

Durham E-Theses

“Late Quaternary ice sheet dynamics and palaeoceanography in the Baffin Bay region”

CODLING, PETER

How to cite:

CODLING, PETER (2017) *“Late Quaternary ice sheet dynamics and palaeoceanography in the Baffin Bay region”*, Durham theses, Durham University. Available at Durham E-Theses Online:
<http://etheses.dur.ac.uk/12676/>

Use policy

The full-text may be used and/or reproduced, and given to third parties in any format or medium, without prior permission or charge, for personal research or study, educational, or not-for-profit purposes provided that:

- a full bibliographic reference is made to the original source
- a [link](#) is made to the metadata record in Durham E-Theses
- the full-text is not changed in any way

The full-text must not be sold in any format or medium without the formal permission of the copyright holders.

Please consult the [full Durham E-Theses policy](#) for further details.

Peter Codling

“Late Quaternary ice sheet dynamics and palaeoceanography in the Baffin Bay region”

There remains a lack of data surrounding the timings and dynamics of the initial retreat of the Greenland ice sheet (GIS) from its maximum extent at the end of the last glacial maximum (LGM), with poor chronostratigraphic constraint also present on the timings of major Baffin Bay detrital carbonate events (BBDC) during the last deglaciation. This study presents new high-resolution data from two cores extracted from the deep abyssal plain of central Baffin Bay. Two separate radiocarbon dates have been extracted using foraminifera which have been used in the development of an age-depth model; estimating the base of the longer gravity core 'GC01' to be approximately 22 ka in age. Samples adequate for radiocarbon dating are few and far between due to intense dissolution of biogenic carbonate in both cores. Measurements of elemental concentrations indicate that significant changes in sediment provenance occurred in central Baffin Bay over the last 22Ka. Substantial amounts of sediment influx from western Greenland occurred during the LGM until approximately 15.8 ka BP when the GIS began its initial stages of retreat as the marine area of Baffin Bay increased. Thereafter the use of sedimentological, geochemical and biological markers alongside radiocarbon dating has captured two separate periods of ice sheet instability associated with the BBDC 1 and BBDC 0 estimated to have occurred between 14.1-13.6 ka BP and 12.7-11.4 ka BP respectively. Further analysis of elemental concentrations attributes these two BBDC events to both be associated with large amounts of sediment influx from northern Baffin Bay i.e. the break-up of the Laurentide (LIS) and the Innuitian Ice Sheets (IIS). When plotted as a timeseries against GISP2 and NGRIP ice core records and regional records of marine palaeoenvironmental, change it is clear that BBDC 1 and BBDC 0 occur out-of-phase with Heinrich event 1 or Heinrich event 0. Instead, BBDC 1 appears to start during the later stages of the Bølling Interstadial and continue into the Allerød Interstadial, peaking during the Older Dryas Stadial. BBDC 0 is generally coeval with the Younger Dryas Stadial although likely ends before the start of Heinrich event 0 in the North Atlantic. Due to BBDC events occurring during both interstadials and stadial periods this would also suggest that the initial trigger for the start of BBDC events are not necessarily linked to temperatures changes on Greenland, supporting Jackson et al., 2017. Therefore, indicating that the LIS and IIS were likely decoupled from the North Atlantic climate mode during the last deglaciation.

“Late Quaternary ice sheet dynamics and palaeoceanography in the Baffin Bay region”

Peter Codling

Thesis submitted for the
degree of Master of
Science

Department of
Geography
Durham University

December, 2017

Contents:

Chapter 1: Introduction:	1
1.1 Importance of Ice Sheet Research	1
1.2 Central Baffin Bay.....	1
1.3 Thesis aims and objectives.....	2
1.4 Study area and Core Selection:	3
Chapter Two: Review of previous research in Baffin Bay	5
Section 2.1 Present-day conditions in Baffin Bay:	5
2.1.1 Introduction: History of Early Study in Baffin Bay:	5
2.1.2 Baffin Bay- Present-day Oceanographic Conditions:	5
2.1.4 Present-Day Ice flux through Baffin Bay:	9
Section 2.2: Global drivers of climate change during the Quaternary:	10
2.2.1 Introduction: The Quaternary:.....	10
2.2.2 Internal (Sub-Milankovitch) processes in Baffin Bay and the North Atlantic:	10
2.2.4 Baffin Bay Detrital Carbonate Events (BBDC):	13
Section 2.3: Baffin Bay through the Quaternary: Ice Dynamics:	14
2.3.1 Introduction:	14
2.3.2 Ice Sheet inception and growth/decay in Baffin Bay:.....	14
Section 2.4 Oceanographic Changes in Baffin Bay:.....	20
2.4.1 Carbonate Dissolution Cycles:.....	20
2.4.2 Long-term Records of Sea-ice and Productivity Changes:	22
2.4.3 Late Pleistocene and Holocene Productivity:	26
2.4.4 The Younger Dryas and the Holocene Transition:	26
2.4.5 The Early-Mid Holocene:.....	27
2.4.6 The Late Holocene - Recent Oceanographic Change in Baffin Bay:.....	28
Chapter 3: Methods:	30
3.1 Introduction:	30
3.2 Core Sedimentology:.....	30
3.3 Multi-core Scanner XRF, MSCL and core X-Rays:	30
3.4 Particle Size Analysis:	31
3.5 Biological Analysis: Foraminifera	31
3.4.1 Sample Preparation:	32
3.5.2 Sample Analysis:.....	32
3.6 Geochemical Analysis:	32
3.6.1 Biomarker Extractions:.....	32
3.6.2 Osmium Isotope Analysis:.....	35
3.7 Radiocarbon Dating:	36
3.8 Pb-210 Dating:.....	36

Chapter 4: Results:	38
4.1 Introduction:	38
4.2 Chronology: Description:	38
4.3 Core Sedimentology: Descriptions:.....	40
4.3.1 GC01: Sedimentological Description:.....	40
4.3.2 BC06: Sedimentological Description:.....	44
4.4 XRF geochemical and Physical properties: Descriptions:	46
4.4.1 GC01: XRF geochemical and Physical properties: Description:	46
4.4.2 BC06: XRF geochemical and Physical properties: Description:.....	49
4.5 XRF: Ca, K and Ti total counts (Semi-Quantitative Minerology): Description:.....	50
4.5.1 Calcium total counts: GC01:.....	50
4.5.2 Potassium total counts:GC01:.....	50
4.5.3 Titanium total counts: GC01:	50
4.5.4 Calcium total counts: BC06:	50
4.5.5 Potassium total counts:BC06:	50
.....	51
4.5.6 Titanium total counts: BC06:.....	52
4.6 GC01: Geochemical Analysis: Osmium Isotopes Ratios: Description:	53
4.7 Biological Analysis: Foraminifera:	53
4.7.1 Biological Analysis: Foraminifera Abundances: GC01: Description:	56
4.7.2 Biological Analysis: Foraminifera Abundances: BC06: Description:.....	56
4.7.3 Biological Analysis: Foraminiferal Ecology: Description: GC01:.....	56
4.7.4 Biological Analysis: Foraminiferal Ecology: Description: BC06:	57
4.8 Biomarker Extractions: IP ₂₅ :	57
Chapter 5: Interpretations:	58
5.1 Chronology: Timeseries development and associations:	58
5.2 Lithofacies associations: GC01 and BC06:.....	58
5.3 GC01: Interpretations:	60
5.4 BC06: Interpretations and correlations to GC01:	62
5.5 Summary of Interpretations GC01 and BC06:.....	64
Chapter Six: Discussion:	65
6.1 Introduction:	65
6.2 The Timings and Dynamics of BBDC Events in central Baffin Bay during the last deglacial (15.5- 10. 5 ka BP):	65
6.3 The Dynamics of the LGM in central Baffin Bay (22-15. 6 ka BP):	70
6.4 Interpretation of osmium Isotopes in Central Baffin Bay Deep Water:	71
6.5 Summary of Central Baffin Bay Sediment Influx and Oceanographic Change (22-10. 5 ka BP):	72

6.6 Summary of Ice Sheet Instability (22-10. 5 ka BP):	75
6.7 The Role of Ocean circulation changes and Climatic Forcing of major ice sheets surrounding Baffin Bay:	77
Chapter Seven: Conclusions:.....	79
7.1 Conclusions:	79
7.2 Future research in central Baffin Bay:	82
7.3 Recommendations for future analysis (GC01 and BC06):.....	82
References:.....	84
Appendices:	99
8.1 GC01 Foraminifera Data Log:	99
8.2 BC06 Foraminifera Data Log:	116
8.3 XRF data GC01:.....	119
8.4 XRF Data BC06:.....	133

List of Tables:

Table 1: Code and description of lithofacies.....	31
Table 2: Specific information regarding the amounts of Jule's Standard used for biomarker extractions from GC01.....	34
Table 3: Radiocarbon ages from GC01.....	38
Table 4: BBDC events timings.....	66

List of Figures:

<u>Figure:</u>	<u>Description:</u>	<u>Page Number:</u>
1.1	Present-day bathymetry including the approximate positions of major ocean currents which operate within Baffin Bay.	3
2.1	Modern-day ocean currents that operate around Greenland and in Baffin Bay.	6
2.2	Monthly sea-ice concentrations in Baffin Bay	8
2.3	Correlations between the GRIP Summit record, Greenland, and the records of foraminifera.	14
2.4	Comparisons of Baffin Bay detrital carbonate events to GISP2 record (Andrews et al., 1998).	15
2.5	Model of ice sheet break-up in Baffin Bay using 100-year intervals.	17
2.6	Bathymetric map of Baffin Bay showing the locations of core GC01/BC06 in relation to grounding lines of the Uummannaq ice stream (UIS) and the Disko ice stream (DIS), Smith Sound ice stream (SSIS) and the Lancaster Sound ice stream (LSIS).	20
2.7	LGM ice margins of the LIS, GIS and IIS during the last glacial maximum (Stokes et al., 2016).	21
2.8	Carbonate dissolution cycles in Baffin Bay (Asku, 1983).	22
2.9	Representation of different sea-ice conditions and the respective IP ²⁵ and phytoplankton biomarker responses with the PIP ²⁵ index (Belt et al., 2013).	25
2.10	Sediment delivery in Baffin Bay (Hiscott, Asku and Nielsen, 1989).	26
2.11	Possible four major sediment sources for core JR175 BC06.	27
3.1	process of extraction and partial purification of IP ²⁵ (Belt et al., 2012).	35
3.2	Gamma activities from BC06.	37
4.1	Age versus depth plot for GC01.	39

4.2	High-resolution combined images showing the physical and magnetic properties of core GC01.	42
4.3	X-rays of GC01 showing various lithofacies.	43
4.4	High-resolution combined images showing the physical and magnetic properties of core BC06.	44
4.5	X-Rays of BC06 showing various lithofacies.	45
4.6	High resolution combined images showing geochemical properties of GC01.	48
4.7	High resolution combined images showing geochemical properties of BC06.	49
4.8	High resolution images showing selected elements normalised against potassium for GC01.	51
4.9	High resolution images showing selected elements normalised against potassium for BC06.	52
4.10	$^{187}\text{Os}/^{188}\text{Os}$ results extracted from GC01.	53
4.11	Foraminiferal abundances for GC01.	54
4.12	Foraminiferal abundances for BC06.	55
5.1	High resolution combined images showing geochemical properties of GC01 showing lithofacies associations.	59
5.2	High resolution combined images showing geochemical properties of BC06 showing lithofacies associations.	62
6.1	Comparisons of key data extracted from GC01 with GISP2 and NGRIP during the last 22ka.	66
6.2	Geological map of Baffin Bay's bathymetry and major ocean currents (Simon et al., 2014).	69
6.3	Ice sheet extent in West and East Greenland from the LGM to the early Holocene (O'Cofaigh et al., 2013).	70

6.4	Oceanographic change in Baffin Bay between 10.5-22Ka.BP.	73
6.5	Summary of ice sheet instability between 22-10.5Ka.	75

Statement of Copyright:

“The copyright of this thesis rests with the author. No quotation from it should be published without the author's prior written consent and information derived from it should be acknowledged.”

Acknowledgements:

First of all, I would like to thank Dr. Jerry Lloyd and Prof. Colm O'Cofaigh for their advice throughout this research masters and also for giving me the incredible opportunity to accompany them on their research expedition to northeast Greenland this year.

Additionally, I would also like to thank my friend Daniel Aldridge for teaching and giving me access to various graphics packages used for the purposes of this thesis and his constructive comments throughout. Finally, I would like to thank my parents and Jennifer Toothill for supporting me throughout the entire course of this research masters.

Chapter 1: Introduction:

1.1 Importance of Ice Sheet Research

Recent observations have identified significant changes in outlet glacier behaviour around the Greenland Ice Sheet (GIS), including ice stream acceleration, thinning and retreat of tidewater glacier calving margins (Joughin et al., 2008; Rignot and Mouginot, 2012; Nick et al., 2013). This has led to a major increase in research investigating the dynamics of the GIS over recent and longer timescales to try and improve our understanding of the driving mechanism. It is important to monitor changing dynamics of these outlet glaciers (surface mass balance and iceberg calving), and ice sheets as a whole, in order to best model future sea-level change and how this may influence atmosphere-ocean interactions across the globe. Therefore, understanding the past responses of large ice sheets to climate and ocean forcing allows for better placement of the current ice sheet dynamics into longer-term contexts (Jennings et al., 2017), providing valuable data for future ice sheet modelling. Observations over the last two decades have demonstrated the complexity of the GIS with marine-terminating glaciers often exhibiting different behaviour to one another despite their close proximity, likely due to differences in underlying topography and small-scale local effects (Joughin et al., 2012; Enderlin and Howat, 2013). It is also apparent that the GIS is losing mass via surface melt too (Zwally et al., 2002), with increases in ice flow velocity attributed to higher amounts of summertime melting, further contributing to global sea-level rise. However, the accurate modelling of ice sheet responses to climate change requires improved understanding of the timings and dynamics associated with rapid retreats and advances of major ice sheets (Stokes and Tarasov, 2010), with the drivers of ice sheet retreat still poorly understood (Simon et al., 2014). It is therefore vital that further research is undertaken to develop a robust chronology of past ice sheet variability and the driving mechanisms behind past changes. At present it remains difficult to differentiate whether the modern-day GIS ice margin dynamics are caused due to a mix of mass balance and internal dynamics (Stokes et al., 2012) or climate/ocean warming (Holland et al., 2008; Straneo et al., 2012).

1.2 Central Baffin Bay

Investigating the extent and dynamics of the Laurentide Ice Sheet (LIS) and GIS has been the focus of scientific research for over a century, with scientists placing a strong emphasis on the reconstruction maximum ice sheet extent during the last glacial maximum (LGM) (England, 1999; Dyke, 2002; Ó Cofaigh, 2013) and their subsequent decay during the last deglaciation (Funder and Hasen, 1996; Bennike and Bjorck, 2002; Young et al., 2012). However, the chronology of ice sheet break-up around the margins of central Baffin Bay remains poorly constrained, with previous studies choosing to focus on well-known major discharge events from Hudson Strait into the Labrador Sea and the northwest Atlantic Ocean (e.g. Hulbe et al., 2004; Stanford et al., 2011; Álvarez-Solas, 2011).

There have been some studies investigating ice margin instability and the links to palaeoceanography of Baffin Bay (e.g. Asku and Piper, 1978; Asku, 1987; Andrews et al., 1998; Knudson et al., 2008; Jennings et al., 2017),

but our understanding of the dynamics of the northern sectors of the LIS, GIS and the Inuitian (IIS) since the LGM is still relatively limited.

The location of Baffin Bay is unique, offering the opportunity to study three major ice sheets, including the LIS, GIS and IIS that all flanked Baffin Bay during the Quaternary to the west, east and north respectively (see Figure 1.1). Although as demonstrated on multiple occasions in the literature attempts at developing a chronostratigraphic framework of ice margin variability has been met with great difficulty (e.g. Andrews and Eberal, 2011; Schroeder-Adams and Van Rooyen; 2011; Seidenkrantz, 2013) due to lack of biogenic carbonates which are either scarce or have been dissolved in the glaciomarine sediments found in central Baffin Bay. Chronological developments have therefore tended to be based on high-resolution palaeomagnetic and cosmogenic $^{10}\text{Be}/^9\text{Be}$ ratios (Simon et al., 2012; 2016) in order to establish a well constrained record of ice sheet dynamics. However, exact timings of major discharge events identified in Baffin Bay (Andrews, 1998) are still poorly constrained, highlighting the need for establishing a robust chronology of ice sheet variability since the LGM. Whilst continuing to investigate the potential driving mechanisms controlling ice margin variability.

1.3 Thesis aims and objectives

This study aims to develop a record of ice sheet instability and ocean productivity changes through the Late Quaternary for central Baffin Bay. To achieve this a multi-proxy approach will be used. The incorporation of sedimentological, geochemical and biological proxies as well as radiocarbon dating will be used to interpret environmental changes from a sediment core in central Baffin Bay and also the reconstruction of ice sheet dynamics and associated productivity changes over time. In doing so, the study will contribute to a greater understanding of the changing sediment provenance linked to variability in ice dynamics of the ice sheets fringing Baffin Bay over the last 22,000 years. To achieve this aim, the following objectives have been developed:

- To develop a chronology of palaeoenvironmental change from core BC06 and GC01 collected from central Baffin Bay using ^{14}C dating from the last 22,000 years.
- To identify major lithofacies in GC01 and BC06 based on sedimentological and geochemical proxies.
- To identify changes in benthic and planktonic foraminiferal abundances and reconstruct the palaeoceanographic evolution of central Baffin Bay.
- Combine the sedimentological, geochemical and biological proxies to develop a chronology of environmental change in central Baffin Bay linked to ice sheet dynamics and palaeoceanographic evolution of the Baffin Bay region, complementing previous and ongoing work in the region.

1.4 Study area and Core Selection:

Baffin Bay is a semi-enclosed basin which is located between the west coast of Greenland and the Canadian Arctic Archipelago, extending approximately 1400 km north-south and 550 km east-west (see Figure 1.1). It is connected to the Arctic Ocean through a series of relatively shallow and restricted straits, (Jones and Lancaster Sounds and the Nares Strait) with the bay also connected to the North Atlantic Ocean via the Davis Strait to the south. The bathymetry of Baffin Bay shows that Baffin Bay is characterised by a large abyssal

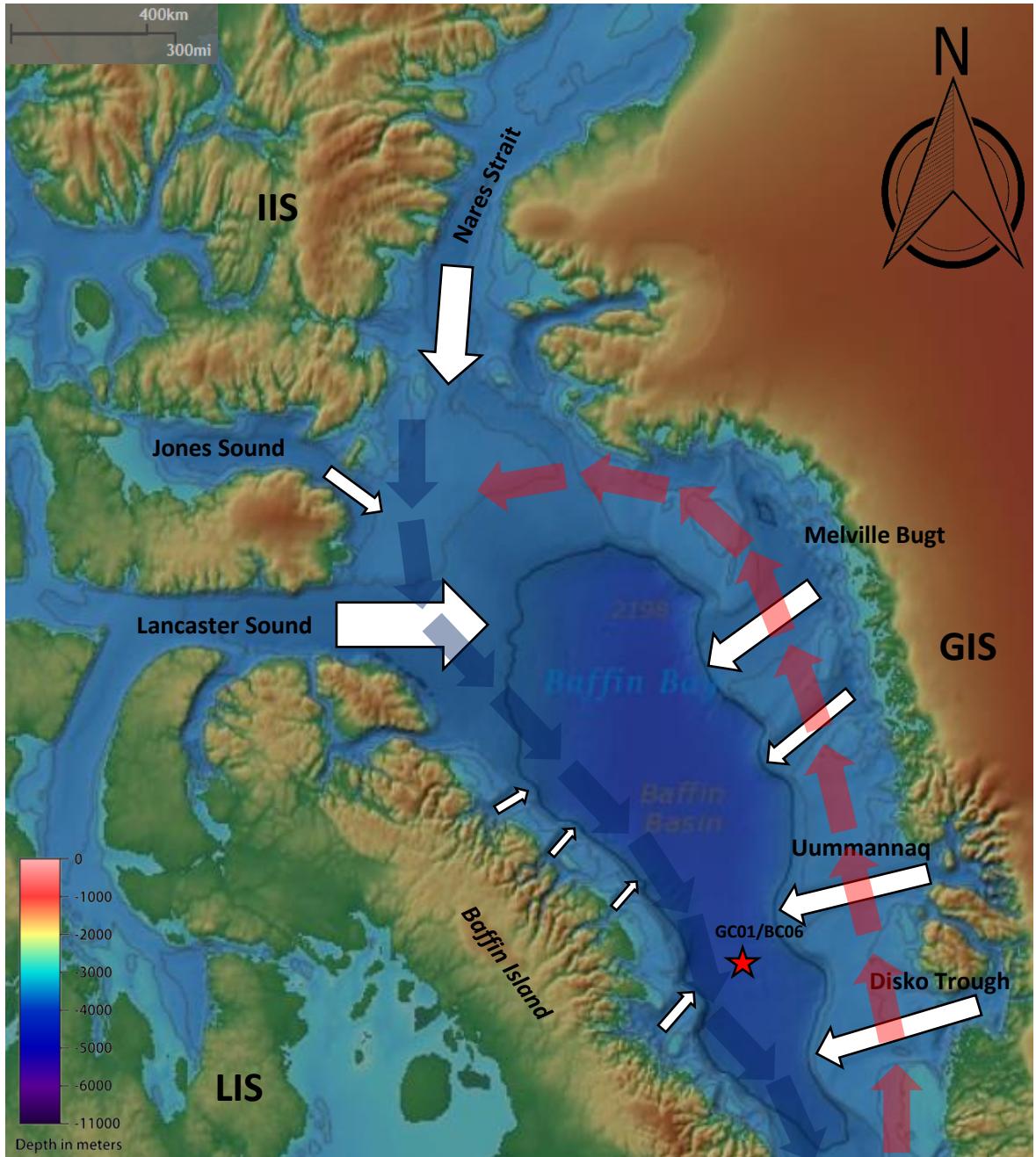


Figure 1.1: Present-day bathymetry including the approximate positions of major ocean currents which operate within Baffin Bay, also shown are all major channels into Baffin Bay; Lancaster, Jones and Smith Sounds in relation to the georeferenced locations of cores GC01 and BC06 (shown by red star). White arrows show the approximate locations of major trough systems surrounding Baffin Bay. Original bathymetric base map provided by (NOAA, 2016).

plain in its centre which reaches depths of over 2400 m, with the continental shelves around the bay generally being around 200-600 m deep.

Around the margins of Baffin Bay, the continental shelf shows significant variability with the average widths in western Greenland reaching some 350-400 km from the coast whereas off the coast of Baffin Island the average width of the continental shelf here is approximately 150 km. Further work by Asku (1983) evidences that these shelves have been dissected by several deeper transverse channels, with the shelves breaking at 400-600 m down steep slopes that run into the abyssal plain, before rising again towards the Davis Strait to the south and the Lancaster Sound to the north. The deep troughs that dissect the western Greenland continental shelf commonly end in large trough mouth fans (Ó Cofaigh et al., 2013), with an extended shelf also present in northern Baffin Bay dissected by the major trough of Lancaster Sound and associated large fan system.

The two cores used for the purposes of this study were collected during the RRS James Clark Ross (JR175) expedition which operated between August and September 2009. The aim of the cruise was to collect marine geophysical data from west Greenland and the abyssal plain of Baffin Bay. The two cores used in this study are box core 'JR175-BC06' and gravity core 'JR175- GC01' (hereafter referred to as BC06 and GC01) which were both collected at the same location, 'Lat. 69° 56.01_N', 'Long. 63° 03.4_W' at a water depth of 2034 m, (see Fig.1.1). The longer gravity core is 1.68m in length whereas the box core is 0.48m. The box core was used as well as the gravity core to collect an undisturbed and higher resolution record for the most recent time whilst still gaining a longer record of ice sheet dynamics and productivity changes from the gravity core. The two cores were extracted from the deep abyssal plain in central Baffin Bay, northwest of the Disko Trough and just southwest of the Umnanak Trough, west Greenland (Figure 1.1). To the west lies Baffin Island, Canada. Following the extraction, both cores were stored at +3 °C at Durham University Science Site, UK, until analysis was begun in October 2016.

Chapter Two: Review of previous research in Baffin Bay

Section 2.1 Present-day conditions in Baffin Bay:

2.1.1 Introduction: History of Early Study in Baffin Bay:

The present-day oceanographic conditions in Baffin Bay and central west Greenland have been the focus of several major studies in recent decades (Grumet et al., 2001; Tang, 2004; Lloyd et al., 2011; Sheldon et al., 2016). The first records of human expeditions into the area dates back to approximately 983 AD; Dunbar (1951) exhaustively lists these initial marine observations, although interestingly it would appear that it was at this time that an early connection between Baffin Bays surface circulation and ice drift was first noted. Moving forward into the latter part of the 19th century it was clear through more extensive mapping of the region that warmer waters entered the bay through the Davis Strait, located south of Baffin Bay, and that cold water flowed southward down the western side of Baffin Bay (Hayes, 1867). Petterson (1900) also notes the presence of three-layered structure to the ocean water found within Baffin Bay, (see section 2.1.2 for more detail). During the 20th century there was numerous oceanographic expeditions which set out purposely to explore in greater detail the marine and environmental dynamics operating within the region. Most noteworthy was the work by Smith, (1937) and Kiilerich, (1939) that gave the first in-depth description of the geostrophic flow of water in the Davis Strait and the major baroclinic currents influencing Baffin Bay, building upon the previous descriptions put forward by (Hayes, 1867 and Petterson 1900).

2.1.2 Baffin Bay- Present-day Oceanographic Conditions:

Due to Baffin Bay's northern geographical location and unique bathymetry, the hydrographic conditions are of much interest in terms of developing a better understanding of the interaction between the Earth's oceanic and atmospheric systems. Studies have focused on the three areas where water can enter the bay; at Nares Strait (Munchow et al., 2006), Smith Sound (Melling et al., 2001) and at Lancaster Sound (Fissel et al., 1982). This was then combined with research from the Davis Strait (Mauritzen, 1996; Cuny et al., 2005) to give a broader picture of the oceanographic conditions operating within Baffin Bay. The collective research over recent decades reveals that the modern-day oceanic circulation in Baffin Bay is in-part influenced by cold, low salinity waters flowing down from the Arctic through the Nares Strait, however, (see Fig 2.1), this cold water tends to flow down the western side of Baffin Bay, known as the Baffin Current (BC) (Williams, 1986), before exiting via the Davis Strait then into the Labrador Sea, finally flowing south past Labrador to become the Labrador Current (LC) (Mertz et al., 1993). The work of Muench (1971) investigates in detail the specific water masses of Baffin Bay with a three-layer division based on temperature, salinity and depth put forward; the division is laid out as follows; the surface layer (0-150 m), the intermediate layer (150-300 m to 1200-1300 m) and the bottom layer (1300 m to the ocean floor). The surface layer is a mix of cold Arctic and warmer Atlantic water, because of this mixing of different water masses this layer receives the largest seasonal and geographical variations of all three layers (Muench, 1971), however the layer generally consists of cold, low salinity water. The intermediate layer is comprised of more saline and relatively warmer water and is often

called Baffin Bay Atlantic Water (Asku, 1983), which although originating from the Atlantic is then cooled through mixing with the cold surface layer. Below this, cold water, known as Baffin Bay Bottom Water (Asku, 1983), dominates, within this layer levels of salinity are very stable with no temperature or salinity changes detectable below 1800 m (Tan and Strain, 1980).

Furthermore, on comparison to previous studies of water body characteristics in the Arctic ocean and also in the Eurasian basin (e.g. Palfrey and Day, 1968; Jones et al., 1995), the results collected from Baffin Bay indicate that Baffin Bay Deep Water has similar characteristics to water masses originating from the Arctic Ocean. Indicating that Baffin Bay bottom water is partly of Pacific origin which flows into the Arctic Ocean through the Bering Strait and then enters Baffin Bay through the Canadian Archipelago (Tang et al., 2004).

Baffin Bay lies north of the planets zonal flow of westerly winds, there is a clear east-west gradient in terms of air temperature during the winter months with this decreasing significantly in summer (Tang et al., 2004). During winter, it has been consistently measured that the highest air temperatures are found along southern

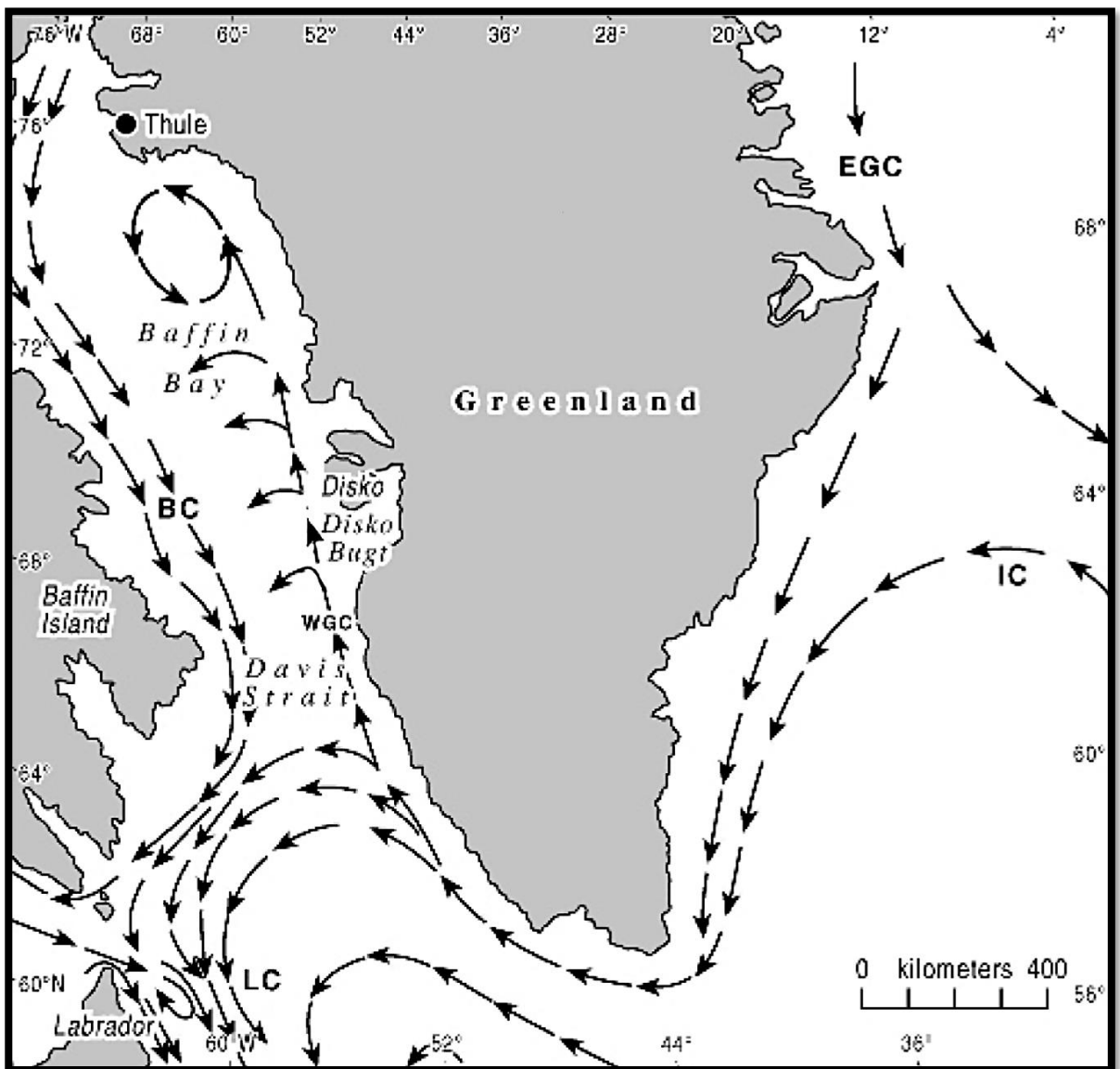


Figure 2.1: Modern-day ocean currents that operate around Greenland and in Baffin Bay. All currents have been abbreviated as follows; West Greenland Current (WGC), Baffin Current (BC), Labrador Current (LC), East Greenland Current(EGC), Irminger Current (IC). Modified from (Lloyd, 2006).

Greenland and in the eastern part of the Davis Strait, with a 'warm tongue' of water extending up from the southeast around Kap Farvel, (see Fig 2.1), whereas the coldest temperatures are found in the northwest. It is this variation in air temperature which plays such an important role in present-day interannual sea-ice cover in Baffin Bay, with the 'warm tongue' likely associated with the West Greenland Current (WGC) often preventing the south-eastward progression of winter sea-ice. Many studies have observed that even in the 'heavy' ice years ice thickness in the Davis Strait has remained very variable since at least 1950 when detailed observations began proper (Kaminski, 1955; Crane, 1978; Parkinson et al., 1989; Valeur et al., 1996; Parkinson et al., 1999), observing that even in the 'heavy' ice years ice thickness in the Davis strait has remained very variable since at least 1950 when in-depth observations began proper.

Despite cold inflow from the Arctic and its northerly latitude, Baffin Bay is not completely dominated by sea-ice year-round, large interannual variations in sea-ice cover have been observed (Parkinson and Cavalieri, 1989; Wang, 1994; Tang et al., 2004), with the Bay being almost completely free of sea-ice during September each year. As discussed by Tang et al., (2004) throughout the ice season there is always more ice cover over towards the western side of Baffin Bay, with significantly less ice in the eastern half, with this being linked to the relatively warm flows of water associated with the WGC. The WGC is of North Atlantic origin and is mixture of the cold, low salinity East Greenland Current (EGC) and the warm, saline, North Atlantic Irminger Current (IC). These two currents mix off the southeast coast of Greenland before flowing around Kap Farvel and then northward to become the WGC, (Figure 2.1), although some of the WGC is deflected westwards at the Davis Strait which forms a counter-clockwise gyre in the Labrador Sea (Buch and Stein, 1989). The dynamic processes associated with the mixing between the two ocean currents has been extensively discussed by Myers (2007); with the amount of mixing of the IC and the ECG once deflected around Kap Farvel is shown to be highly variable even over relatively short timescales, despite this variation, the WGC's influence has been shown to be felt as far north as northern Baffin Bay (Lewis et al., 1996). It is here that the northward flow of the WGC is then stopped upon reaching large counter-clockwise gyres located in Baffin Bay, the flows then join up with the cold, low salinity BC and flows back southward.

Monthly Ice Concentration

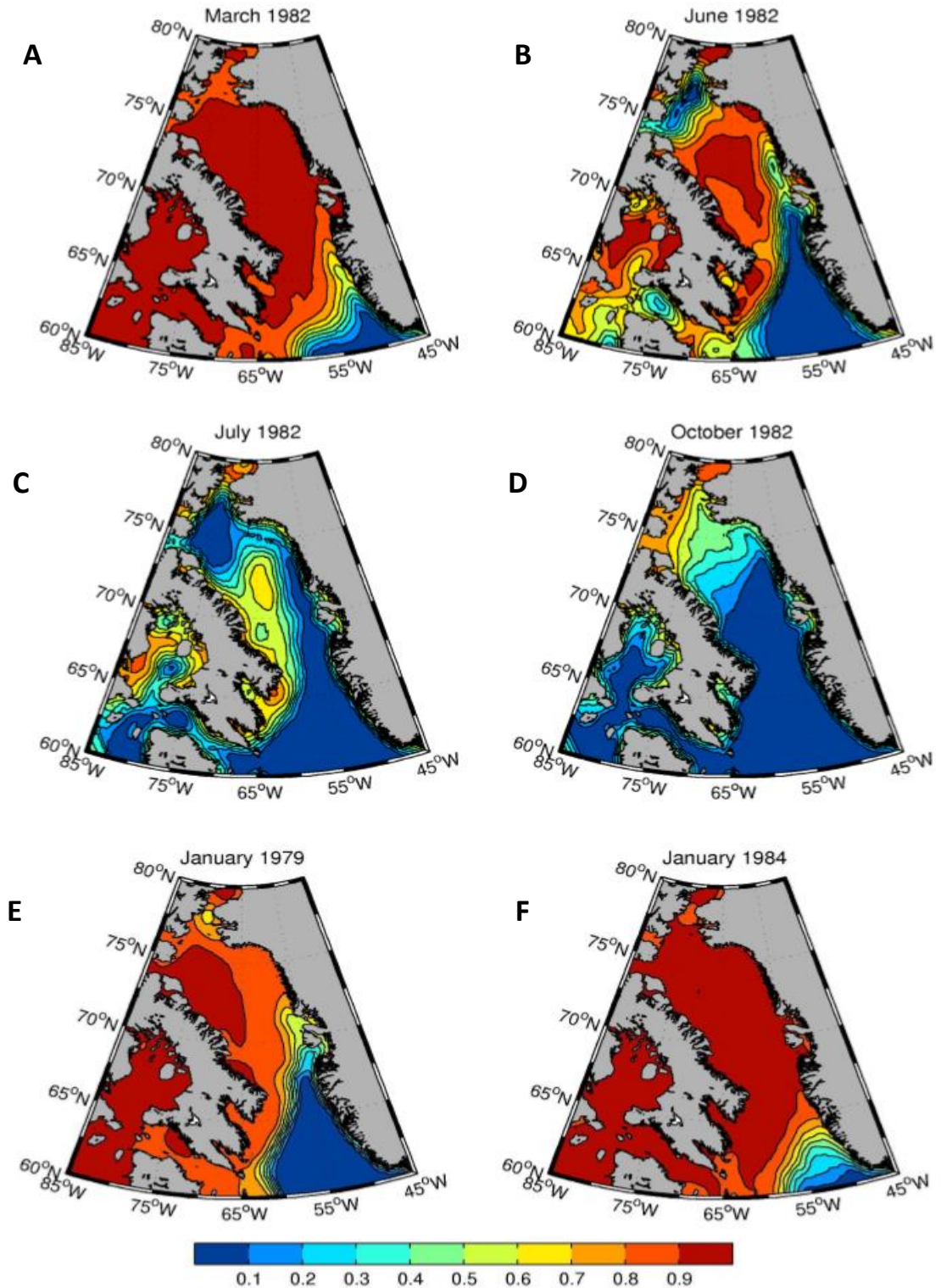


Figure 2.2: Monthly sea-ice concentrations in Baffin Bay showing the annual variations from; early spring (A) sea-ice maximum, early summer, (B) mid-summer, (C) and mid-autumn, (D) when sea-ice is at its lowest concentrations before the winter re-freeze. (E) and (F) show an inter-annual comparison between an ice 'light' year in 1979 and an ice 'heavy' year in 1984. (Modified from Tang et al., 2004).

2.1.4 Present-Day Ice flux through Baffin Bay:

Data regarding annual amounts of ice flux through Baffin Bay is difficult to come by. However there have been a few attempts to estimate this based on reconnaissance flights and, more recently, satellite data (e.g. Dunbar, 1973; Dey, 1981). Based on these relatively crude datasets, the influx of ice into Baffin Bay occurs mainly during the warmest summer months from northern channels due to the fact that these channels are covered with landfast ice through the rest of the year halting ice flow. The main channels which allow ice influx are the Lancaster and Jones Sounds, but it should be noted that some ice influx does indeed occur from the Arctic through the Nares Strait. As discussed by Sadler; (1976) the influx of ice via Nares Strait despite being significant is still much less than from the Canadian Archipelago sources. Regarding the calving of icebergs, the majority of icebergs that enter Baffin Bay are not produced from the smaller glaciers located on the Canadian Archipelago but from the large glaciers on the west coast of Greenland, with some 12-40,000 icebergs entering Baffin Bay each year most notably from Umnanak and Disko Bay in central west Greenland (Valeur et al., 1996). Icebergs that are produced from these two areas either flow north or south depending on the exact location of their calving and their overall size, to be carried south these icebergs are transported westwards by a re-circulating arm of the WGC into the southerly flow from the Baffin Current. The smaller icebergs are usually carried away south or south-eastwards by the Labrador Current and melt, sometimes reaching as far south as the Grand Banks off the coast of Newfoundland, Canada (Tang et al., 2004). Those which flow north with the WGC, tend to be either calved north of Disko Bay or are over 1 million tons (Tang et al., 2004), these then flow into northern Baffin Bay before being picked up by the Baffin Current which flows south hugging the continental shelf of the Canadian Archipelago. The highest concentrations are found in the centre of the Baffin Current where waters are at their coldest, the drift of these icebergs has been extensively mapped (Marko, Birch and Wilson, 1982), with measurements of drift indicating intermittent periods of rapid movement in between periods where movement is almost zero due to icebergs becoming trapped in landfast ice, (see Figure 2.2).

Section 2.2: Global drivers of climate change during the Quaternary:

2.2.1 Introduction: The Quaternary:

The Pleistocene epoch is the first of the two formal epochs which make up the Quaternary period (last 2.5Ma); with the end of the Pleistocene occurring approximately 11.7 ka BP and the present warm period known as the Holocene (11.7 ka- present) beginning with the Preboreal at the end of the Younger Dryas. The Pleistocene is characterised by very large pseudo-periodic fluctuations in global ice volumes (Broecker and Donk, 1970; Hays et al., 1976; Kominz et al., 1979) with at least twenty glacial cycles evidenced to have occurred during the epoch, (see Figure 2.4); whereas the Holocene has been comparatively stable but with it too experiencing notable, although much less extreme, shifts in climate.

2.2.2 Internal (Sub-Milankovitch) processes in Baffin Bay and the North Atlantic:

The growth of northern ice sheets such as the Laurentide Ice Sheet over North America and the Fennoscandian Ice Sheet over Europe have been discussed extensively (Manabe and Broccoli, 1985); with synoptic modelling suggesting that strong westerly winds blew along the northern flank of the Laurentide ice sheet. This northerly sourced air mass then acted to cool Baffin Bay and Labrador at the surface, with the air cold enough at higher latitudes to freeze these subpolar waters. However, it is understood that as these large ice sheets begin to retreat it led to the subsequent weakening and eventual break-down of these regional wind patterns (Webb et al., 1993), as overtime, shifts in atmospheric circulation results in major climatic changes at regional scales (Charles and Fairbanks, 1992). Nevertheless, it must be noted that these changes in atmospheric circulation at regional scales are likely to be driven by a combination of interconnected internal processes; with it being apparent through extensive work within the field of palaeoceanography that

fluctuations in ocean density, temperature and salinity are of major importance to the global climate system. However, oceanography sits within a complex system of other climatic feedback loops which makes it exceedingly difficult to identify the different components of the atmosphere-ocean-terrestrial relationship which are causally linked. Despite this, high resolution proxy records obtained from both ice and deep-sea sediments suggest that over the last 130 ka there have been significant changes in ocean water movement in the North Atlantic (Keigwin et al., 1994; McManus et al., 2002). Such variations in ocean circulation operate at Milankovitch frequencies reviewed previously, but also at much shorter frequencies (Chapman and Shackleton, 2000) between the major glacial-interglacial cycles. This movement of ocean water is evidenced by changes in ocean surface micro-fauna such as the distribution and abundance of planktonic foraminifera, but also from lithostratigraphic variations, such as the presence of ice rafted debris (IRD) in ocean cores

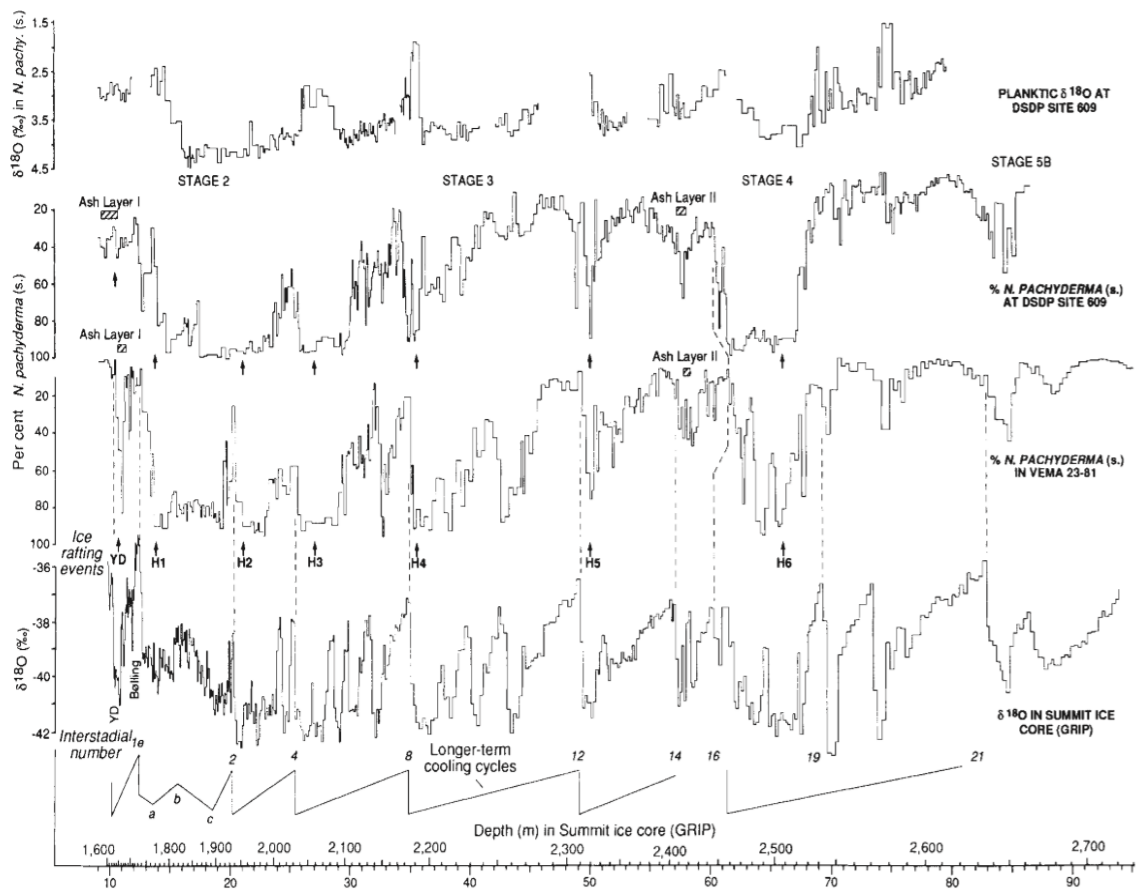


Figure 2.3: Correlations between the GRIP Summit record, Greenland, and the records of foraminifera at site DSDP 609 and at site V23-81, with six Heinrich events shown to have occurred in the last glacial-interglacial transition, with the dashed lines used in order to match the ice-core records to the marine records. The heavy arrows mark the points at which IRD counts reached their maximum levels. Also shown are the longer-term cooling cycles which are defined by (Bond et al., 1993) by grouping the millennium scale Dansgaard-Oeschger cycles and Heinrich events together. Between 20-80 ka BP shifts in the ocean-atmosphere were grouped into a series of cooling cycles which became known as the Bond Cycles, with each lasting approximately 10-15 ka characterised by an asymmetrical saw-tooth pattern as each cycle culminated with a cold stadial followed by an abrupt shift to warmer conditions (Bond and Lotti, 1995). (Taken from Bond et al., 1993).

extracted from the North Atlantic and Baffin Bay. The reasons for the onset of these incursions of polar water into the mid-latitudes during the last glacial-interglacial transition appear to have coincided with repeated melt fluxes of the Laurentide Ice Sheet (Bond et al., 1993); with this in turn having a partial effect on the

position of the polar front. However equally as important during these transitional periods appears to have been the strength of the thermohaline circulation and more specifically the variability in the amount of North Atlantic Deep-Water (NADW) formation (Lowe and Walker, 2007). This large-scale conveyor belt is of critical importance in transporting heat from the tropics into the polar regions. However, during glacial periods a reduction in the salinity of the North Atlantic could act to reduce the rate at which NADW is formed and subsequently slow down the thermohaline circulation conveyor during smaller sub-Milankovitch climatic events (Broecker et al., 1990); with perhaps a complete shut-down possible during the major Northern Hemisphere glaciations (Broecker, 1992).

Nevertheless, despite there still being debate around the mechanisms which drive these rapid climatic events within the paleoclimatic community, they are often seen as prime examples of the high level of interaction which occurs between Earth's oceanic-atmospheric-cryospheric system (Broecker, 1994). Previous work set out to analyse these rapid sub-Milankovitch climatic events (Heinrich, 1988; Zaucker et al., 1994) has identified two different types of climatic changes known as Heinrich events and Dansgaard-Oeschger (D-O) events. The latter were first reported from the GRIP summit ice cores by Oeschger and Dansgaard, (1985); who identified twenty-five separate D-O events between the LGM and the last glacial-interglacial transition. These events are characterised by an abrupt warming to near-interglacial levels, with this occurring in a matter of decades, followed by a gradual cooling. However, the former, known as Heinrich events occurred during the coldest intervals between each D-O event with six being formally identified in the last 80ka, characterised in the North Atlantic deep-ocean record by sudden increases in IRD counts which are indicative of the purging of icebergs from the Laurentide and Greenland ice sheets (Rahman, 1995).

2.2.4 Baffin Bay Detrital Carbonate Events (BBDC):

The Baffin Bay sedimentary record indicates that ice rafting events took place on millennial time-scales (Hiscott et al., 1989) throughout the Quaternary. These events formally termed Baffin Bay Detrital Carbonate (BBDC) events (Asku, 1981) and have since been tentatively linked to mass iceberg discharges during Heinrich events in the North Atlantic (Andrews et al., 1998). Although it is likely that the input from Baffin Bay would have been small in comparison to locations further south, such as in the Hudson Strait, which has been recognised as the main source of iceberg discharge (Dowdeswell et al., 1995). Interestingly data presented by Parnell et al., (2007) from central Baffin Bay does suggest that BBDC events may have been more influential in transporting material into the North Atlantic than first thought, with sediments associated with Heinrich events reaching as far as Portugal (Peck et al., 2006) whilst still containing high concentrations of dolomite, rather than the calcitic sedimentology associated with Hudson Bay (MacLean et al., 1977). Recently a framework for sediment-source differentiation has been proposed, (Simon et al., 2012) states that the LIS and IIS did indeed respond to high-frequency fluctuations in climate such as Dansgaard-Oeschger events during MIS2 and MIS3, whereas the GIS appears to be more responsive to changes in oceanographic conditions such as the in strength of the WGC. This is further supported in the sedimentary framework

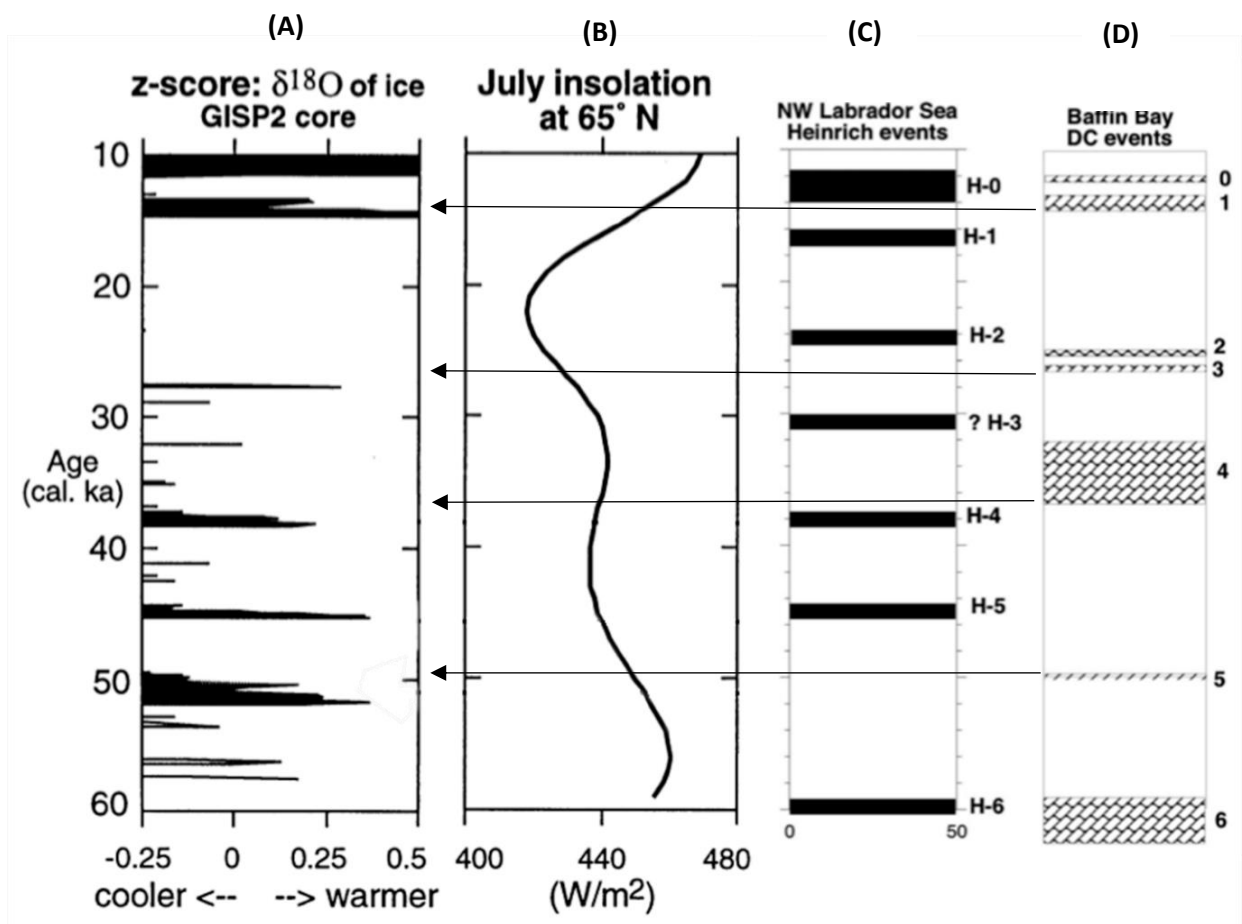


Figure 2.4: (A) Normalised $\delta^{18}\text{O}$ from GISP2, highlighting major MIS 2 and MIS3 interstadials, (B) July insolation for 65°N, (C) Ages of Heinrich events in the Northwest Atlantic, (D) ages for Baffin Bay detrital carbonate events. Note miss-matching of BBDC and Heinrich events excluding BBDC and H-0. (Modified from Andrews et al., 1998;2014).

presented in Andrews et al., (2014) which shows the GIS as the main source of sediment into Baffin Bay, however this record is interrupted approximately every 7ka.BP between 51-14 ka BP by detrital carbonate incursions, sourced from the erosion of Palaeozoic outcrops in Northern Baffin Bay and the Canadian High Arctic (Bond and Lotti, 1995). However due to problems associated with carbonate dissolution in Baffin Bay there are still issues with obtaining an exact chronology of these BBDC events. Due to differences in radiocarbon age models between studies it is difficult to say whether these events are synchronous with calcite-dominated Heinrich events from further south in Labrador or, as suggested by (Andrews et al., 2014), BBDC and Heinrich events are controlled by different driving mechanisms.

Section 2.3: Baffin Bay through the Quaternary: Ice Dynamics:

2.3.1 Introduction:

Despite there being a large amount of evidence for climatic change in the North Atlantic Region, it is now understood that in order to better understand glaciological/climate episodes such as D-O and Heinrich events studies should be focused on areas which are particularly sensitive to changes in climate. Baffin Bay and the Labrador Sea are two of the unique locations which were likely have been subject to large fluctuations in oceanographic conditions during the Quaternary. As Baffin Bay has been in close proximity to multiple ice sheets, the region is likely to be of critical importance in the study of large-scale glacial meltwater events (Williams and Fillon, 1986; Berger, 1990; Fairbanks et al., 1992).

2.3.2 Ice Sheet inception and growth/decay in Baffin Bay:

In recent years glacier dynamics and the links to ice sheet growth and decay have received increasing attention. This in part is likely due to the recent observed rapid increase in mass loss from the GIS (e.g. Rignot and Kanagaratnam, 2006; Rignot et al., 2011) which has potential to raise global sea-levels significantly in the next century (Nick et al., 2013). Despite this, relationships between high-frequency ice sheet dynamics during the LGM in Baffin Bay remain poorly understood, with only few studies focusing on the area (e.g. Andrews and Ebrel, 2011; Simon et al., 2012). However, Baffin Bay's unique location means that through the Quaternary it is likely to have been influenced by multiple ice streams (Simon et al., 2014) from central west Greenland, the north-eastern Laurentide and also the southern Innuitian Ice Sheets.

Although the onset of the LGM has been conventionally defined through the use of sea-level records (e.g...) and is defined as the most recent point at which global ice sheets reached their maximum integrated volume (Mix, Bard and Schneider, 2001) this does not take into account temporary regional variability of ice sheet maxima. It is therefore important to note that although the global LGM is thought to have occurred between 26.5 ka to 20 ka. BP in response to significant global-scale climate forcing (Clark et al., 2009), it is likely that the onset of deglaciation of some ice sheets occurred later after 19 ka due to regional controls on glacier mass balance (Dyke and Prest, 1987).

During the LGM sea-levels were also likely to have reached their lowest levels approximately 20 ka BP (Bard, Fairbanks and Hamelin, 1992). This period of maximum ice extent was followed by mass ice sheet break-up with the LIS having completely disappeared from Hudson Bay by approximately 6.8 ka BP (Carlson et al.,

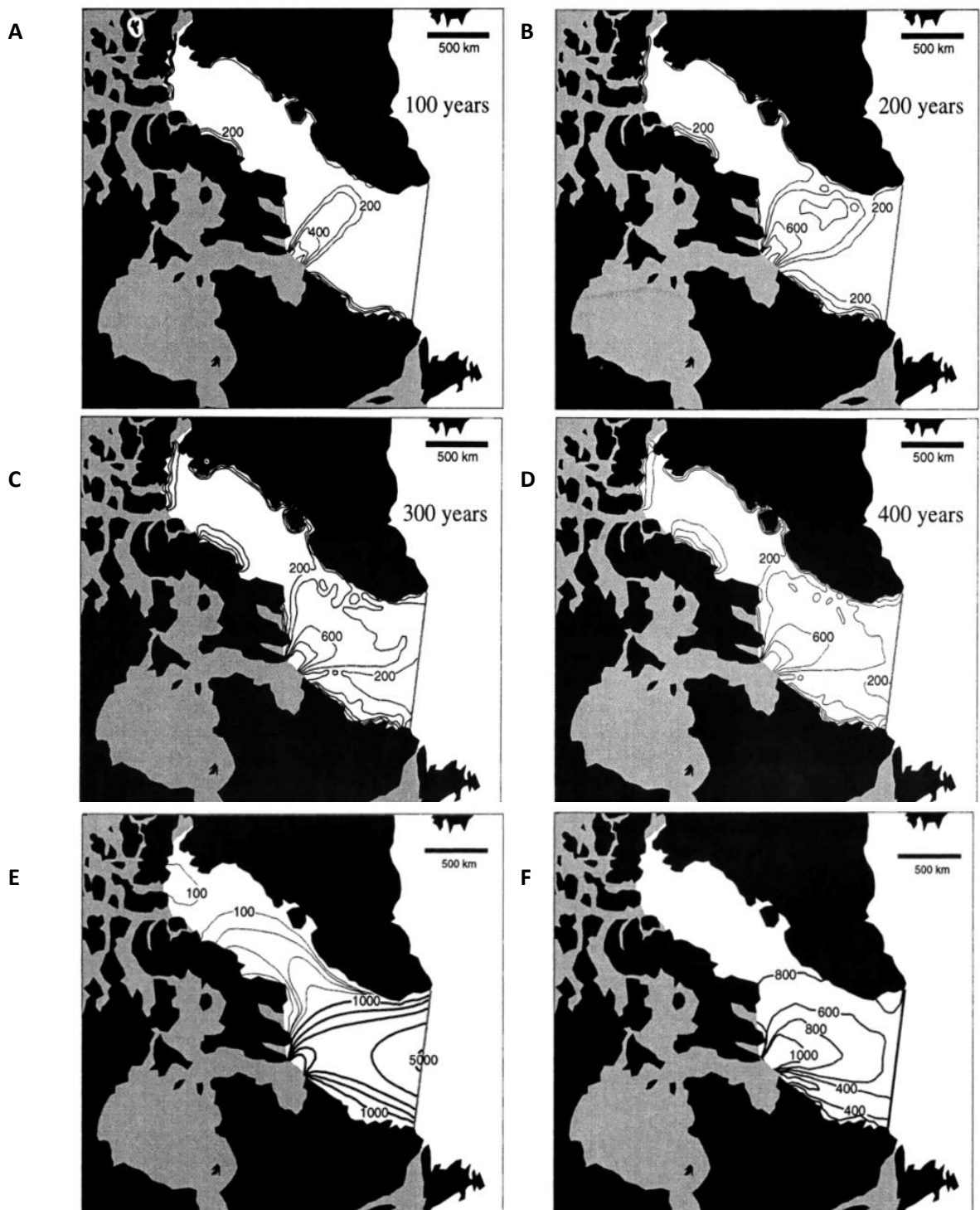


Figure 2.5: Model of ice sheet break-up in Baffin Bay using 100-year intervals. **(A)** and **(B)** show the development of large scale thickness gradients firstly in the Labrador Sea before progressively extending north as basal melting/freezing processes begin to start soon after ice sheet inception. This has been shown by (Bond et al., 1997) to fit with millennial scale climate oscillations such as D-O cycles. Notice that the ice sheet in Baffin Bay grows at a much slower rate as even after 300-400 years of ice sheet break up further south **(C)** and **(D)** only minor gradients are present along Baffin Island and the west Greenland coast. **(E)** shows steady ice speed during break-up with ice flowing rapidly through the Labrador Sea, however north of the Davis Strait there is much slower flows of ice. **(F)** displays the ice shelf thickness, due to large basal gradients being present in the Labrador Sea large amounts of basal melting occurred along the deep keel of the shelf with basal freezing occurring upslope in along the ice sheets flanks. (Modified from Hulbe et al., 1997).

2008). The chronology of retreat of the LIS since the LGM is the best constrained record of the demise of a

large ice sheet to date, with evidence suggesting that ice was likely removed from the Baffin Bay region in stages (Miller et al., 2005). What was known as the Foxe Dome of the LIS covered almost the entirety of Baffin Island during the Quaternary glaciations, with the limits of its extent thought to have been either on the islands eastern coast (Miller et al., 2002; Briner et al., 2007) or perhaps even as far as the continental shelf edge (Dyke et al., 2002). The exact location of the LIS margin on Baffin Island therefore remains unclear.

To the north of Baffin Bay several large outlet glaciers occupied the Lancaster and Jones with the largest of these ice streams likely having reached the shelf break (Miller et al., 2005), grounding at 900 m depth during the LGM (Li et al., 2011). However, by around 14 ka BP the coast of Baffin Island was likely ice-free and by just after 11 ka BP outlet glaciers began to retreat at rapid rates up to their respective fjords heads, some retreating from outer fjord to fjord head in less than 1000 years between 10.5 and 9.6 ka BP (Briner et al., 2003). The influence of the Younger Dryas in Baffin Bay has been subject to some debate; however, there is an increasing amount of evidence suggesting that glaciers did readvance on Baffin Island (Falconer et al., 1965; Andrews and Ives, 1978) and also in central west Greenland (O’Cofaigh et al., 2013; Sheldon et al., 2016; Oksman et al., 2017) but perhaps starting as late as 9.9 ka BP on Baffin Island. The readvance does appear to be out of phase with the North Greenland Ice Core Project (NGRIP) and also other sea surface temperature (SST) records from the North Atlantic. This has led to an alternative hypothesis which attributes this early Holocene readvance on Baffin Island to regional climate forcing that was not temperature triggered, but instead was a response to increased precipitation between 11-10 ka BP (Cuffey and Clow, 1997). This factor combined with the presence of what remained of the LIS is suggested to have been sufficient to keep down summer temperatures in areas downwind of the LIS, at least enough to allow for a positive mass balance on Baffin Island, in what was otherwise regarded as the warmest phase of the Holocene.

The GIS is presently the only remaining ice sheet in the Northern Hemisphere, allowing a large amount of data to be collected regarding the chronology of its past maximum ice extent and subsequent deglaciation. Data now suggests that during the LGM and also during previous Pleistocene glaciations large areas of the continental shelf were glaciated (Funder and Hansen, 1996). The Disko Bugt and Uummannaq troughs in central west Greenland are located adjacent to this research projects study site and have been subject to extensive work (Bennike and Bjorck, 2002; Lloyd et al., 2005; Jennings et al., 2014; Sheldon et al., 2016), with suggestions that deglaciation did not occur in the inner part of the bay until 9.6ka.BP. Additionally, despite limited data, it is likely that grounded ice did indeed extend to the shelf edge of central west Greenland during the LGM and before this during previous Quaternary glaciations (Bennike and Bjorck, 2002; O’Cofaigh et al., 2013) with retreat dating from 13.8 ka BP as the relatively warm WGC established just before 14.0 ka BP, possibly enhancing ice retreat in the Disko and Uummannaq troughs (Jennings et al., 2017).

It is likely that retreat occurred first in the Uummannaq trough with ice retreating from the shelf-edge occurring around 17.1 ka BP with retreat in Disko perhaps not occurring till 16.2 ka BP (Jennings et al., 2017). There is now increasing evidence that despite a period of ice retreat from the shelf-edge in Disko trough between approximately 16.2 till 12.2 ka BP, perhaps by as much as 100km (O’Cofaigh et al., 2013), that during the Younger Dryas cold stage a significant readvance occurred over a relatively short period of time (see Figure 2.11) with ice reaching as far as the outer shelf.

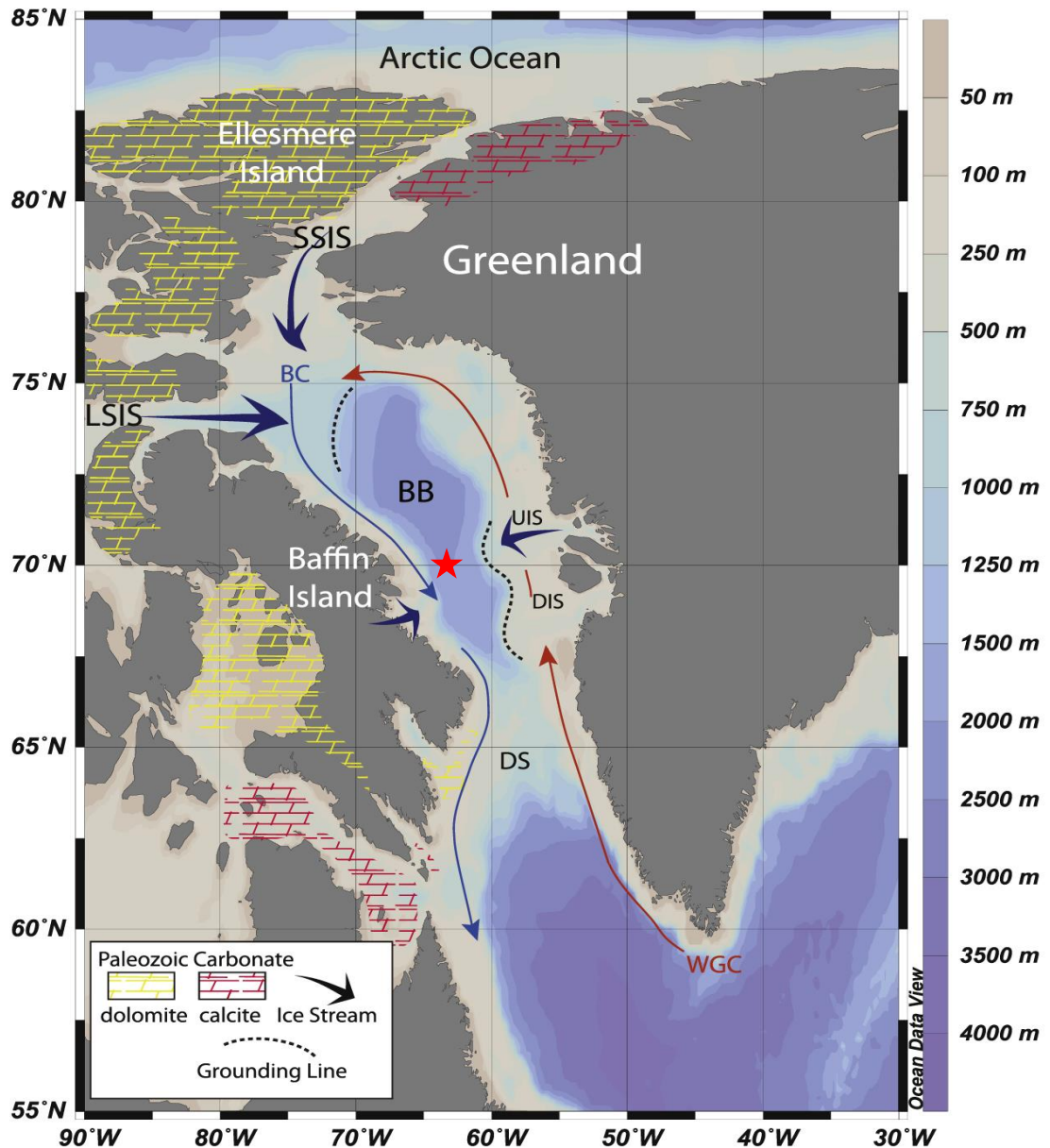


Figure 2.6: Bathymetric map of Baffin Bay showing the locations of core GC01/BC06 in relation to grounding lines of the Uummannaq ice stream (UIS) and the Disko ice stream (DIS), Smith Sound ice stream (SSIS) and the Lancaster Sound ice stream (LISIS). Major ocean currents are also shown; the northward flowing west Greenland current (WGC) is represented by the red line and the Baffin Bay current is represented by the blue line flowing south. Edited from (Jennings et al., 2017).

Evidence from Sheldon et al., (2016) suggest that during the Younger Dryas some ice streams in west Greenland stabilised until the end of the cold stage when fjord glaciers began to retreat rapidly after 9.5 ka BP due to increases in insolation with the present day inland ice margin being reached around 8 ka BP (Funder and Hansen, 1996). The GIS margin then retreated behind the present-day ice margin at around 6.0 ka BP during the Holocene Thermal Maximum (HTM), but then readvanced once more during a period of Neoglaciation (Davis, 1985) with this readvance also occurring both on Baffin Island and in the Canadian Arctic islands in the north of Baffin Bay (Weidick and Bennike, 2007).

The third ice sheet that surrounded Baffin Bay to the north, located across the Queen Elizabeth Islands (QEI) of the Canadian High Arctic, was the Innuitian Ice Sheet (IIS). The IIS most likely coalesced with the LIS to its south and also with the GIS to its east (England et al., 2006), although the prior to MIS 2, there is generally poor constraint regarding the dynamical behaviour of the IIS. It is also possible that the build-up of the IIS

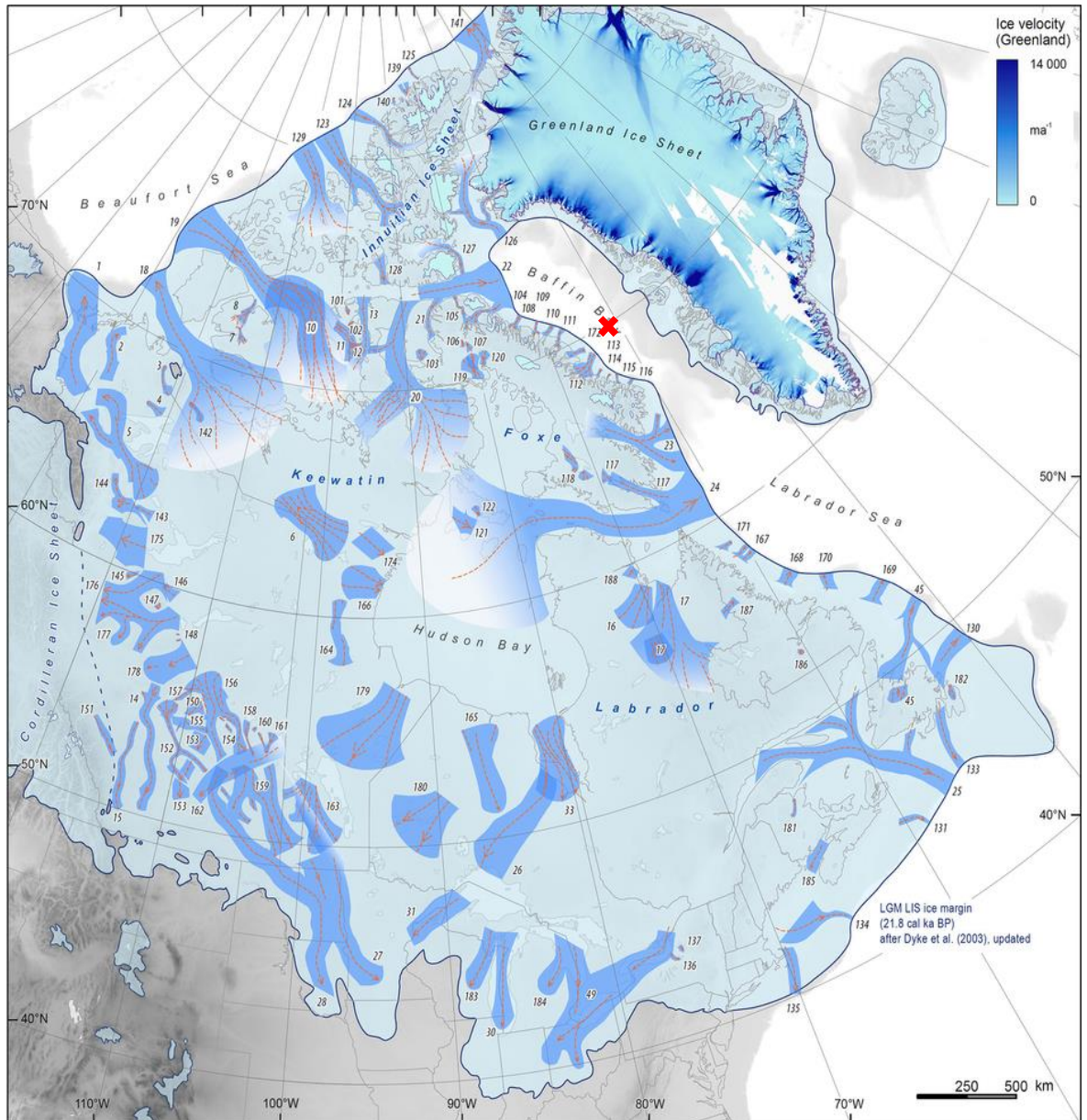


Figure 2.7: LGM ice margins of the LIS, GIS and IIS in relation to the relative positions of cores GC01/BC06 (marked via the red cross) at 21.8ka.BP. Palaeo-ice-streams are shown in dark blue shading. Modern-day ice velocities are shown for Greenland, underlying topography is based on data from model GTOPO30 using digital 506 elevation data. (Modified from Stokes et al., 2016).

occurred as late as 19 ka BP during MIS 2 (Blake, 1992; Dyke et al., 2002; England et al., 2006), meaning that the IIS and LIS maximum extent were not reached at the same time, with the IIS reaching maximum extent after the LGM. The reasons for the out of phase build-up of the IIS have been subject to debate but is likely to be due to a combination of factors, which are explained in detail in (England et al., 2006), but can be spilt into three main sections here. The first being the effect of the GIS buttressing the eastern flank of the IIS providing increased stability via the blocking of trunk glaciers in to the Nares Strait (England et al., 2006), further strengthening ice flow onto the polar shelf, (see Fig.2.12 for maximum ice extent). The LIS appears to

have also played a major role in the IIS late advance as at the LGM when global sea-levels were lowest, and the LIS at its largest, allowed for glaciers from the IIS to expand through inter-island channels and fjord systems on QEI (England et al., 2006). Atmospheric circulation due to the sheer size of the LIS likely split the prevailing mid-latitude jet-stream (Bromwich et al., 2004), deflecting it north and south around the LIS providing a significant increase in precipitation over QEI. Geological evidence suggested that break-up of the IIS was underway by 9.0 ka BP in the Nares Strait and that Baffin Bay and the Arctic Ocean were fully connected again by approximately 7.5 ka BP.

Section 2.4 Oceanographic Changes in Baffin Bay:

2.4.1 Carbonate Dissolution Cycles:

Work by Asku, (1983) went some way to establish a record of foraminiferal change through the Quaternary in Baffin Bay, suggesting a cyclic pattern of high and low biogenic carbonate which when used alongside the

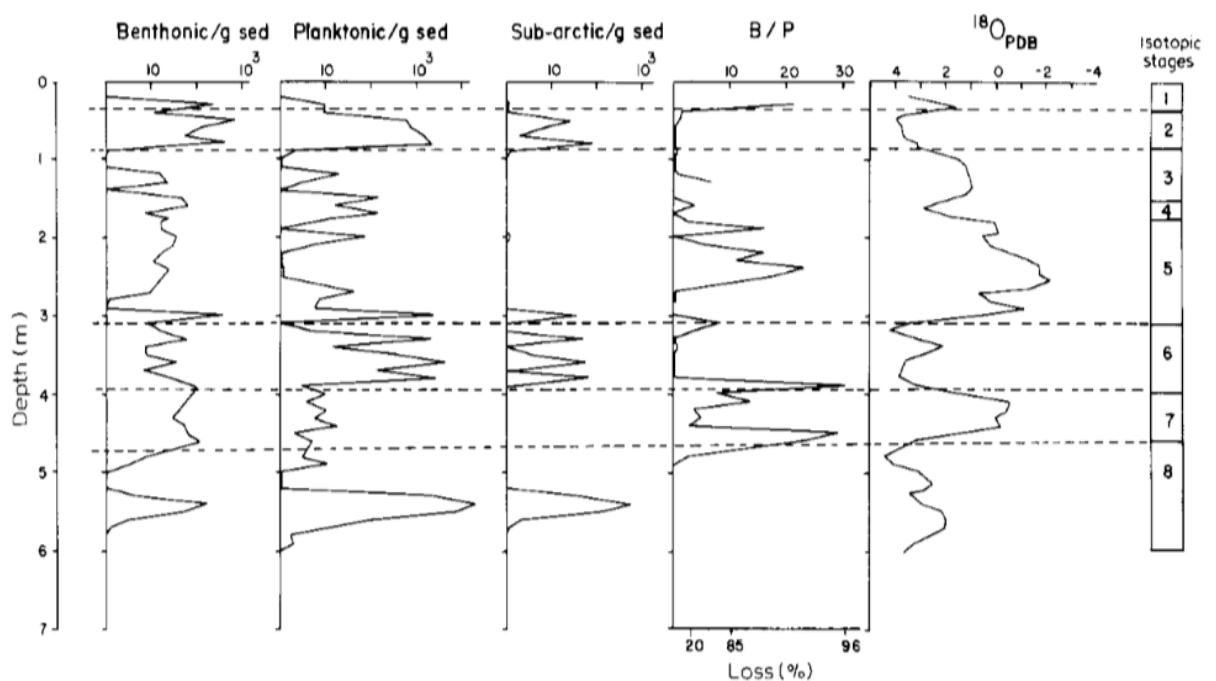


Figure 2.8: Matching of foraminiferal abundances of Benthonic foraminifera per gram sediment (column one); planktonic foraminifera per gram sediment (column two); sub-arctic planktonic foraminifera per gram sediment (column three); ratio of benthonic to planktonic foraminifera (column four) and delta oxygen 18, all plotted against the depth of the core. Showing that low biogenic carbonate stages coincide with high benthonic/planktonic ratios and interglacial isotope stages. (Taken from Asku, 1983).

oxygen isotope record appears to show a clear pattern. Glacial periods record oceanographic conditions which are rich in faunal matter, therefore having high levels of biogenic carbonate, whereas interglacial periods are characterised by low levels of biogenic carbonate; hence during interglacials there is generally a much poorer preservation of biogenic carbonate on the sea floor (Asku, 1983).

It is therefore possible that due to this inverse correlation between the oxygen isotope signature and the concentrations of fauna that dissolution of foraminifera is responsible; based on test size, porosity, microstructure and wall thickness of foraminifera, planktonic species are more susceptible to this process of

dissolution compared with benthic species (Ruddiman and Heezen, 1967). Based on this evidence it has enabled the matching of specific cycles of biogenic carbonate to marine isotopes, i.e. specific glacial and interglacials through the Pleistocene and the Holocene, (see Figure 2.13).

Through matching specific marine isotope stages to biogenic carbonate dissolution cycles and then combining this with what is currently known about the present-day oceanographic conditions in Baffin Bay, it has been possible to reconstruct palaeowater mass changes. It would appear that during the current interglacial Baffin Bay water chemistry characteristics were likely similar to other past interglacials, (see Figure 2.13), with MIS five, seven, and nine all appearing to have been characterised by similar oceanographic conditions to present (Asku, 1983). Since Baffin Bay is a semi-enclosed basin which is connected via several restrictive straits to the Arctic Ocean such as the Smith, Jones and Lancaster Sounds and the Nares Strait, it is therefore inferred that during interglacials water would flow into Baffin Bay via these passages. However, despite increases in flow from the Arctic Ocean the amount of inflow from the Nares Strait is only responsible for a fraction of Baffin Bay Bottom Water formation as the rest is likely to be mixed with Baffin Bay Atlantic and surface water (Jennings et al., 2011). Therefore, during glacials the opposite occurs with a significant reduction in net mass transfer from the Arctic Ocean (Kellogg, 1976), but also because of decreased surface run-off, with the colder conditions combined with evidence for a partial or complete shut-down of the thermohaline circulation (Broecker, 1992). It is therefore likely that sea-ice formation would have been possible down to 45°N (McIntyre et al., 1976), which would reduce significantly both the bottom and surface influx into the Arctic Ocean. This could then lead to very stagnant bottom conditions in Baffin Bay, with Asku (1983) suggesting that this reduction in net mass transfer from the Arctic Ocean resulted in the shutdown of formation of Baffin Bay Bottom Water. During the transition from glacial to interglacial it is expected that a chemical equilibrium would then become established again leading to the dissolution of carbonate to occur and allowing Baffin Bay Bottom Water production to eventually reach a stable phase.

These cycles of dissolution appear not to be limited to the major glacial/interglacial phases but are also evident during shorter stadials and interstadials (e.g. Asku, 1983). During shorter cold stadial periods foraminiferal assemblages are well preserved, whereas during interglacials and interstadials foraminiferal losses are estimated to be up to 90% in Baffin Bay (Asku, 1983). This under saturation of calcium carbonate in Baffin Bay is likely due to a combination of very low water temperatures and higher concentrations of carbon dioxide being present.

2.4.2 Long-term Records of Sea-ice and Productivity Changes:

Long-term sea ice records of sea ice variability are sparse for Baffin Bay with the majority of studies largely focusing on large-scale iceberg rafting events (e.g. BBDC events outline above). However, sea-ice concentrations in Baffin Bay can be determined, at least in part, by the use of foraminifera (Seidenkrantz, 2013); with high benthic/planktonic foraminiferal ratios suggestive of perennial sea-ice cover (Scott et al., 1989). In contrast during ice edge retreat very high productivity levels often allow for phytoplankton blooms (Perrette et al., 2011) with these conditions often shown to simultaneously cause benthic foraminifera to diminish in abundance due to reduced oxygen (Jennings and Helgadottir, 1994). Planktonic foraminifera have also been shown to be only found in very low abundances under permanent sea ice or in some cases not at all (Carstens et al., 1997). However, during periods of near-perennial sea-ice cover in Baffin Bay the influx of terrigenous calcareous materials into the area appears to act to preserve benthic foraminifera (Hald and Steinsund, 1996), but only for a short period of time before productivity lowers and conditions become too harsh to support foraminifera. The dominance of agglutinated foraminifera has been suggested to be not directly related to sea-ice cover but instead likely a reflection of corrosive bottom-water conditions (Seidenkrantz, 2013). Despite this, the use of foraminifera as a sea-ice proxy remains in its early stages with further study into species specific response to changes in sea-ice necessary, alongside the comparison of these changes to already well-established sea-ice proxies such as IP²⁵ which is discussed below.

IP²⁵ is now an established biomarker for the reconstruction of sea-ice in the Northern Hemisphere in which a specific mono-saturated hydrocarbon is produced by diatoms that live within sea-ice (Belt et al., 2006) during periods of perennial sea-ice cover. Using IP²⁵ alone in order to reconstruct sea-ice concentrations can be problematic (Belt et al., 2013), especially in the case of Baffin Bay which is likely to have experienced both permanent ice cover during cold stages and also perhaps near no sea-ice during warm stages, which are both represented by a complete absence of IP²⁵ (Belt et al., 2013). The use of brassicasterol which is a phytoplankton-derived biomarker (Volkman, 1986) has recently been combined with IP²⁵ to create the PIP²⁵ index (Muller et al., 2011) which aims to provide a more quantitative reconstruction of sea-ice, (see Figure 2.14).

In regard to the application of IP²⁵ to sediments from Baffin Bay studies have tended to focus on Northernmost Baffin Bay and the Canadian Archipelago (Vare et al., 2009; Brown et al., 2011) and also off the coast of Labrador (Pearce et al., 2012; Weckström et al., 2013) with few if any studies applying IP²⁵ to deep central Baffin Bay, particularly so prior to the Holocene. Results from northern Baffin Bay (e.g. Vare et al., 2009) show that during the Holocene, spring sea-ice concentrations were at their lowest after 10 ka BP till 6.0 ka BP with a slight rise occurring after this until approximately 4.0 ka BP when spring sea-ice significantly increased at the end of the Holocene thermal maximum. Thereafter higher resolution data shows that changes in sea-ice concentrations during the late Holocene showed two distinct periods of low spring sea-ice between 1.2 ka – 0.8 ka BP and then high 0.8-0.4 ka BP coeval with the Medieval Warm Period (MWP) and the following Little Ice Age (LIA), (Kinnard et al., 2011). Although the occurrence of IP²⁵ in one particular

location could simply be a representation of localised sea-ice conditions rather than across Baffin Bay, so further study from a variety of locations is needed.

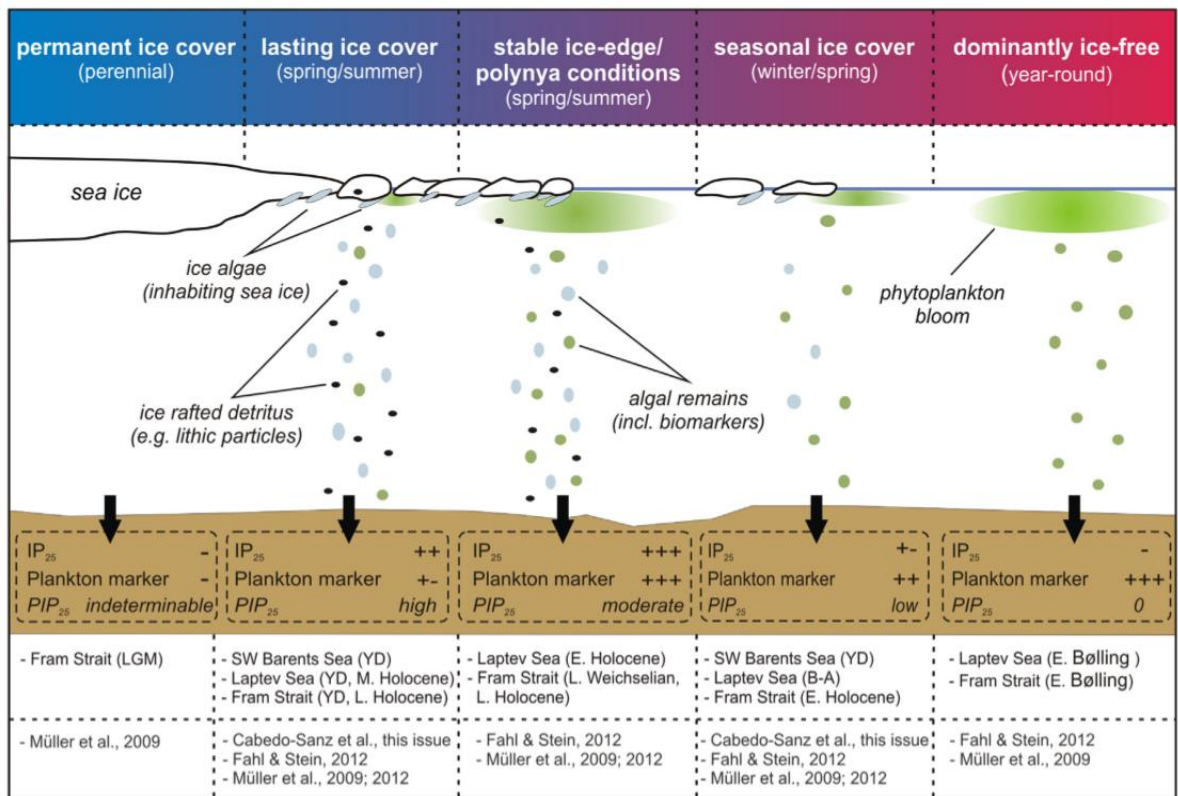


Figure 2.9: Representation of different sea-ice conditions and the respective IP²⁵ and phytoplankton biomarker responses with the PIP²⁵ index shown below each of the five environmental conditions with examples of studies with each respective PIP²⁵ index also listed. (Modified from Belt et al., 2013).

2.4.3 Sediment Delivery in central Baffin Bay:

Baffin Bay is flanked to the west by Baffin Island, to the east by Greenland, and is connected to the Arctic and Atlantic Oceans both to its north and south respectively. However, the continental shelves of Baffin Island and west Greenland are quite different, with the shelf of west Greenland being some 200 km wider and 100 m deeper than on Baffin Island, (see Figure 1.1).

Although both shelves exhibit large transverse troughs which run from the mouth of large fjords all the way into deep central Baffin Bay, data collected by (Askv and Piper, 1987) shows that the shelf break occurs at approximately 250 m along Baffin Island whereas the along west Greenland this does not occur until around 400-500 m depth. Large cross-shelf troughs which were formed by fast flowing ice streams associated with the GIS terminate on the continental slope as major trough-mouth fans (O’Cofaigh et al., 2013; Jennings et al., 2017) with the two largest systems in central west Greenland associated with the Uummannaq and Disko ice streams. Estimates of sediment accumulation rates (SARs) in Baffin Bay are difficult to gauge with any accuracy from site to site due the severity of dissolution of foraminifera preventing radiocarbon dating of all but glacial-deglacial transitions (e.g. Jennings, 1996). Although it is accepted that generally SAR are low throughout Baffin Bay (Andrews, 1990; Gilbert et al., 1998; Praeg et al., 2006), especially so on the abyssal

plain (estimated at 2-5 cm/ka)- (Asku and Piper, 1987). Sediment supply is likely primarily from break-up of ice shelves, very much in contrast to sedimentation patterns further south in Labrador (e.g. Hillaire-Marcel et al., 1994).

Especially relevant for this study is the work by Andrews and Eberl, (2011) who attempted to pinpoint sources of sediments that flowed into central Baffin Bay during the last 12.1 yrs (no direct ages were achieved) using core BC06 (box core used in this study). Interestingly, results appear to show significant changes in sediment sources during the Holocene transition. During peaks in detrital carbonate it would seem that the main source is from northern Baffin Bay, although other research also points towards the possibility of a large contribution from multiple ice streams from Baffin Island to Homes Bay (Azetsu-Scott et al., 2010). Despite this, initial evidence presented by (Andrews and Eberl, 2011) does give a rough idea

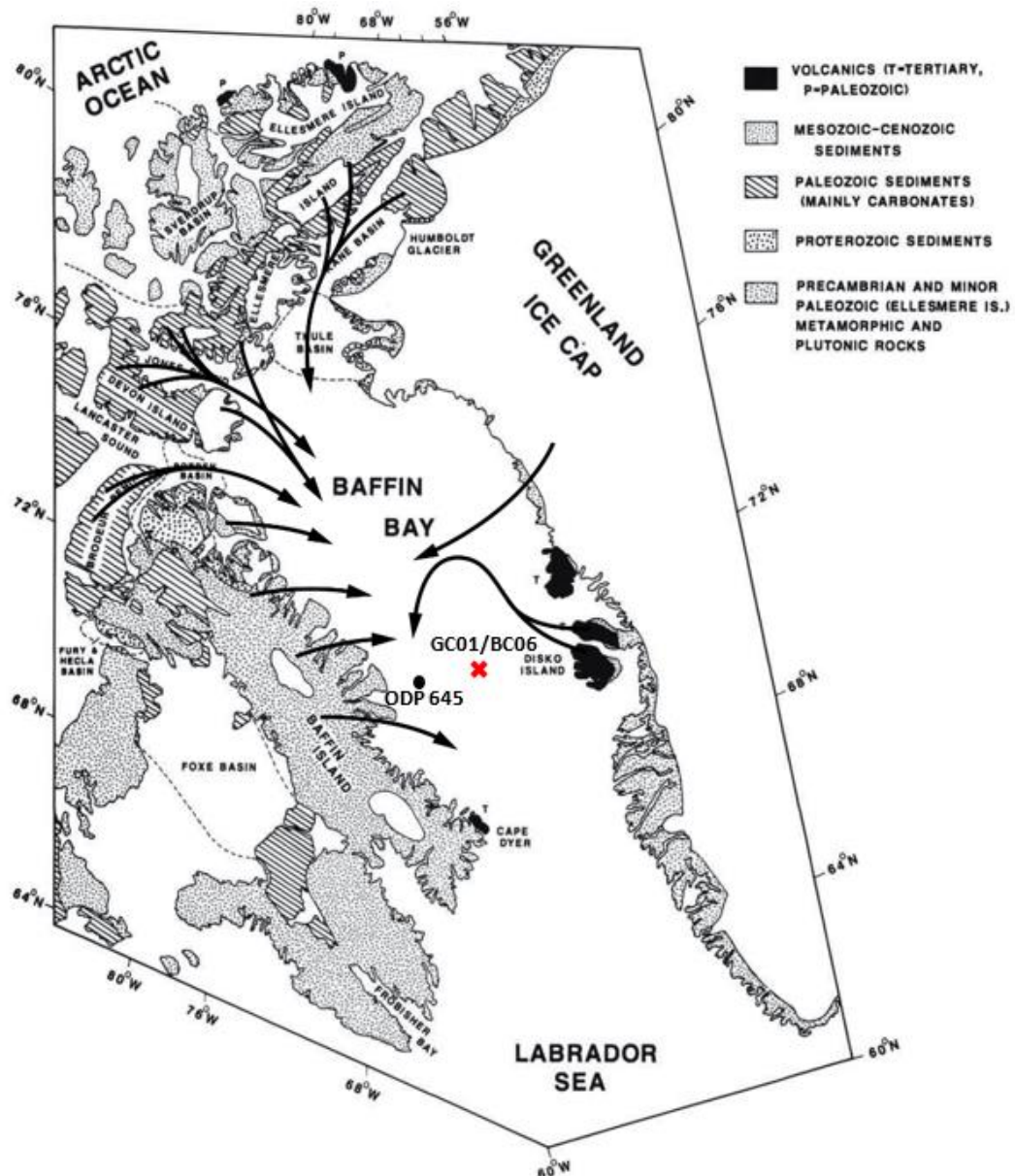


Figure 2.10: Geological map of the major landmasses that surround Baffin Bay with important sedimentary basins outlined by dashed lines and named. Overlain is a schematic representation of the transport paths of detritus with the exact paths to central Baffin Bay scaled using the known drift patterns of modern-day icebergs, exact paths are still uncertain. Original paths were plotted in respect to ODP site 645 (shown by black dot) in relation to this study (shown by red cross). (Modified from Hiscott, Asku and Nielsen, 1989).

of sediment source, with the Jakobshavn trough notably contributing very little due to its geographic location being well to the south, whereas the Umanak Trough and sediments derived from Baffin Island appear to be largest non-carbonate sources. The Umanak Trough looks to be of key importance due to both its near adjacent geographical location and its sensitivity to climatic changes in relation to this projects study site with significant influxes of material shown to have occurred prior to peaks in carbonate, (see Figure 2.16).

There is considerable evidence for debris flows occurring many times during Quaternary glaciations on both Baffin Island and west Greenland continental slopes (Hiscott, Asku and Nielsen, 1989; Li, Piper and Campbell, 2011) with this causing transport via mass-flows towards central Baffin Bay. The lithology of sediment deposited in central Baffin Bay during glacial periods, is characterised by turbidites which interbed with hemipelagic muds from both Baffin Bay and west Greenland (Asku and Piper, 1987), with ice rafted debris (IRD) only usually reaching the abyssal plain during large-scale glacial retreat. The most likely source being the ice-shelves on Ellesmere Island and also from ice-choked channels in the Lancaster Sound area, (see

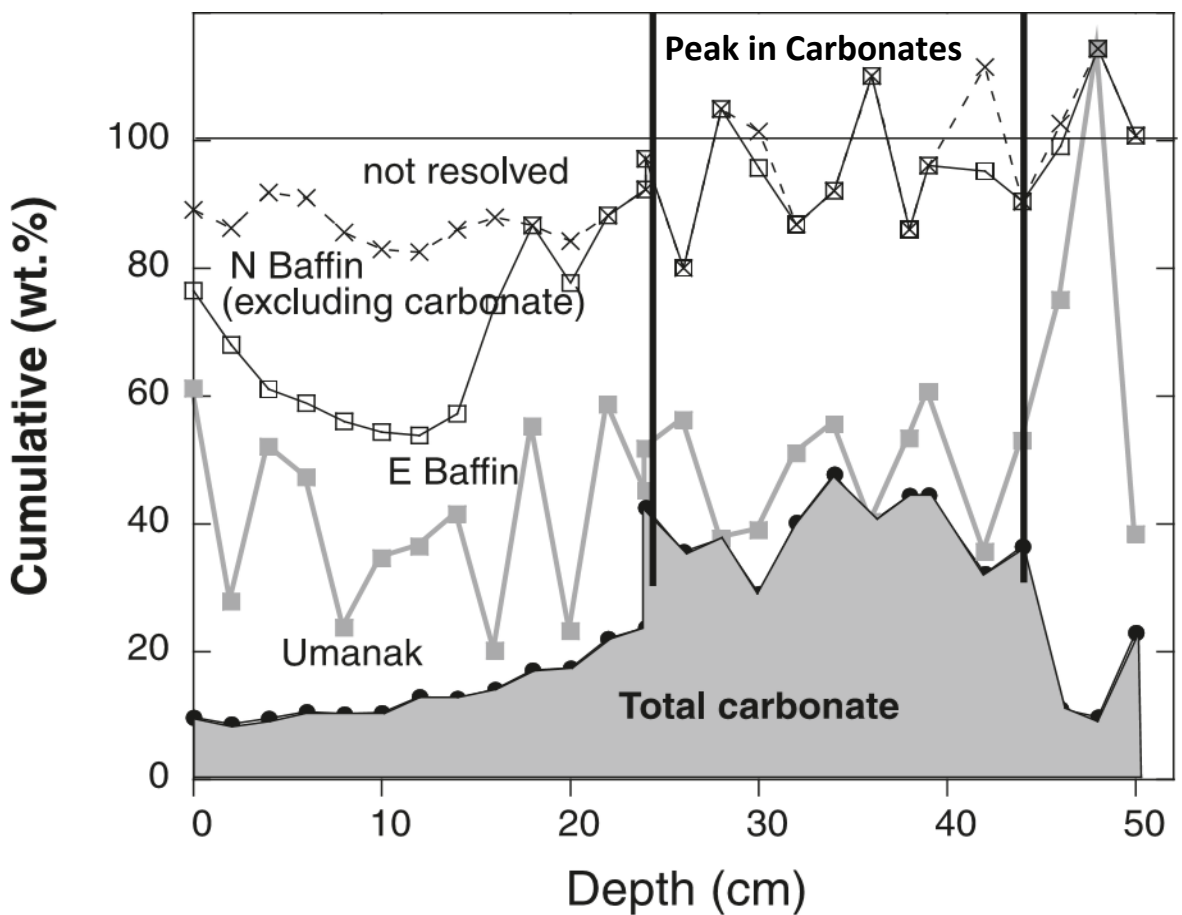


Figure 2.11: Possible four major sediment sources for core JR175 BC06 in central Baffin Bay are displayed for the first 50cm of the core against total levels of carbonate; North Baffin Bay (excluding and including carbonates), East Baffin Bay, Umanak. These are expressed as cumulative weight wt.% and total wt.% of carbonate respectively. Wt.% of sediment from N Baffin remains unresolved as wt.% was less than 100% when calculated. Bold vertical black lines delimit maximum peaks in carbonate. (Modified from Andrews and Eberl, 2011).

Figure 2.15). Conversely interglacial periods have been shown to be dominated by Hemipelagic sediments in several cores extracted from central Baffin Bay (Hiscott, Asku and Nielsen, 1989; Andrews and Eberl, 2011).

2.4.3 Late Pleistocene and Holocene Productivity:

There has been limited research focussing on longer-term oceanographic change in Baffin Bay prior to MIS2. This is likely due to the fact that there remain issues regarding the accurate dating of materials past 40 ka BP.

However, it appears that it is possible to at least reconstruct ocean productivity back to MIS 7, with evidence from Baffin Bay suggesting dissolution of biogenic carbonate, which occurs cyclically on interglacial/glacial timescales (Asku, 1987), productivity of surface waters was therefore likely significantly higher during interglacials than during glacial periods. Hence, during glacial times sea ice in Baffin Bay was extensive which likely resulted in closed sea-ice cover (Stein and Stax, 1990); as during these times it is possible that the weakening or perhaps complete absence of the relatively warm WGC resulted in decreased productivity in the surface waters within Baffin Bay (Hamel et al., 2002).

Therefore, during interglacials it is expected that the productivity increased due to an enhancement in the strength of the WGC; however maximum tends to occur at the sea-ice margin (Sakshaug and Holm-Hansen, 1984); illustrated by planktonic foraminiferal blooms occurring directly in front of the sea-ice edge during MIS 1, 5 and 7. These findings suggest that although the location of the sea-ice edge plays an important role in determining the amount of productivity in the surface waters of Baffin Bay, the relationship is likely to be more complex than this. Hence it more probable that multiple variables are responsible for high cyclic productivity responses in Baffin Bay. Variability in the relatively warm WGC alongside variations in the strength of other ocean currents operating outside of Baffin Bay; with the Labrador, current and also the larger North Atlantic Drift are likely also playing major roles in determining productivity through time (Asku, 1989).

2.4.4 The Younger Dryas and the Holocene Transition:

The transition from the last cold stage (MIS2) into the current interglacial (MIS1) has been heavily studied in recent decades across the North Atlantic region (e.g. Dowdeswell et al., 1995; Coope et al., 1998). Partly due to the fact that proxy records from this time are available in much higher temporal resolution; allowing more opportunities to link different proxy records together and also for a more accurate chronology of events to be established.

Studies of oceanography from Baffin Bay have focused heavily on the northernmost part of the bay, due to this being the location where there is a significant water exchange from the Arctic Ocean (Jones et al., 2003). This is also the region where the relatively warm high salinity WGC meets the cold polar waters, which are transported out of the Arctic Ocean through the Nares Strait, (see Figure 1.1). The area is characterised by high levels of productivity (Dunbar and Dunbar, 1972) especially so within the Polynya in northernmost Baffin Bay. Foraminiferal abundances indicate that deglaciation of the area occurred at approximately 12.5 ka BP with stratigraphical evidence of a basal diamicton overlain by sediments rich in calcareous benthic foraminifera after approximately 12.3 ka BP (Knudsen et al., 2008). It is during this period (12.3 – 10.9 ka BP) that it is likely that there was seasonal if not occasional perennial sea ice cover in the region (Levac et al., 2001); with no open connection to the Arctic Ocean. There is mounting evidence (Asku and Piper, 1979; Asku,

1983; Knudsen et al., 2008) that the lack of inflow from the Arctic Ocean during this period would have allowed the WGC to penetrate perhaps further than 72 N into Northernmost Baffin Bay shortly after deglaciation. This is supported by the foraminiferal record; as up until 11.2 ka BP planktonic foraminifera are continuously at low abundances, whilst benthic foraminifera show a sudden increase, which as Knudsen et al., (2008) suggests would indicate nutrient-rich subsurface waters. Interestingly, biogenic carbonate appears to show less dissolution during this cooler period. However, it was not until after 10.9 ka BP that there was a significant change in subsurface waters (Knudsen et al., 2008); with more open water conditions in Baffin Bay indicated by rises in the abundances of planktonic foraminifera as the strength of the WGC increased and became more influential in the bay, which also supports previous studies (e.g. Bennike, 2004).

2.4.5 The Early-Mid Holocene:

Despite the period from 10.9-9 ka BP being shown to have been dominated by the relatively warm WGC there is evidence that the strength of the current varied, especially so in the early part of the Holocene. Due to these increasingly warmer conditions continuing over a prolonged period it is likely that sometime between 8.2-7.3 ka BP Baffin Bay underwent a period of rapid environmental change (Levac et al., 2001; England et al., 2006; Knudsen et al., 2008) as the Nares Strait opened to flow from the Arctic Ocean. However, there is evidence that suggests that the HTM perhaps occurred during this period in Baffin Bay (Levac et al., 2001), with sea-surface temperatures likely to have reached maximum values around 7.8 ka BP but definitely by 6.4 ka BP. Interestingly, during this period opening connections to the Arctic Ocean via the Nares Strait occurred creating very different oceanographic conditions across Baffin Bay (Knudsen et al., 2008). Near-coastal areas on the eastern side of the bay were likely influenced more by the WGC and for longer than areas in central Baffin Bay where much more variable, and at times severe, surface water conditions prevailed, shown by low abundances of planktonic foraminifera. Therefore, suggesting that coastal areas, even in northern Baffin Bay, received less sea-ice than more central locations off the continental slope of west Greenland (Knudsen et al., 2008), most likely due to the WGC's influence.

The mid-Holocene appears to be dominated by agglutinated foraminifera at several different core sites located across Baffin Bay; including the more coastal waters of Disko Bugt (Lloyd, 2006) but also in central Baffin Bay (Asku, 1983) where agglutinated foraminifera dominated by 6.0 ka BP, much earlier than in the shallower waters. Due to Arctic Water being of low-salinity and rich in carbon dioxide (Osterman and Nelson, 1989), this would have caused the dissolution of calcareous foraminifera in central Baffin Bay earlier than in more coastal locations (between approximately 6.0- 2.5 ka BP). However, there remains significant uncertainty regarding how exactly Baffin Bay Bottom Water is formed.

2.4.6 The Late Holocene - Recent Oceanographic Change in Baffin Bay:

Foraminiferal records extracted from the central west Greenland coast (Seidenkrantz et al., 2008) indicate that between approximately 2.9-2.0 ka BP there is evidence for a period of much more stable, stratified water mass due to a reduction in the strength of the WGC. A surface cooling event, dated between 3.6-3.0 ka BP, is picked up in cores extracted from deeper marine sites in the Labrador Sea (Lassen et al., 2004; Seidenkrantz et al., 2007) and in northern most Baffin Bay (Levac et al., 2001). Although, due to the latitudinal differences between the sites temporal variations exist. As might be expected this cooling event occurs earliest in the deep ocean record extracted from the Nares Strait (Levac et al., 2001), with increased sea-ice formation by approximately 3.6 ka BP with evidence for a second wave of cooling occurring at 3.0 ka BP (Knudsen et al., 2008). This wave of 'neoglaciation cooling' extended south with the polar front over the course of the next 700 years culminating in a strong IRD event around 2.8 ka BP in the North Atlantic (Bond et al., 1997).

From the more recent period (2.0 ka BP – present) it becomes possible to pick out smaller climatic events such as the Roman Warm Period (RWP) 2.0-1.3 ka. BP, the Medieval Warm Period (MWP) 1.5-1.1 ka BP, and the Little Ice Age (LIA) 0.3 ka BP, due to greater temporal resolution within paleoclimatic records. However, it should be noted that the climatic periods mentioned above were originally recorded in European climate records and there is evidence (e.g. Seidenkrantz et al., 2008) that records are not synchronous across the North Atlantic sector during these shorter events. The RWP signal in central west Greenland exemplifies this non-synchronous behaviour; with vegetation studies (Fredskild, 1983) and also oceanographic evidence (Lassen et al., 2004; Roncaglia and Kuijpers, 2004) suggesting that climatic conditions in the Greenland were much colder than those recorded in Europe (e.g. Lamb, 1995). Atmospheric temperatures have been shown to have been cold enough to support glacial advances along the North Icelandic Shelf (Strotter et al., 1999; Jiang et al., 2002). Despite this, benthic foraminifera collected from the coast of central west Greenland (Lloyd, 2006) do suggest that there was a response during the MWP and the LIA. There is evidence of a retreat of the Jacobshavn Isbrae glacier during the MWP and then a subsequent advance during the LIA as colder conditions developed; interestingly a similar pattern of glacial retreat can also be found in northern Baffin Bay (Knudsen et al., 2008) during the MWP.

However, it should be noted that although the RWP and the MWP were relatively warm in Baffin Bay, surface water temperatures were shown to be quite low during the MWP despite warmer atmospheric temperatures (Seidenkrantz et al., 2008). Additionally, it is also likely that surface temperatures were only a little warmer during the RWP than during another well-known modern cold period during the 'Dark ages' (Seidenkrantz et al., 2008), whereas it would appear that during the LIA there is a clearer signal for colder conditions. This appears to create a complex oceanographic set-up within Baffin Bay; as it would appear despite there being some synchronicity between conditions in Baffin Bay and terrestrial North-western Europe. It is therefore likely that during these two warm and cold periods different atmospheric and oceanographic set-ups must have been in operation to create such different bottom and subsurface water conditions. Sutton and Hodson (2005) suggest that subsurface water conditions are controlled mostly by large-scale ocean circulation such as Atlantic Multidecadal Oscillation (AMO); whereas surface-water conditions are perhaps controlled by

changes in atmospheric circulation and freshwater discharge from melt plumes. Another important atmospheric variable which must also be considered is the relationship between the North Atlantic Oscillation (NAO) and how this may influence the oceanography of Baffin Bay. Buch, (2002) suggests that a positive NAO has the power to raise subsurface temperatures within Baffin Bay although this has only been tested on relatively short-term timescales.

Chapter 3: Methods:

3.1 Introduction:

This chapter will give a detailed description of the methods used to address the research questions outlined in chapter 1. The nature of this project required the use of multiple proxies ranging from biological analysis to geochemical and isotopic analysis. Radiocarbon dating was also performed.

3.2 Core Sedimentology:

Core logging was undertaken for both GC01 and BC06 after x-rays had been taken to detect changes in stratigraphy and establish major lithofacies within each core. As it was clear that in certain areas large amounts of clastic material was present intra-core and not clearly visible from the surface. In order to log lithofacies the method outlined in (Ben and Evans, 1998) was modified using the coding displayed in Table 1.

Further information was noted during core logging regarding each cores lithology, grain size, changes in sediment colour were recorded using a Munsell Soil Colour chart and a description noted of each separate layer downcore. Sediment that was over 2 mm in size was interpreted as ice rafted debris (IRD), this was counted primarily using x-ray images of both cores which were divided up into 1 cm segments using the

Lithofacies:	Description:
Fl	Clay, fine lamination often with minor fine sand and very small ripples.
Fp	Intraclast/outsize clast.
Fs	Silt, massive, very fine to very coarse.
Sf	Sand, massive, very fine to medium grain size.
Sl	Sand, Horizontal and draped lamination.
Dcm	Diamict, clast-supported and massive.

Table 1: Code and description of lithofacies found in cores GC01 and BC06 extracted from the abyssal plain of Baffin Bay.

'ImageJ' software package. This allowed for contrasts to be adjusted accordingly for the clear identification of intra-clasts and IRD deposits. All IRD data was then plotted against depth downcore.

3.3 Multi-core Scanner XRF, MSCL and core X-Rays:

Both GC01 and BC06 were ran through Geotek multi-core scanner prior to sediment extractions in order to provide x-ray fluorescence (XRF) and also magnetic susceptibility (MSCL) XYZ data on each core. The use of the MSCL-XYZ provides high resolution XRF data which is very repeatable. X-rays of both cores were also taken using 'Geotek: Vertical X-Ray CT System' which produces a detailed 2D X-ray image which was very useful for the identification of clasts and sedimentary structures. Once taken each core was analysed using the ImageJ software package.

3.4 Particle Size Analysis:

Particle Size Analysis (PSA) was undertaken at 4cm intervals downcore with approximately 0.5 g of material extracted from the core for each sample before being weighted and placed into a 50 ml centrifuge vial. 20 ml of (6% conc) hydrogen peroxide (H₂O₂) was then added to each sample in order to allow for the break-down of organic matter and then left in a boiling water bath for 24 hours to aid oxidation. Due to some samples having very high amounts of calcareous foraminifera, the decision was made to then add hydrochloric acid (10% conc) and then place in a boiling water bath for 5 minutes in order to dissolve the foraminifera and give a better representation of particle size. However due to the differing concentrations of foraminifera between samples some samples took significantly longer than others for reactions to stabilise, with some taking days rather than hours. Once digestion of all organic matter (including foraminifera) had taken place, and the remaining supernatant liquid was transparent (slight yellow colour tinge) and all gas ceased to be emitted, samples were then centrifuged at 4000 rpm for 4 minutes. The supernatant liquid was decanted and the samples were topped up with distilled water. This process was repeated twice to ensure all hydrogen peroxide was removed, thereafter 20ml of Sodium Hexametaphosphate solution was added to each sample. Once added samples were individually stirred to aid deflocculation they were analysed separately in the 'Coulter LS 13 320' laser diffraction particle size analyser equipped with laser granulometer and Polarisation Intensity Differential Scattering (PIDS). The measurement range of the particle size machine is between 0/04-2000 µm and produces is very reproducible data. Data was then analysed using GRADISTAT (Blott and Pye, 2001).

3.5 Biological Analysis: Foraminifera

The use of foraminifera as proxies for palaeoceanographic reconstructions in northern Baffin Bay and west central Greenland has been documented extensively in the literature (Levac et al., 2001; Lloyd, 2006; Seidenkrantz, 2013). This study has chosen to use a range of different foraminifera to aid in the reconstruction of oceanographic conditions in central Baffin Bay through the Quaternary.

Planktic foraminifera due to their upper water column habitat are useful organisms for assessing sea ice concentrations (Vilks, 1975) and also as a measure of productivity, both of which are reviewed in detailed in (section 2.4.2). Benthic foraminifera were also chosen in order to investigate palaeoceanographic change in Baffin Bay due to their well-documented sensitivity to changes in a range of ecological parameters including ocean temperature, salinity and food supply (Murray, 1991). This study also uses agglutinated foraminifera which have been shown to be sensitive to bottom water dissolved oxygen concentrations (Kaminski et al., 1995; Bernhard and Gupta, 1999).

The decision was made to use a range of different foraminifera to give this study the best chance at reconstructing not only palaeoceanographic conditions but also to support identification of facies layers and whether they are ice distal or ice proximal. Hence providing evidence for ice sheet advance, retreat and extent during the Quaternary in central Baffin Bay.

3.4.1 Sample Preparation:

A record of foraminifera (benthic, planktonic and agglutinated) has been developed for both GC01 and BC06. Samples were extracted from GC01 initially at 4 cm intervals however this was then increased to 2 cm throughout and every 1cm for the first 62cm to give the highest temporal resolution possible. Foraminifera was extracted from BC06 at 1 cm intervals throughout the entire core. Much attention was paid when preparing samples for analysis with a standard volume of sediment (1 cm³) extracted from each core by measuring displacement of water in a measuring cylinder. Samples were then placed in a plastic vial and soaked overnight in distilled water to allow for the sediment to disaggregate. Thereafter each sample was then wet sieved at 500 µm and then 63 µm as most foraminifera are present within this fraction (Scott et al., 2001). Reasons for not sieving at a finer level are due foraminifera below 63 µm being very difficult to identify due to the majority likely to have been juvenile specimens.

3.5.2 Sample Analysis:

After being left to soak overnight samples were taken to be analysed under a Leica microscope. 300 benthic, planktic and agglutinated specimens from each sample were picked whilst suspended in distilled water, and then placed on microscope slides for identification. The initial aim was to count at least 300 benthic species, however due to severe amounts of dissolution of foraminifera (see section 2.4.1 for more information) it was not always possible to pick 300 or even 100 benthic, planktic or agglutinated specimens as in some instances there was zero identifiable foraminifera present. However, the agglutinated species *Rhizammina algaeformis* was likely overcounted due to tubular fragmentation of each individual species into multiple pieces. Despite benthic foraminifera being initially selected as the main proxy for this investigation during analysis it became clear that benthic species diversity was very low as were absolute abundances in both cores. In total 19 benthic species were identified, which in itself is very low, with three species dominating as the other 16 are only present in low abundances (1-5 foraminifera per sample). Agglutinated foraminifera species were also identified in the same manner, but for the purposes of this study planktics were all grouped as *Neogloboquadrina pachyderma* (Darling et al., 2000). All species identification follows the work of (Feyling-Hanssen, 1964; Qvale and Nigram, 1985). As well as identification from specimen counts total abundances of all foraminifera per sample were also counted and divided into benthic, planktonic and agglutinated assemblages. The abundances were then converted to percentages and plotted against depth.

3.6 Geochemical Analysis:

Geochemical analysis was used in this study to support both biological and sedimentological analysis. This study uses a variety of analyses including Osmium isotopes (¹⁸⁷Os/¹⁸⁸Os), and also a series of biomarkers (IP²⁵, Sterols, Alkenones).

3.6.1 Biomarker Extractions:

In order to assess long-term sea-ice concentrations specific biomarkers were extracted from GC01. Extraction intervals were selected from throughout the core based on XRF data. Eleven samples weighing approximately 3 g were then freeze-fried overnight and ball-milled to produce homogenised sediment. These samples were then carefully decanted into 7ml neutral glass vials and capped with aluminium lined polypropylene screw caps to prevent any contamination, with a twelfth vial added to serve as a blank which contained no sediment. An internal standard (Jule's standard, see table 3.2) was added to each of the 12 samples (blank included) in order to allow for quantification of biomarkers. DCM/MeOH (ratio of 2:1) was then added to each sample before ultrasonication (ca.15 minutes) to allow for sediments to disaggregate fully and the solvent to penetrate through all of the sediment. Samples were then centrifuged for ca. 30 seconds each at 2500 rpm and the supernatant decanted by pipette into new 7ml vials. This step was then repeated two more times until the supernatant was transparent. After which the total organic extracts (TOE) were evaporated under a slow stream of nitrogen (25 °C) and then weighed. It was then necessary to partially purify the TOE's before analysis via Gas Chromatography Mass Spectrometer (GC-MS). Once the TOE's had dried out hexane was then added to enable re-suspension of sediments (1ml) before ultrasonication for ca. 5 minutes. TOE's were then transferred into the chromatography column as illustrated in (Figure.3.2), all columns were rinsed first with 3ml of hexane. This allowed for the elution of non-polar hydrocarbons which was named fraction one and was collected in clean 7ml vials and placed under nitrogen steam at 25 °C, TOE-2 (see Figure.3.2). Once dried TOE-2 was then stored in the fridge until fractionation began. Filtered extracts were dissolved in hexane and drawn into a syringe and placed into new columns to achieve fractionation as illustrated in (Figure.3.2). Columns were rinsed with hexane between each sample. Each fraction was collected in clean 7 ml vials and clearly labelled. For the purposes of this study; fraction one: IP²⁵, fraction two: Alkenones, fraction three: Sterols. An archive of the original TOE's was also kept. The internal standard used in each sample was Jule's Mix Standard, (see Table 3.2 for more information). Once fully evaporated, each fraction was transferred from the 7 ml vials into gas chromatography 2ml vials and topped up using dichloromethane (DCM), the decision was made to run the samples concentrated so only 1 ml of DCM was used per sample.

Gas Chromatographic Instrumental Conditions:

Fraction one (IP²⁵) was ran through the GC-MS in SIM only mode using a 60 m column. Following injection,

<u>Jule's Mix Standard</u>	<u>Mass (micro grams)</u>	<u>Solution Concentration (micro grams)</u>	<u>Volume Added (micro Litres)</u>	<u>Mass Standard per Sample (micro grams)</u>
F1, 5-alfa-cholestane	4568	0.18272	20	3.6544
F1, heptatriacontane	2835	0.1134	20	2.268
F2, 2-nonadecanone	6168	0.24672	20	4.9344
F3, 5- alfa- androstan-3beta-ol	2527	0.10108	20	2.0216
Hexane (Solvent)	25000	-	-	-

Table 2: Specific information regarding the amounts of Jule's Standard used for biomarker extractions from GC01.

the column was held at 60 °C for 2 minutes, then increased at 12 °C per minute to 150 °C. The temperature then rose at a rate of 6 °C per minute till reaching 310 °C where it was held for 25 minutes before cooling back down to 60 °C. Quantification of IP²⁵ was achieved by integrating peak areas of IP²⁵ and the internal standard used, which is then multiplied by the response factor to account for differences in mass spectral responses of IP²⁵ and internal standards.

Flame Ionisation Detector Instrumental (FID) Conditions:

Fraction 3 (Sterols) and fraction 2 (Alkenones) were initially run through the FID before being run through the GC-MS using the same instrumental conditions outlined above. However, the conditions used for the FID were a little different. Again, a 60 m column was used, following injection column was held at 70 °C for 2 minutes, then increased at a rate of 12 °C per minute until a temperature of 170 °C was achieved. Temperature then increased at 6°C per minute until a temperature of was achieved 310 °C this was sustained for 35 minutes before cool down to 70 °C. Samples were then topped up with DCM and the vials lids changed and replaced with new ones before being ran in the GC-MS to allow for quantification, fraction 2 was ran using the CIMS method for quantification purposes.

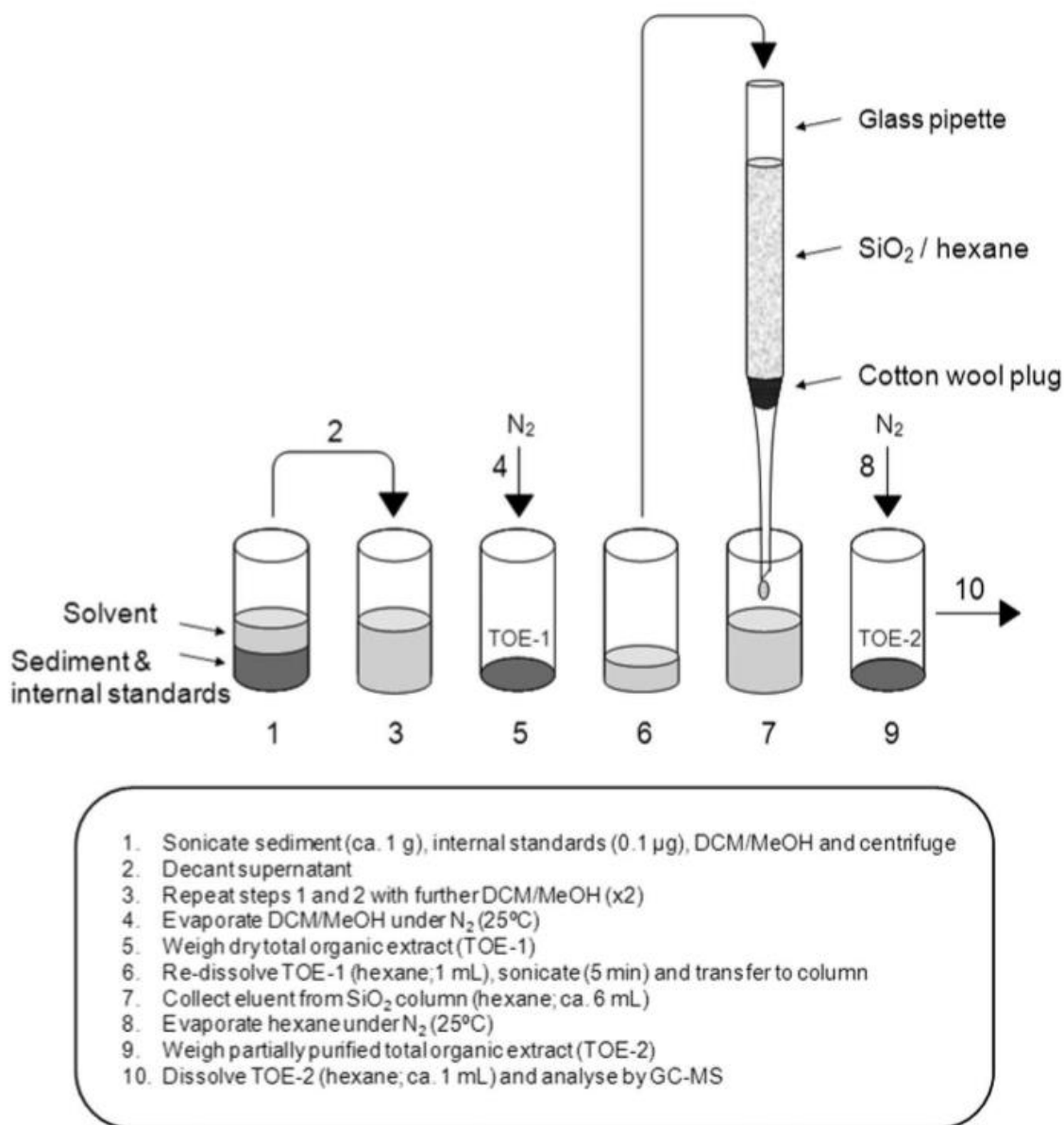


Figure 3.1: Diagram showing the process of extraction and partial purification of IP²⁵ from sediment extracted from GC01. (Taken from Belt, 2012).

3.6.2 Osmium Isotope Analysis:

Isotopic analysis was undertaken on GC01 from six separate sediment samples which were carefully selected based on sedimentology and XRF data analyses prior to extraction. Sediments were taken directly from the core and then freeze-dried overnight ready for ball-milling the next day. Rhenium and Osmium abundances and isotopic compositions were then determined using isotope dilution negative thermal ionization mass spectrometry. Samples were then digested in a carius-tube with an already known amount of osmium tracer solution along with an acid medium (8 ml of 0.25g/g Cr^{VI}O₃-4 N H₂SO₄) at 220 °C for 48 hours (Rooney et al., 2016). Afterwards Osmium was isolated using and purified from the acid medium using CHCl₃ solvent which was then extracted into HBr and micro-distilled. Rhenium was then isolated and purified using NaOH- C₃H₆O solvent and anion chromatography. Once isolated the Rhenium and Osmium fractions were loaded onto Ni and Pt filaments, in order to gauge their respective isotopic composition respectfully a ThermoElectron TRITON mass spectrometer was used along with Faraday collectors and a secondary electron multiplier. In order to calculate uncertainties for each individual sample procedural blank samples were used during analysis.

3.7 Radiocarbon Dating:

Due to the severe dissolution of foraminifera previously mentioned establishing a chronology has been difficult. However, it has been possible to extract two radiocarbon dates from GC01. The first date uses benthic foraminifera only, although with the large amounts of foraminifera needed it was deemed necessary to not use just a single species but instead use *casidulina neoteritis* and *triloculina* which were the most dominant species. The second radiocarbon date used planktonic foraminifera, which although is not ideal for comparison purposes due to its upper water column habitat, it remained the only viable option as benthic foraminifera were only present in very low abundances further downcore. A Delta R value of 140 +/- 30 was applied to all dates in order to correct for isotopic fractionation and marine reservoir effects, which is in line with previous studies of Baffin Bay and west Greenland (Lloyd et al., 2011; Bernier et al., 2014; Jennings et al., 2014; Jackson et al., 2017), and also with regional values of reservoir corrections from Baffin Island, Arctic Canada (Coulthard et al., 2010).

3.8 Pb-210 Dating:

Lead-210 dating was performed on the upper 16 cm of BC06. This involved extracting sediment directly from the box core and then freeze-drying the sediment overnight, at least 20 grams of wet sediment was extracted for each sample. After which the sediments were ball-milled and carefully placed into vials then sealed with hot wax ready for dating. The gamma counts were performed over the course of several months using Ortec Lo-AX Series Detector, with gamma counts displayed initially using Gamma Vision software before being transferred into Microsoft Excel, (see Figure 3.1). Unfortunately, this dating method proved unsuccessful with gamma activities appearing to fluctuate down core between reaching possible background levels and then going back up again, (displayed in Figure. 3.1). Therefore, it was not possible to determine the exact point where equilibrium was reached within the core.

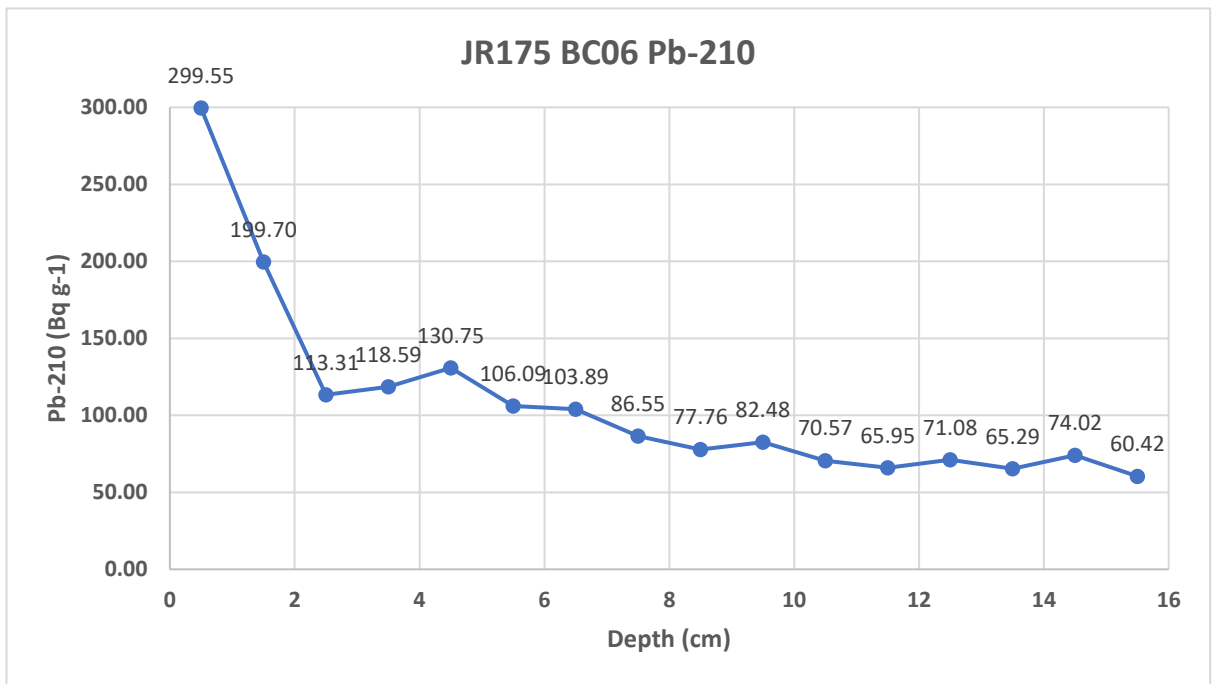


Figure 3.2: Gamma activities for BC06 for the upper 16cm of the core. Total amounts of Pb-210 output are plotted above each sample point with net errors calculated to 1 sigma included in this measurement.

Chapter 4: Results:

4.1 Introduction:

This chapter presents the results of core analysis of GC01 and BC06. The chapter has been divided into five main sections which include; **1)** A chronology obtained from radiocarbon dating of foraminifera extracted from GC01 **2)** detailed descriptions of sedimentological and physical characteristics of GC01 and BC06 **3)** XRF data for GC01 and BC06 **4)** Geochemical analysis of GC01 **5)** Biological analysis using benthic and planktonic foraminifera as a record of oceanographic change. Results will then be interpreted in chapter 5.

4.2 Chronology: Description:

Two radiocarbon dates were obtained from the extraction of foraminifera from GC01 at 59 cm and 29 cm. The decision for these specific depths was based upon both the abundance of foraminifera at each and also the results of the XRF displayed in this chapter. The dates have been corrected for isotopic fractionation effects and also marine reservoir effects with a delta R value of 140 ± 30 yrs used, which is in line with previous studies of Baffin Bay and west Greenland (Lloyd et al., 2011; Bernier et al., 2014; Jennings et al., 2014; Jackson et al., 2017), and also with regional values of reservoir corrections from Baffin Island, Arctic Canada (Coulthard et al., 2010). The calibrated and raw radiocarbon ages are displayed in Table 1 and were calculated using the MARINE 13 database. All radiocarbon ages in this study were measured by BETA Analytic.

Core Name:	Sample Depth (cm):	Lab Code:	Sample Material:	Radiocarbon Age (^{14}C yr. BP $\pm 2\sigma$ range):	Lower Calibrated age (cal. yr. BP):	Upper Calibrated age (cal. yr. BP):	Mean Calibrated age (cal.yr.BP. BP)
JR175-GC01	57-59 cm	Beta-470332	Planktic Foraminifera	12310 \pm 40	13462	13780	13621
JR175-GC01	27-29 cm	Beta-468820	Benthic Foraminifera	10560 \pm 40	11270	11790	11500

Table 3: Radiocarbon ages from GC01, extracted from central Baffin Bay. All dates were calculated to the 95%, 2σ uncertainty range.

The age-depth relationship presented in Figure 4.1 shows the bottom most layers of GC01 to be approximately 22 ka in age, however due to very low amounts of foraminifera throughout GC01 additional

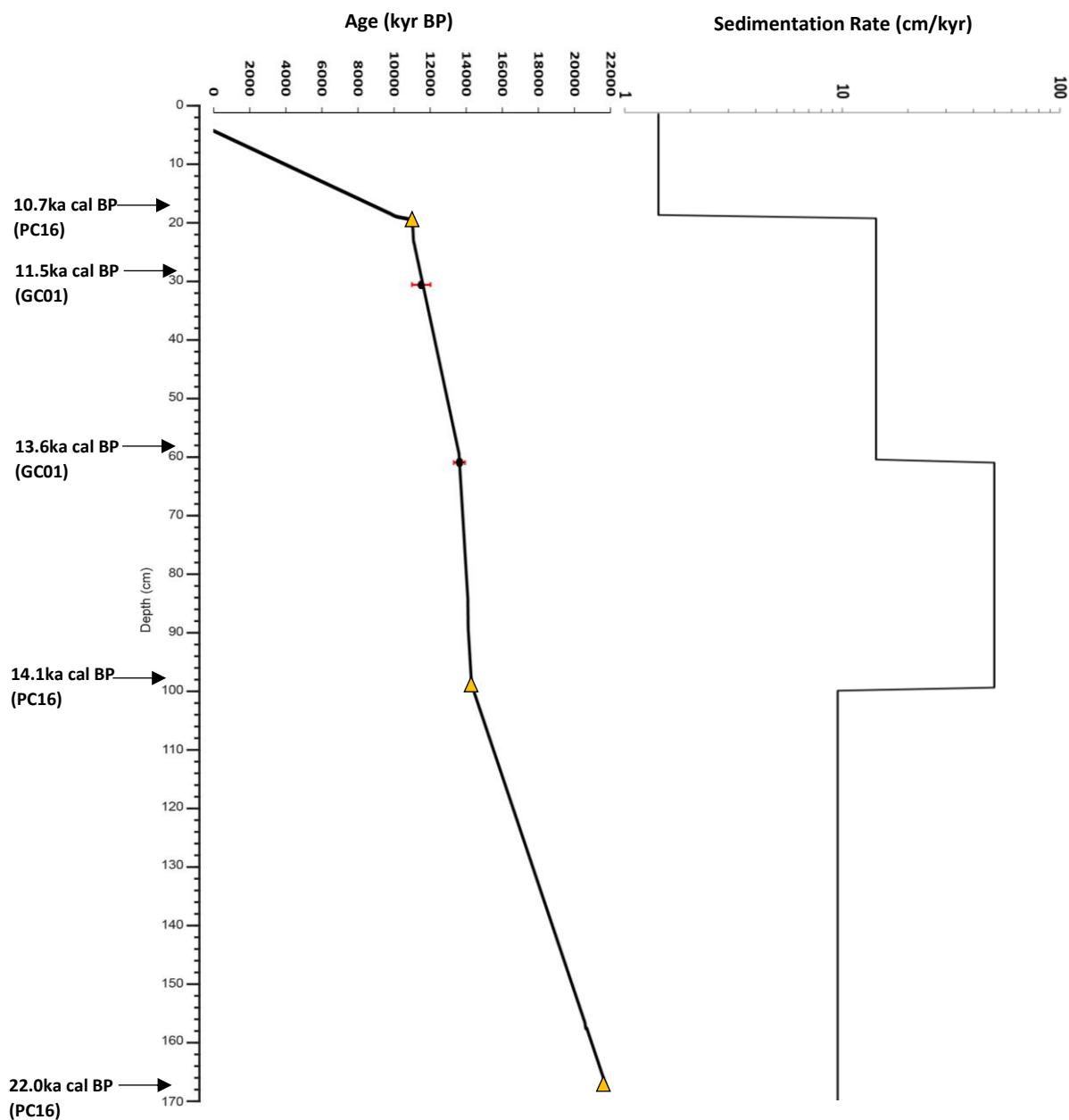


Figure 4.1: Chronology for GC01. Age versus depth plot showing the positions of radiocarbon dates within GC01 (represented by black circles) associated error bars indicate minimum and maximum ages (95% 2 Sigma uncertainty range). Sedimentation rates are shown (log scale) which were calculated between each radiocarbon date interval. Due to only two radiocarbon dates being extracted from GC01 sedimentation rates are averaged using tie points from (Simon et al., 2014), shown using yellow triangles. Due to the absence of calcareous foraminifera between 168 cm and 98 cm in GC01 two tie-points are used at these depths from (Simon et al., 2014) in order to allow for the calculation of sedimentation rates through the entirety of GC01.

For detailed descriptions of the different lithofacies presented in the core log for GC01 in this figure see 'core sedimentology' section below.

radiocarbon tie-points have been used from (Simon et al., 2014) in order to give a more detailed overview of sedimentation rates through time. This age-depth model shows that sedimentation rates were approximately 9.5 cm/kyr between 168-97 cm with increasing rates to 50 cm/kyr between 96- 58 cm. Above 56 cm

sedimentation rates decrease to 14.2 cm/kyr until 19 cm with a significant drop to 1.4 cm/kyr in the uppermost 18 cm of GC01. The locations of radiocarbon tie-points were carefully selected based a range of parameters including core lithology, physical, geochemical properties and the direct radiocarbon dates obtained from GC01.

Lead-210 dating was also performed on BC06 but as previously mentioned in chapter 3 gamma activities vary between reaching background and then rising back up again as displayed in Fig.3.1. It is for this reason that the lead-210 dating results will not be used for age estimation in this study.

4.3 Core Sedimentology: Descriptions:

Descriptions of the sedimentology of both GC01 and BC06 are presented here. All lithofacies and colour changes for GC01 (Fig. 4.2 and 4.3) and BC06 are described in detail (Fig.4.4 and 4.5).

4.3.1 GC01: Sedimentological Description:

The gravity core (GC01) shows significant changes in lithology from 168cm upwards which is clearly visible in Fig.4.1 by the presence of alternating clay (FI) to horizontally laminated sand units (SI). From 168 cm this alternating pattern is evident with a sand unit between 146-156 cm with a further horizontally laminated sand units (SI) unit present between 116-104 cm with clay (FI) unit's in-between. There are large spikes in sand percentages between 156-138 cm where percentages reach over 60% with sand percentages then rising to over 80% at 132 cm. Levels of silt (Fs) are generally high throughout at approximately 60% with rises to 90% occurring either side of the sand (Sf) unit at 138-136 cm. Amounts of IRD between 168-104 cm are very low and occur within sand units. In terms of grain size distribution clay percentages vary between 20% at 168-158 cm, 138-136 cm and 130-126 cm with percentages falling below 10% during silty/sandy units. Patterns of grain size sorting varies from bimodal during sand units to polymodal during clay units within the first sand unit with the pattern reversing upwards of this point to polymodal during sand units and bimodal during clay units. Magnetic susceptibility shows large increases during silty/sandy units and rapid decreases in clay units with levels at rising between 146-140 cm and reaching their highest between 126-122 cm.

There is further significant variability in the lithology of GC01 between 103-0 cm with sharp changes between fine clay units and diamictons with a number of large amounts of IRD present within diamicton layers. The core exhibits a broadly repeating pattern of clay (FI)-diamicton (Dcm)- clay (FI) -diamicton (Dcm) throughout the first 103cm, with the clay (FI) units also appearing to each have their own narrow band of diamictons (Dcm), with IRD (albeit significantly less than the main two diamicton layers which occur between 76-60 cm and 41-20 cm respectively) present within them. This is evident at 96-94 cm, 91-90 cm, 88-86 cm, 49-46 cm and 10-9 cm. Particle size distribution shows that although clay (0-4 μm) percentages remain relatively stable at around 15-25% throughout this section there are notable dips where percentage fall below 15% with these coinciding with rises in silt and sand during major increases in diamictons and IRD (Fig.4.2). During these layers silt (4-63 μm) percentages rise to between 70-80% with sand (>63 μm) percentages also increasing to between 20-40% at times. Grain size sorting was analysed using GRADISAT and varies from poorly sorted to very poorly sorted throughout with sediment deposited under trimodal or polymodal conditions. Magnetic

susceptibility shows slight increases for the top 103 cm during periods when grain size is larger and IRD is present between 76-60 cm and 41-20 cm with levels decreasing in-between.

Through this analysis of sedimentology, the following lithofacies have been identified (see Fig. 4.2 and 4.3 for detailed visual images of these);

1) Fp with a few large clasts mainly concentrated at 9 cm, colour - dark brown 7.5yr/3/4 (0-19 cm depth), **2)** Dcm, facies change marked with a clear and sharp colour change to dark greyish brown 10yr/4/2 at the point at which Fp are first present, significant IRD is present throughout this facies (19-40 cm depth), **3)** FI marked by sharp and clear colour change to dark grey 10yr/4/1, note narrow Dcm layer marked by colour change to grey 7.5/5/1 in middle of facies layer before returning to FI (41-61 cm depth), **4)** Dcm majority, although Fs initially, which is marked by sharp and clear colour change to dark greyish brown 10yr/4/2, significant amounts of IRD present (62-76 cm depth), **5)** FI sharp colour change to dark grey 10yr/4/1 (77-86 cm depth), **6)** FI (d), narrow band of clasts with significant IRD present before changing back to FI with some intra-clasts present (87-103 cm depth), **7)** SI laminations becoming increasingly vertical with increasing depth (104-109 cm), grey 10yr/5/1. **8)** FI sharp transition from SI with further narrow Sf units present within the facies (110-121 cm depth), **9)** Sf with four small intra-clasts present at 122 cm and one again at 130 cm, colour change to pale brown 10yr/4/1 between 138-142 cm as sediment rapidly changes from FI to silt to FI and then to SI (122-155 cm depth), **10)** FI transition is sharp at 156 cm and continues until end of core GC01.

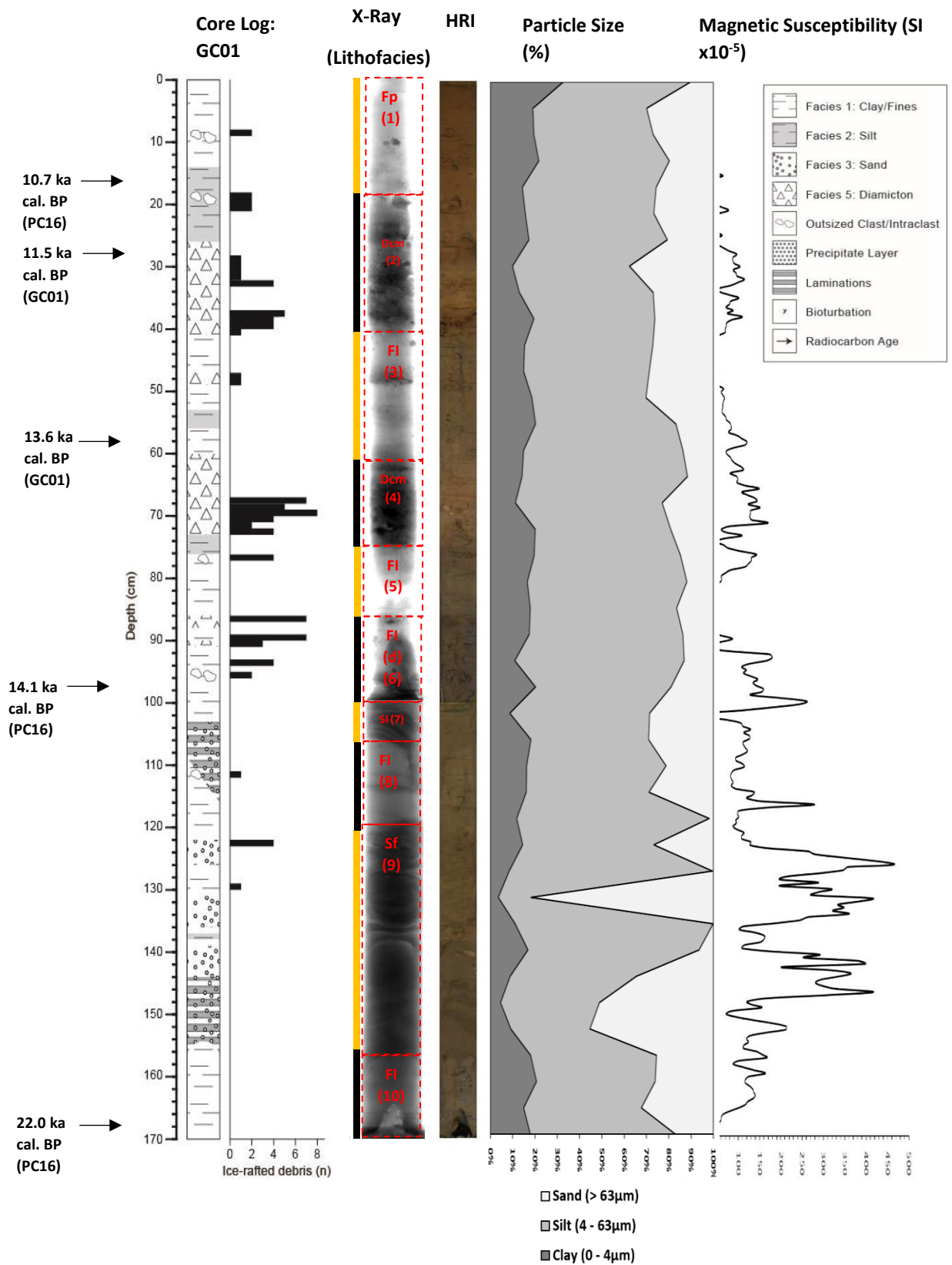


Figure 4.2: High-resolution combined images showing the physical and magnetic properties of core GC01. Moving from left to right; simplified core log illustrating changes in stratigraphy with IRD counts plotted against depth downcore; combined x-rays taken using the Geotek: Vertical X-Ray CT System shown alongside a HRI: high resolution digital image of GC01; particle size (%) for clay, silt and sand (see key and text for more information) which were measured at 4 cm intervals; magnetic susceptibility measured using a Geotek multi-core scanner. Lithofacies are labelled in red on the x-ray image and delimited by the black and yellow colour bands.

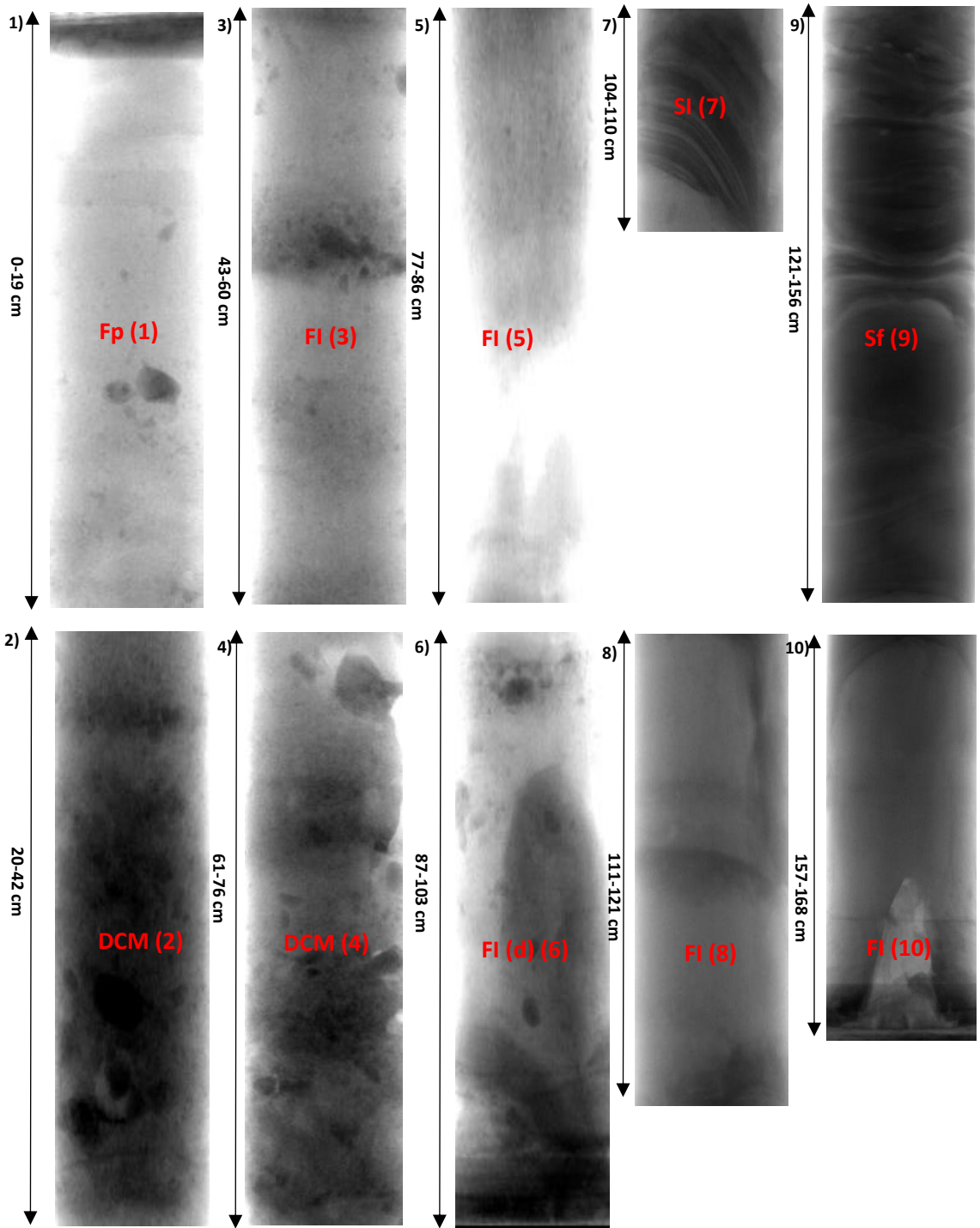


Figure 4.3: X-rays of GC01 showing various lithofacies with length of facies displayed to the left of each. Lithofacies have been numbered and correspond to the description given above.

4.3.2 BC06: Sedimentological Description:

BC06 was extracted from the same site as GC01 and offers a higher resolution look at the uppermost section of GC01 including the second diamicton/IRD layer at the top of the core. The lithology of the core shows three distinct facies, (see Fig. 4.4 for more detail), with the bottom of the core 48-46 cm dominated by a thin clay (FI) layer and low amounts of magnetic susceptibility. There are sharp facies change to diamicton (Dcm) and IRD rich sediment thereafter (45-22 cm). Magnetic susceptibility shows large increases between 46-

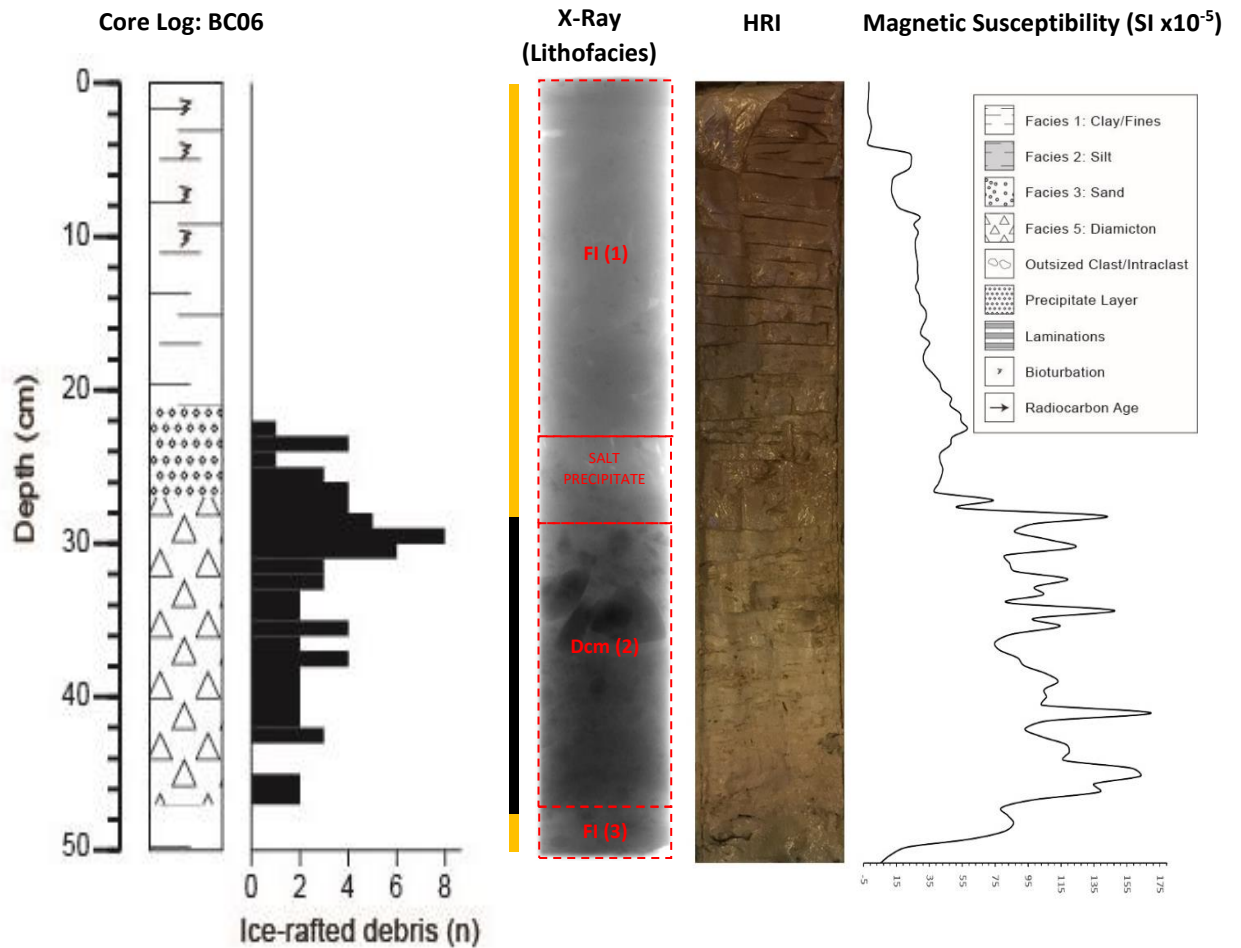


Figure 4.4: High-resolution combined images showing the physical and magnetic properties of core BC06. Moving from left to right; simplified core log illustrating changes in stratigraphy with IRD counts plotted against depth; combined x-rays taken using the Geotek: Vertical X-Ray CT System shown alongside a HRI: high resolution digital image of BC06; magnetic susceptibility measured using a Geotek multi-core scanner. Lithofacies are labelled in red on the x-ray image and delimited by the black and yellow colour bands.

24 cm during diamicton and IRD rich sediment. Interestingly between 27-22 cm there is a salt precipitate layer with amounts of IRD decreasing quickly between 21-18 cm, although more gradually than seen in GC01. Facies then change to clay (FI) after 18 cm until the top of core GC01 with evidence of bioturbation between 11-0 cm. Levels of magnetic susceptibility are generally low throughout the upper most 21 cm of core BC06.

Through this analysis of sedimentology, the following lithofacies have been identified (see Fig. 4.4 and 4.5 for detailed visual images of these);

1) FI throughout with evidence of bioturbation during the top 10 cm, with some small intra-clast present from 17-20 cm, brown throughout 7.5yr/5/4, after 20 cm depth there is a significant amount of salt precipitate present (0-25 cm depth). 2) Dcm, facies change is marked by a sharp and clear colour change to light greyish brown 10 yr/6/2, very large intra and outsized clasts become present after 30 cm before gradually becoming smaller (26-46 cm depth). 3) FI sharp and clear lithofacies change marked by colour change to dark grey 5yr/4/1 (46-48 cm depth).

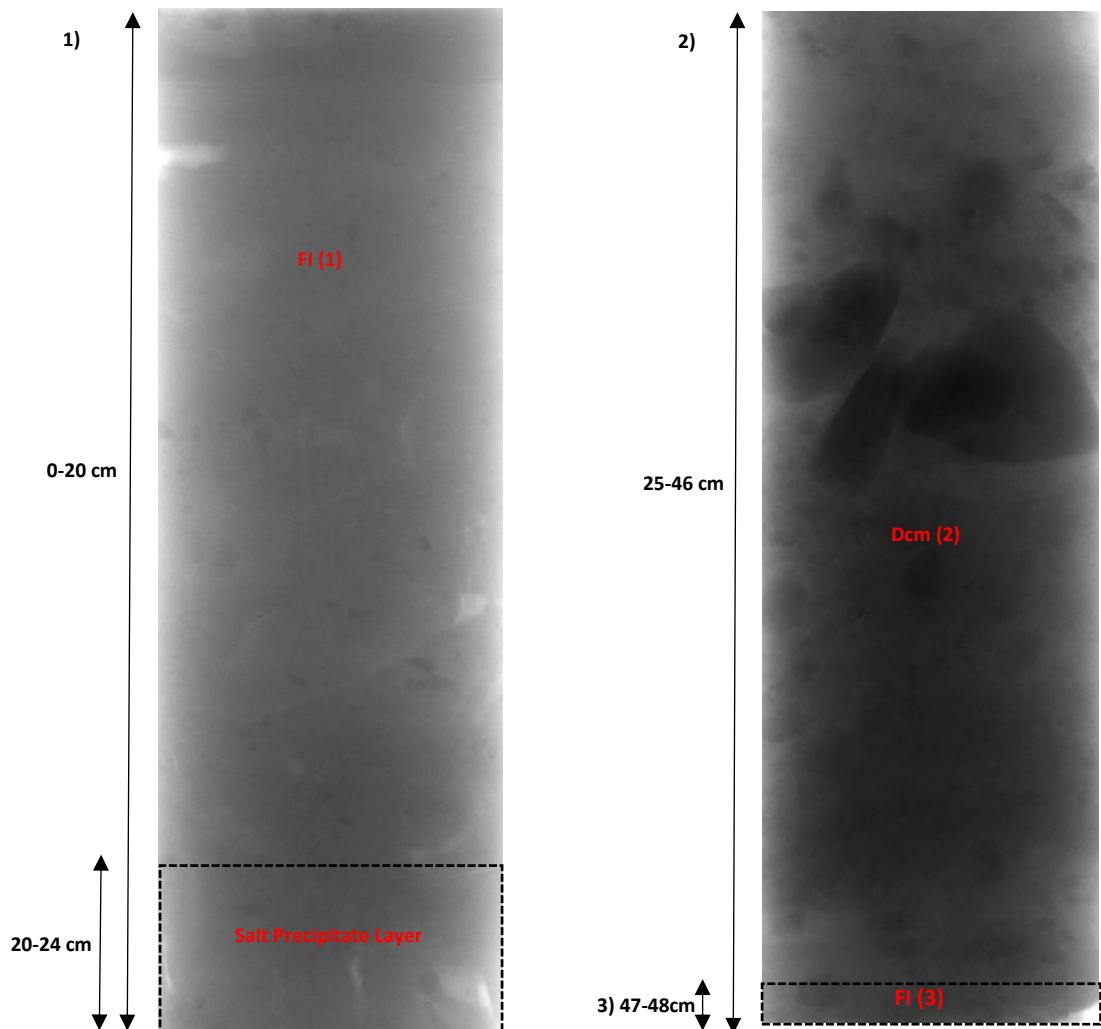


Figure 4.5: X-Rays of BC06 showing various lithofacies with the length of each facies displayed to the left of each. Each lithofacies have been numbered and corresponds to the description given above.

4.4 XRF geochemical and Physical properties: Descriptions:

The elements shown in Fig. 4.5 and 4.6 were chosen from a large number of elements measured using a Geotek multi-core scanner (see chapter 3 for more information). The XRF data presented here has been carefully selected based on extensive reviews of the literature, hence only a select few have been presented for the purposes of this study; Calcium (Ca), Manganese (Mn), Iron (Fe) and Barium (Ba) with all elements normalised against potassium (K). The justification to use these listed elements is as follows; Ca was chosen as an indicator of carbonate deposition in central Baffin Bay from surrounding carbonate outcrops since XRD was not available to measure carbonate directly from either GC01 or BC06. Due to several examples within the literature (Croudace et al., 2006; Polyak et al., 2009; Simon et al., 2012;2014), Mn has been chosen an indicator of changes in redox conditions through time. Fe as a possible measure of changes in sediment transport from non calcium sources in central Baffin Bay. The inclusion of Barium in this study is due to increasing evidence that Ba can be used as a primary productivity proxy throughout the Quaternary (Dymond et al., 1997; Tribovillard et al., 2006; Soua, 2011), although few studies so far have focused on Arctic regions.

4.4.1 GC01: XRF geochemical and Physical properties: Description:

In the lower third of core GC01 (168-104 cm) sedimentology, physical and geochemical properties are quite different to the upper 103 cm with a significant lack of diamicton/IRD layers or noteworthy changes in Ca/Ka ratios, although three short sharp modest rises do occur between 139-122 cm. Working up core, the first sand layer begins at 156 cm with Ca/K values starting low, although Fe/K starts off very high there is a rapid drop at the start of the first SI layer. Moving up core there are clear alternating clay to sand layers as previously described, with these sand units generally coinciding with the three modest rises in Ca/Ka ratios and a rise in levels of Fe/K ratios (see Fig.4.6). Magnetic susceptibility rises significantly during both the SI and SU layers which are present between 158-103 cm. This is the only time IRD is present in the lower third of GC01 although amounts remain low throughout this section of the core until above 103 cm.

From 103 cm upwards in GC01 there is a section of rapidly alternating clay-diamicton layers between 96-87 cm (see Fig.4.2) with increases in IRD within diamicton layers Ca/K levels remain low. Between 88-77 cm the first low calcium layer (LCL) is marked by very low levels of Ca/K, lower than the modest levels present in the lower sections of GC01 (168-89 cm). This change to the first LCL is marked by sharp facies change to clay with no IRD present. At 76 cm Ca/Ka values rise significantly at the start of the first high calcium layer (HCL) peaking at approximately 62 cm before declining again to low levels once more by 58cm. Between 61-41 cm the second LCL begins Sedimentologically, the second LCL is predominantly clay rich with no IRD present, although there is a narrow band of diamictons with small amounts of IRD present between 49-47 cm in GC01 (not present in BC06). Throughout the second HCL there is a repeating pattern both in terms of significant decreases in Fe/ka ratios, increases in IRD, increasing magnetic susceptibility and very high calcium levels returning. The first HCL coincides with significant increases in IRD with higher amount of magnetic susceptibility during this unit, Fe/K values decrease from the start of the first HCL and remain low until 57 cm. This pattern of LCL-HCL is repeated again between 41-22 cm as a second HCL is present marked clearly by a very high and sustained concentration of Ca/Ka. Sedimentologically the second HCL is very similar to the first

with diamicton dominating and high amounts of IRD present along with a lowering of Fe/K ratios and higher magnetic susceptibility. In the uppermost brown mud layer (UBML) 22-0 cm in GC01 there are rapid rises in Mn/K levels (represented by the red layer in Fig. 4.6) with steady rises in Fe/Ka levels also evident along with decreasing amounts of magnetic susceptibility. Ca/K levels are very low through the uppermost 22 cm of GC01.

Ba/K ratios are presented for GC01, (see Fig.4.5). Results indicate that Ba concentrations are very high during the bottommost clay layer (168-157 cm) with two more peaks, also in clay layers, between 138-136 cm and again at 132-129 cm. Between 128-78 cm concentrations of Ba is relatively low, but with some smaller amplitude shifts in peaks present. Interestingly, there are major peaks at the start of each HCL, 76-59 cm and 42-22 cm respectively with low levels of Ba during HCL and in-between during LCL.

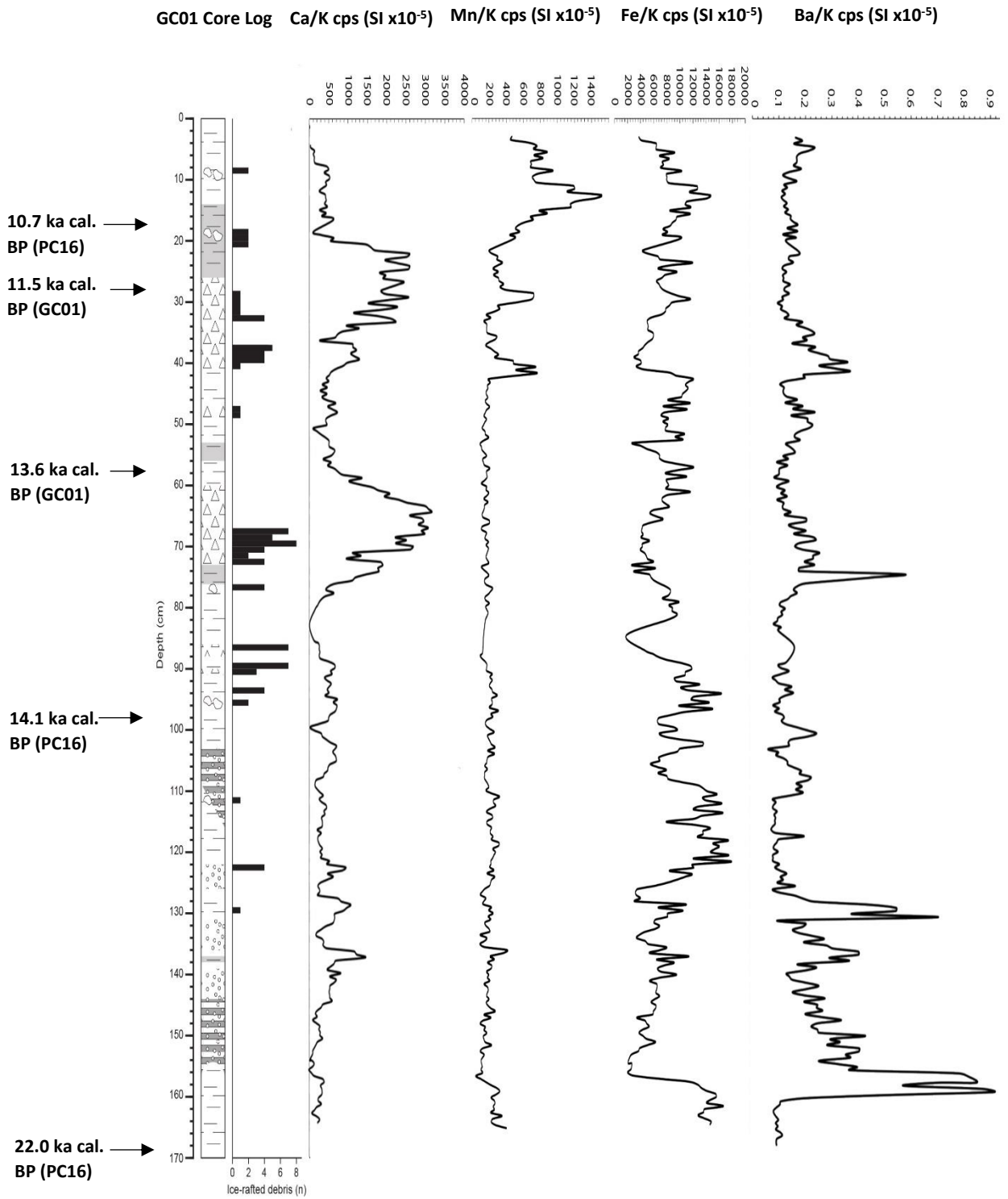


Figure 4.6: High resolution combined images showing geochemical properties of GC01. Moving from left to right; simplified core log illustrating changes in stratigraphy with IRD counts plotted against depth. XRF showing calcium (Ca), manganese (Mn), iron (Fe), barium (Ba) measured against potassium (K).

4.4.2 BC06: XRF geochemical and Physical properties: Description:

The second HDC layer is also present in BC06 with an almost identical pattern of Ca/K, Fe/K ratios to GC01 with slight rises in Mn/K also present at the start of the first HDC layer before rapid decreases as Ca/K levels peak. The uppermost 22 cm of BC06 (represented by the red layer, Fig.4.7) show very high increases in Mn/K with steady rises in Fe/K ratios also evident. Ca/Ka ratios as well as magnetic susceptibility are generally low throughout the uppermost 22 cm of BC06. Changes in Ba/K ratios in BC06 although showing some fluctuations up core remain generally low throughout the entire length of the core. Highest values occur at the bottom of BC06 between 48-46 cm and 18-2 cm with lower values inbetween.

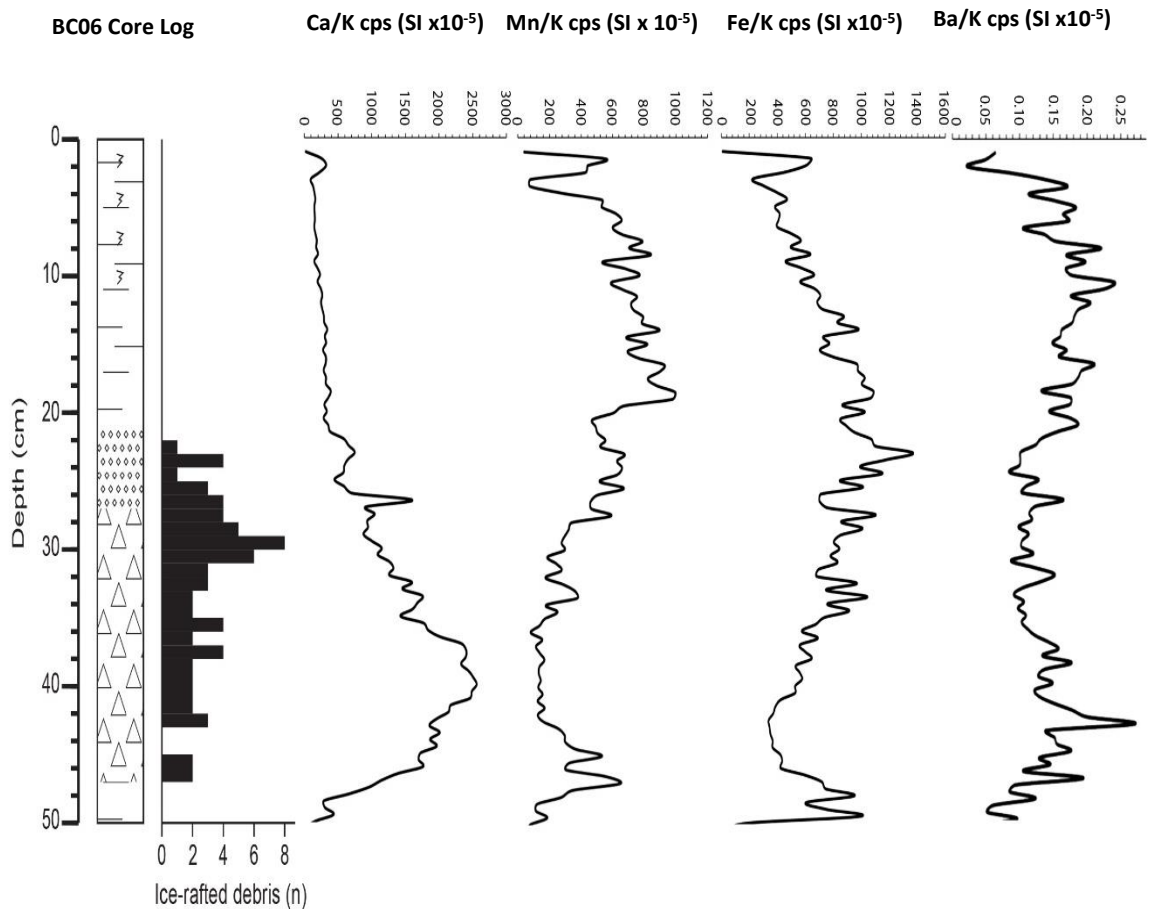


Figure 4.7: High resolution combined images showing geochemical properties of BC06. Moving from left to right; simplified core log illustrating changes in stratigraphy with IRD counts plotted against depth. XRF showing calcium (Ca), manganese (Mn), iron (Fe), barium (Ba) measured against potassium (K).

4.5 XRF: Ca, K and Ti total counts (Semi-Quantitative Minerology): Description:

The concentrations (total counts) of Calcium, Potassium and Titanium are presented in Fig. 4. and Fig.4.9 in an attempt to investigate the variation in mineralogy of both GC01 and BC06. Since this study did not have direct access to X-ray diffraction (XRD) hence the results presented here are from XRF element total element counts only.

4.5.1 Calcium total counts: GC01:

Total counts of calcium in GC01 show large variations up-core with levels typically remaining around 14% between 168-80 cm with rapid but short duration rises approximately 25% occurring at 138 cm (see Fig 4.8). Above 80 cm two well defined peaks in calcium counts occur between 76-59 cm and 42-22 cm with levels reaching over 52%. In between 58-43 cm calcium levels decrease markedly back to approximately 14%. The upper most 18 cm of GC01 is dominated by decreasing levels of calcium beginning at around 20% and gradually falling to 14% at the top of the core.

4.5.2 Potassium total counts:GC01:

Potassium (K) has been used here to represent K-feldspars which show a highly variable abundance downcore in GC01. Levels of potassium from 168-80 cm are around 12% with levels decreasing between 76-59 cm to 8-6%. Above 56 cm levels of potassium rise slightly to 10% before decreasing between 42-22 cm (see Fig 4.8). The upper most 21 cm of GC01 exhibits rises in potassium counts to around 12% until the top of the core.

4.5.3 Titanium total counts: GC01:

Highest total counts of titanium occur between 168-80 cm, 54-42 cm and 16-0 cm in GC01 with levels at around 4%. In between at 79-55 cm and 41- 17 cm counts of Titanium fall to almost 0%.

4.5.4 Calcium total counts: BC06:

Analysis of total counts of calcium in BC06 show that levels start low at approximately 14% between 48-46 cm but rise sharply between 45-22 cm reaching 50% until a gradual decline begins from 36 cm upwards. Total counts of calcium then stabilise at around 13% from 18 cm until the top of BC06 (see Fig. 4.9).

4.5.5 Potassium total counts:BC06:

Potassium counts in BC06 are generally appear very stable at around 10% throughout the entire length of the core. The only notable decreases in potassium counts occur between 48-46 cm with counts at approximately 6% and again between 25-23 cm.

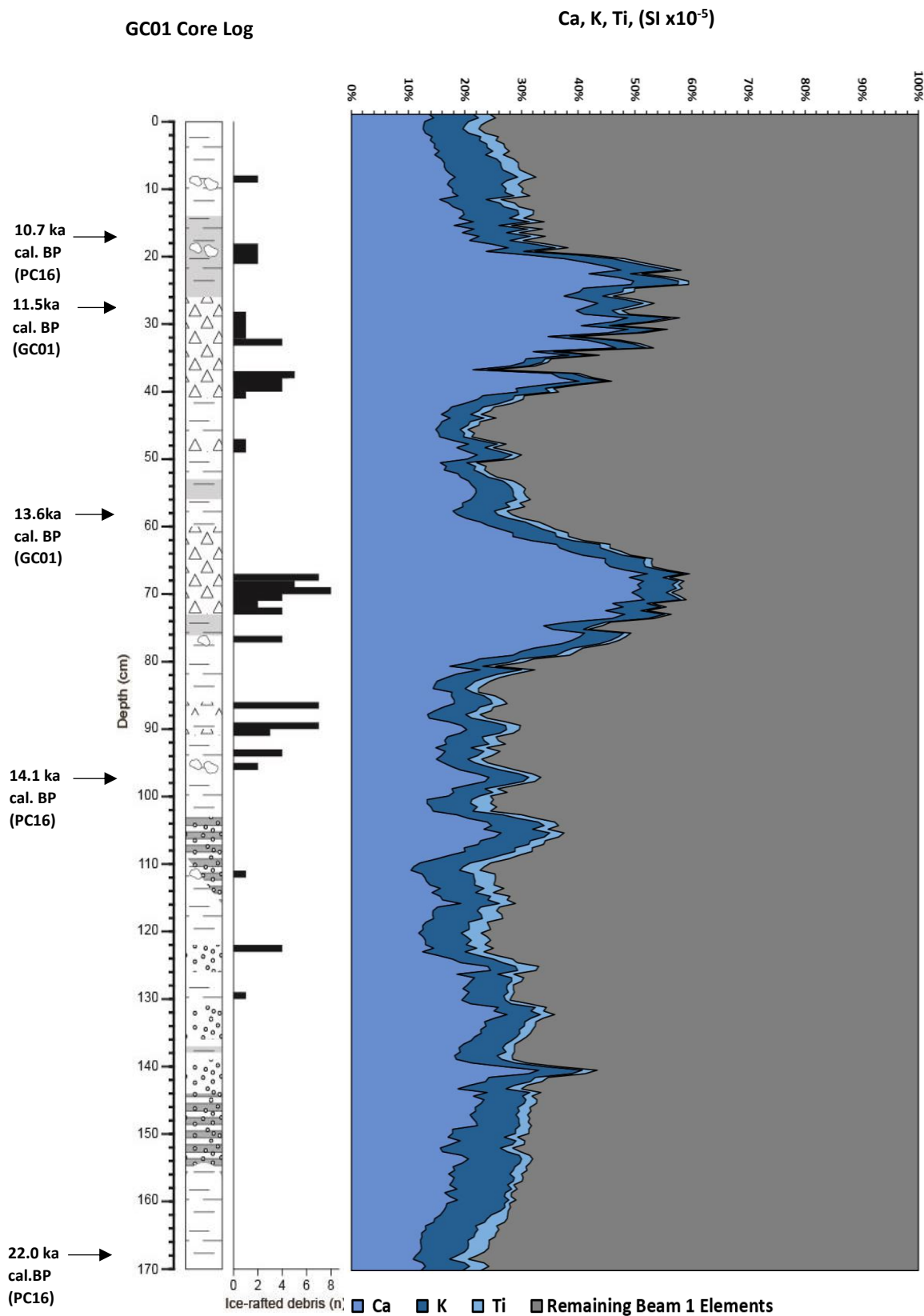


Figure 4.8: High resolution combined images showing geochemical properties of GC01. Moving from left to right; simplified core log illustrating changes in stratigraphy with IRD counts plotted against depth. XRF showing the relative normalised element ratios for calcium (Ca) to Potassium (K), Potassium and Titanium (Ti) to Potassium (K). All other normalised beam 1 elements are represented by the dark grey layer.

4.5.6 Titanium total counts: BC06:

In BC06 total counts of titanium at the base of the core are approximately 4% between 48-46 cm but quickly decrease to 1-0% between 45-32 cm. Counts then gradually rise to around 2-3% between 31-21 cm, increasing to 4% from 20 cm until the top of the core. However there is a reduction in counts between 25-23 cm to 0%.

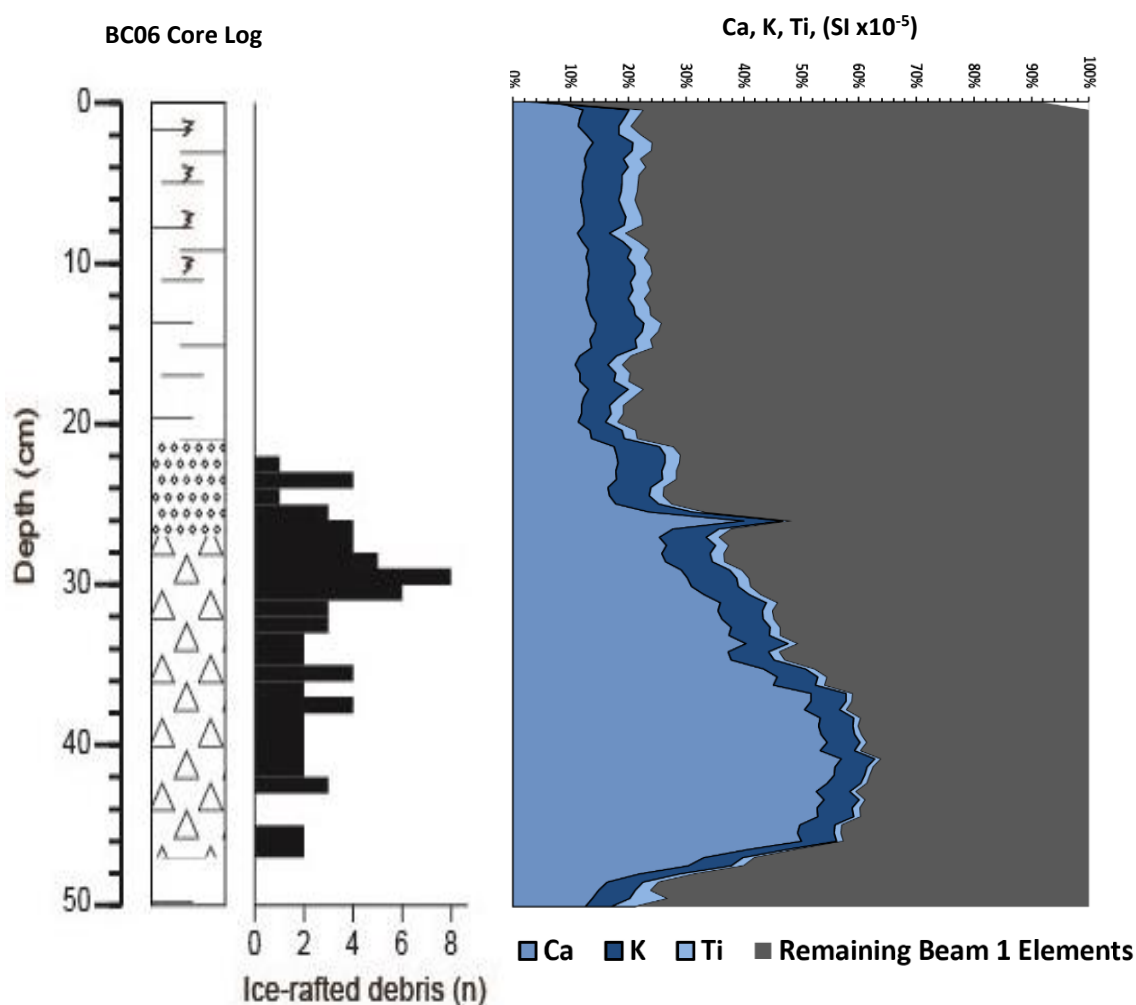


Figure 4.9: High resolution combined images showing geochemical properties of BC06. Moving from left to right; simplified core log illustrating changes in stratigraphy with IRD counts plotted against depth. XRF showing the relative normalised element ratios for calcium (Ca) to Potassium (Ka), Potassium and Titanium (Ti) to Potassium (K). All other normalised beam 1 elements are represented by the dark grey layer.

4.6 GC01: Geochemical Analysis: Osmium Isotopes Ratios: Description:

Osmium isotopic ratios ($^{187}\text{Os}/^{188}\text{Os}$) were measured at six different depths along core GC01 in an attempt to aid in the interpretations surrounding the reconstruct ice sheet inception and break-up during the Quaternary. Furthermore, the results used in this study will further test the use of osmium as a proxy in this context as initially undertaken by (Rooney et al., 2016).

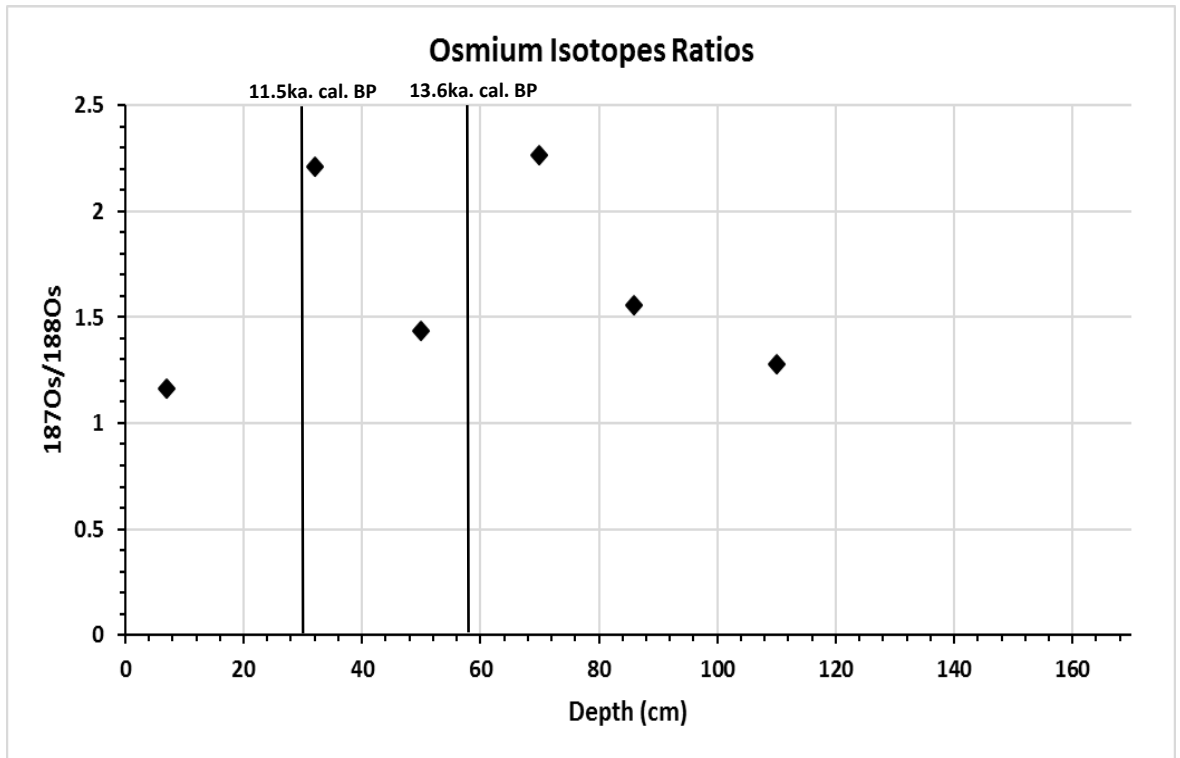


Figure 4.10: $^{187}\text{Os}/^{188}\text{Os}$ results extracted from GC01. Exact depths of extractions are 7 cm, 32 cm, 50 cm, 70 cm, 86 cm and 110 cm. Exact value are as follows; 7cm = 1.16 ± 0.03 , 32 cm = 2.2 ± 0.065 , 50 cm = 1.43 ± 0.028 , 70 cm = 2.26 ± 0.048 , 86 cm = 1.55 ± 0.031 , 110 cm = 1.28 ± 0.025 . Obtained radiocarbon age calibrations are also shown.

The results indicate that isotopic ratios fluctuate down core markedly with values rising from 1.16 at 7 cm to 2.2 at 32 cm, this oscillating pattern continues through core GC01 with another peak in Osmium at 70 cm between two lower values at 50 cm and 110 cm. Giving a range in values from 1.16 to 2.26 within the uppermost 110 cm (see Fig. 4.10).

4.7 Biological Analysis: Foraminifera:

Foraminiferal analysis was undertaken at 2 cm intervals throughout both GC01 and BC06. Volumes of each sample were kept the same to ensure abundance counts were quantitative with 1 cm^3 of sediment extracted and measured via water displacement method as outlined in chapter 3. Due to high amounts of detrital carbonate in certain parts of both GC01 and BC06 it was first thought that foraminifera abundances may have been influenced by the buffering effect. However this appear not to be the case as foraminifera abundances remain very low despite high levels of detrital carbonate in both sediment cores.

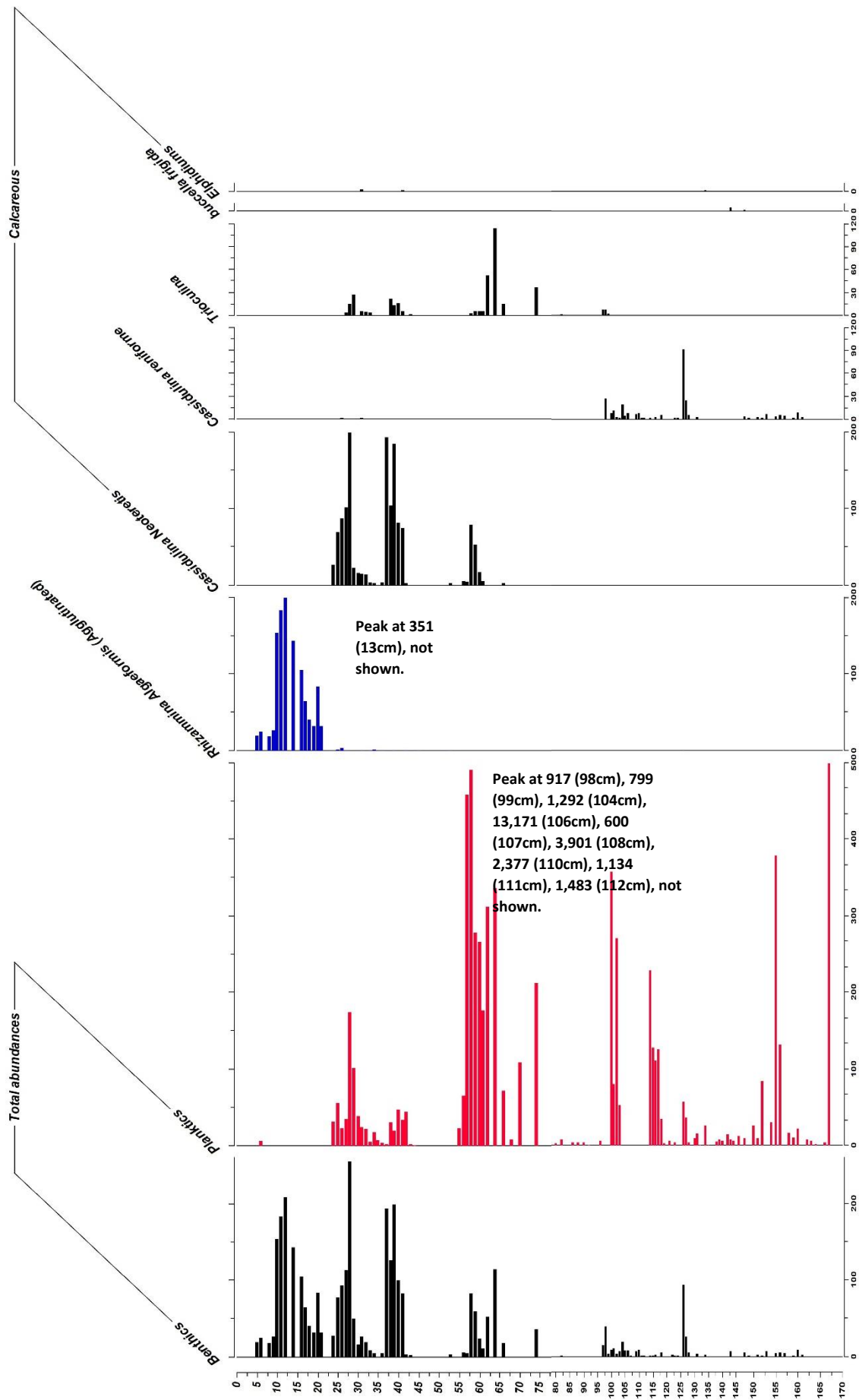


Figure 4.11: Foraminiferal abundances for GC01. Foraminifera have been split to show total abundances of benthic and planktonic species and then divided further into agglutinated (Rhizammina Algaeformis only agglutinated species present) and calcareous species. Total counts of foraminifera are also shown. All data is expressed as a percentage, except total abundances which are absolute abundances per 4ml of displaced sediment (see chapter 3 for more details).

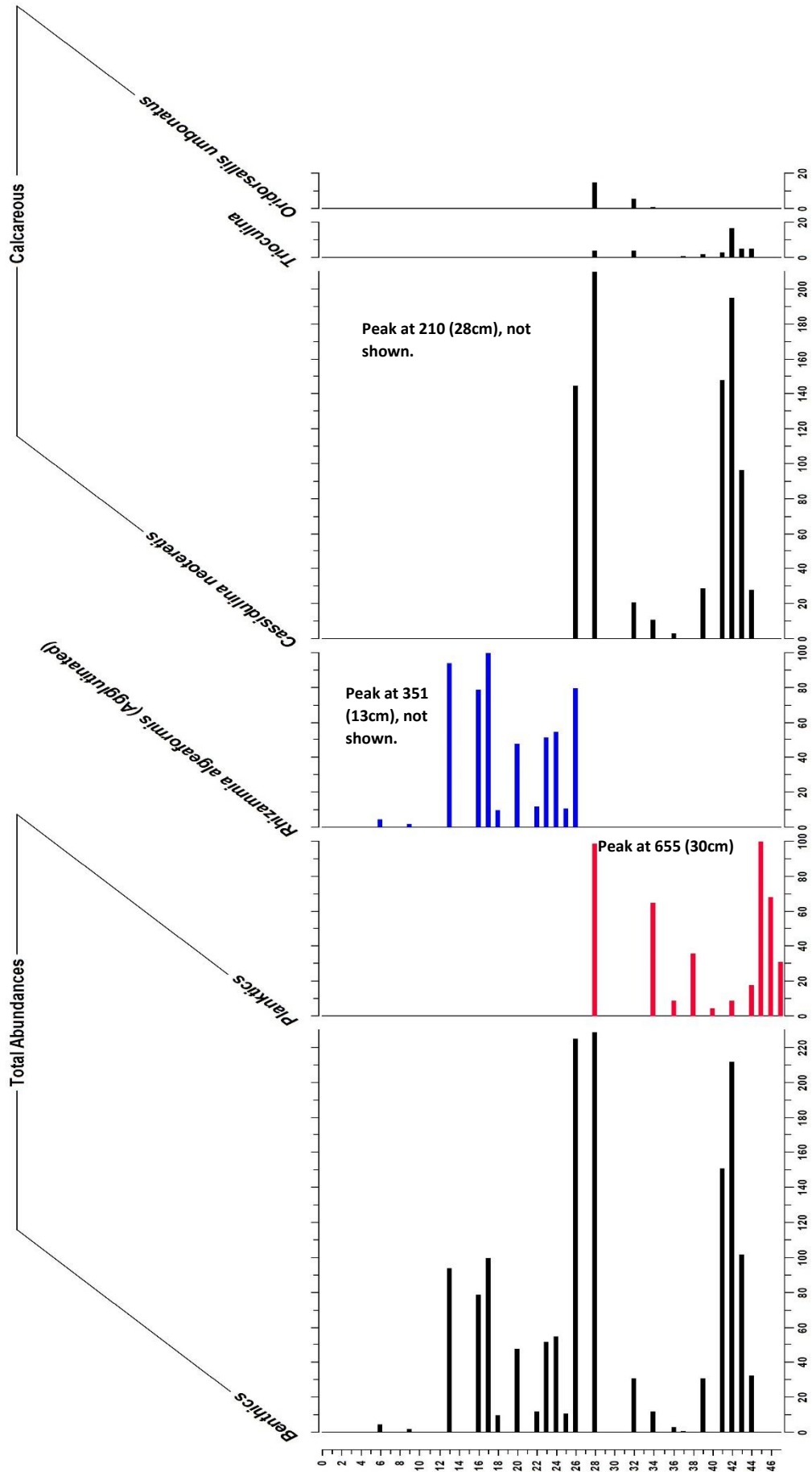


Figure 4.12: Foraminiferal abundances for BC06. Foraminifera have been split to show total abundances of benthic and planktonic species and then divided further into agglutinated (Rhizammina algaeformis only agglutinated species present) and calcareous species. Total counts of foraminifera are also shown. All data is expressed as a percentage, except total abundances which are absolute abundances per 4ml of displaced sediment (see chapter 3 for more details).

4.7.1 Biological Analysis: Foraminifera Abundances: GC01: Description:

Foraminifera abundances are highly variable up core in GC01. The bottom of GC01 is generally devoid of foraminifera except for a peak in planktonic foraminifera at 167 cm with over 500 specimens per sample. Between 154-120 cm foraminifera abundance are extremely low to non-existent (under 30 specimen counts per 1 cm³ sample), with planktonic species dominating assemblages by a ratio of 2:1 to benthics. Between 107-98 cm there are significant rises in planktonic abundances to over 13,000 specimens per 1 cm³ sample whereas benthic foraminifera abundance during this section of GC01 remain low. Almost immediately above 97 cm planktonic foraminifera fall rapidly with near zero foraminifera present between 97-77 cm. Foraminifera abundances again initially increase, albeit barely above 300 specimen counts per sample with benthics remaining relatively low in comparison to planktics which dominate the assemblages between 76-62 cm. Between 61-42 cm there is again a core section with zero identifiable foraminifera before benthic foraminifera dominate assemblages, although rises in amounts of planktonic foraminifera also take place. In the uppermost 22 cm of GC01 assemblages are solely dominated by agglutinated foraminifera with abundances dropping to zero above 10 cm (see Fig. 4.11).

4.7.2 Biological Analysis: Foraminifera Abundances: BC06: Description:

Foraminifera abundances are generally low throughout the entire length of BC06. However, there are fluctuations, with benthic abundances starting off fairly high at around 220 specimens per sample between 44-41 cm with planktonic specimens counts also reaching over 100 per sample. Above this depth there are sharp declines in both benthic and planktonic abundances (see Fig.4.12). Between 28-26 cm there is a rapid increase in benthic foraminifera before a swift transition to agglutinated foraminifera and a complete absence of any calcareous species for the remainder of BC06. Above 12 cm depth agglutinated foraminifera become scarce with zero foraminifera present in the uppermost 6 cm.

4.7.3 Biological Analysis: Foraminiferal Ecology: Description: GC01:

Foraminiferal analysis of GC01 shows a generally low ecological diversity of foraminifera up core. Between 168-128 cm there are very few benthic foraminifera present with only very small amounts of *Casidulina reneforme* present. *Casidulina reneforme* then peaks in abundance at 126 cm with ever decreasing amounts present up core of this until 100 cm when *Casidulina neoteritis* starts to dominate the assemblages. Between 100-98 cm there is an additional eight species of foraminifera, although they are all present in very low abundances. *Casidulina neoteritis* dominates assemblages along with some *tricolina* until approximately 22 cm when assemblages are then dominated solely by the agglutinated species *Rhizammina algaeformis* for the remainder of GC01. Interestingly, GC01 has sections of exceptionally high amounts of planktonic foraminifera which coincide with the slight increase in species diversity between 107-98 cm and then again further up core between 65-55 cm as *Casidulina neoteritis* and *tricolina* also first come into the assemblages.

4.7.4 Biological Analysis: Foraminiferal Ecology: Description: BC06:

Foraminiferal species diversity in BC06 are generally low, with only two benthic species identified throughout the entire length of the core. The bottom of BC06 is dominated by *Casidulina neoteritis*, small amounts of trochammina with planktonic foraminifera also present. There is a peak in *Casidulina neoteritis* between 30-26 cm before a rapid decline in all calcareous species and switch to the agglutinated species, *Rhizammina algaeformis* from 25-12 cm. Above 12 cm little to no foraminifera of any kind are present.

4.8 Biomarker Extractions: IP₂₅:

The sea ice proxy IP₂₅ was not found in any of the 12 samples extracted from GC01.

Chapter 5: Interpretations:

5.1 Chronology: Timeseries development and associations:

Based on the radiocarbon dates obtained from GC01 the core covers the period from at least the Younger Dryas through to the Holocene. The results from the first radiocarbon date would suggest that the sample extracted from GC01 between 59-57 cm is likely to be associated with the end of the Older Dryas stadial, dated at 13.6 ka cal. BP, with the second date extracted at 29-27 cm likely to be of Younger Dryas age, dated at 11.5 ka cal. BP. These dates correlate with previous studies (Andrews and Eberl, 2011; Simon et al., 2014) of late Quaternary climatic change in central Baffin Bay, with dates showing striking similarities to recent work by (Jackson et al., 2017). No direct radiocarbon dates were obtained from the lower sections of GC01 but the chronology for this lower section is based on correlations between proxy data extracted from GC01 (see Fig. 4.6) and other cores in the region (Simon et al., 2016; Jackson et al., 2017). Therefore, using the age-depth model presented, Figure 4.1, it is interpreted that the sediments present between 168-118 cm are most likely associated with the LGM, with the age-model placing the sediment ages around 22-18 ka BP. Although it should be noted that further radiocarbon dates are needed to fully confirm this and this age estimation should be used as a working hypothesis only until further dates can be obtained. For the purposes of this study tie-points have been used (see Fig. 4.1 for more information) in order to create an age-depth model for GC01 and provide an age for the lower sections of the core.

5.2 Lithofacies associations: GC01 and BC06:

It should be noted that in order to achieve these distinctions between sediment units XRF data has also been used (presented in Fig 4.6 and Fig 4.7) and that the high detrital carbonate layers are distinguished using calcium levels as no XRD was available to measure carbonates directly. Therefore, it is the assumption of this study that the high levels of calcium present in both GC01 and BC06 likely indicate high levels of carbonate also. Based on detailed sedimentological descriptions and XRF analysis GC01 and BC06 can be divided into five distinct units up-core.

1) Sand units (S), massive, grey 7.5yr/5/1, 125-121 cm, 136-131 and 148-140 cm (GC01 only). **2)** Sandy units showing horizontal laminations (Sl), grey 7.5yr/5/1, at 116-104 cm and 156-144 cm (GC01 only); **3)** Dark grey 10yr/4/1 clay (Fl) units which are low calcium layers (LCL) located in-between the high calcium layers (HCL) at 86-77 cm and 61-41 cm (these two layers each also have a narrow band of Dcm with IRD present, GC01 only) **4)** Dark greyish brown 10yr/4/2 diamicton (Dcm) layers, which are high in detrital calcium (HDCa) also rich in IRD present between 76-62cm and 40-19cm (GC01 and BC06); **5)** the uppermost brown mud unit (UBM), 7.5yr/5/4, which is primarily made up of clay (Fl) extending from 19-0 cm (GC01 and BC06).

HCL and LCL will therefore be interpreted as high detrital carbonate (HDC) and low detrital carbonate (LDC) layers from this point in for the purposes of the interpretation and discussion chapters.

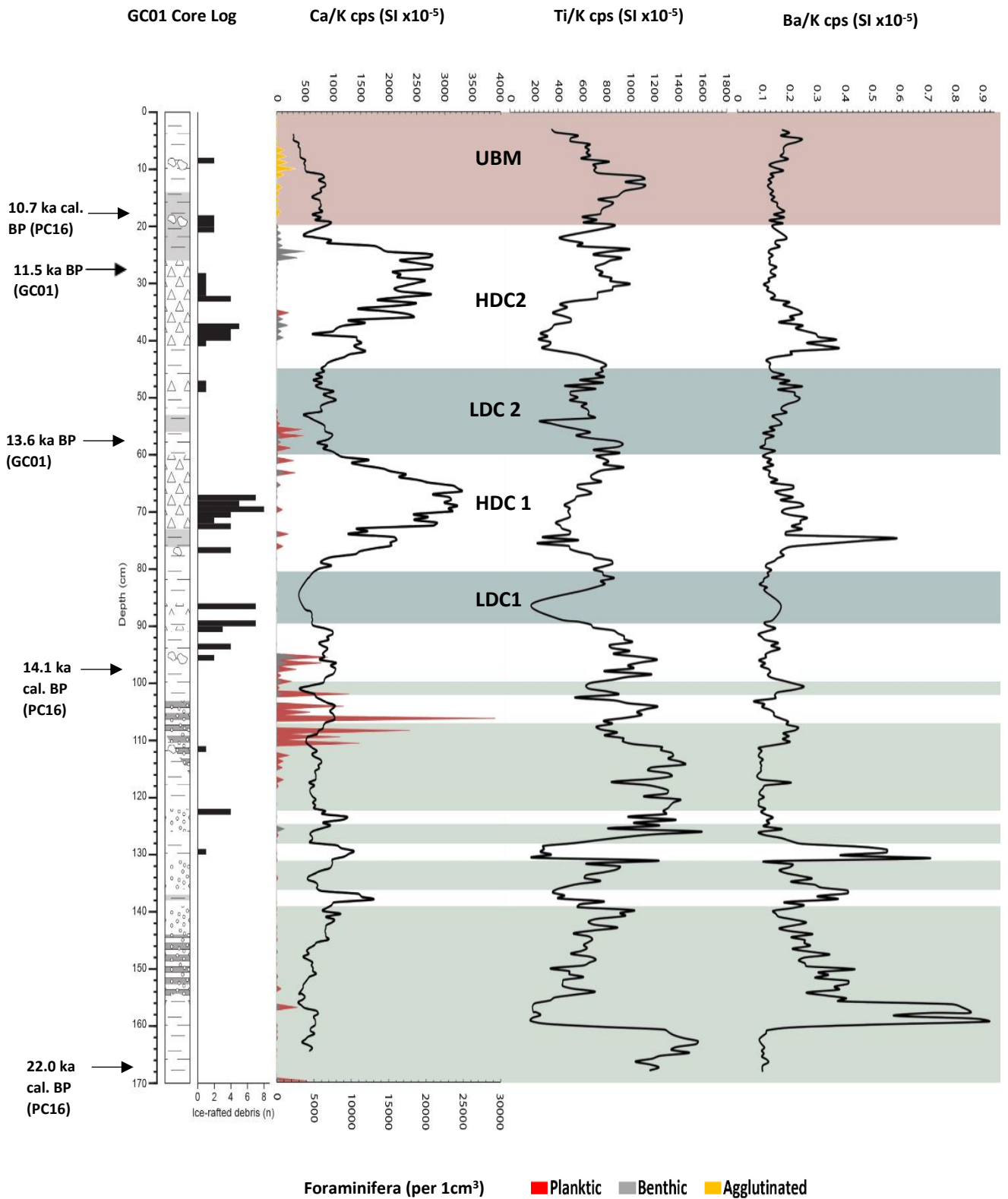


Figure 5.1: High resolution combined images showing geochemical properties of GC01. Moving from left to right; simplified core log illustrating changes in stratigraphy with IRD counts plotted against depth. XRF showing calcium (Ca), manganese (Mn), iron (Fe), barium (Ba) measured against potassium (K). Colour coding has been used in order to split up major lithofacies based on sedimentology, physical and geochemical data. Red layer = uppermost brown mud unit, White layers = high carbonate units, often IRD rich, Dark green layers = low carbonate units, Light green = silty/sandy units. Foraminifera abundances are also shown, split into agglutinated (black), benthics (grey) and planktics (red).

5.3 GC01: Interpretations:

Identification and interpretation of lithofacies are based on sedimentology, physical and geochemical properties, Fig.5.1 and Fig.5.2 have been colour coded in order to give a clear division based on lithofacies interpretation. Based on the data presented in chapter 4 lithofacies have been identified (shown in Fig. 4.8). The interpretation of these lithofacies is now presented below.

Between 168-104 cm GC01 displays low levels of carbonates which occur throughout both laminated sand and Sand units up core with only very small amounts of IRD present within narrow banded FI layers located in between SI and S layers. Interestingly, levels of Ti are highest throughout 168-90 cm of GC01 with levels reducing above this point at approximately 14.5 ka BP. Foraminiferal abundances are near zero between 168-113 cm with a very large spike in planktonic foraminifera between 112-107 cm at 15.0 ka BP, indicating a period of high surface water productivity. The timing of this peak in foraminifera is interesting as it would support recent work (O’Cofaigh et al., 2013) in regards to dating major retreats of Uummannaq from its LGM position at the shelf edge of western Greenland. Higher levels of Ti-rich sediment in central Baffin Bay have also been attributed to sediment sourced from the GIS during the LGM which is present in the sediment record throughout the last 22-14.5 ka BP in GC01. In regards to the distinct sandy units present between 168-104 cm in GC01, it is possible that due to the GIS extending to the shelf edge during the LGM (O’Cofaigh et al., 2013) that large-scale mass movements occurred as sediment built up at the edge of the shelf. This then likely flowed some way down the continental slope with turbidites reaching as far as the abyssal plain of central Baffin Bay as proposed by (Gilbert et al., 1998).

At 97 cm, there is a marked change in lithofacies to clay but with two extremely narrow (>1 cm) bands of diamictons which are rich in IRD present within the larger clay layer. Given the high amounts of planktonic foraminifera, increases in IRD and the age given by the age-depth model (see Figure 4.1) it is likely that the GIS began to retreat from the shelf edge of west Greenland around this time (15.0 ka BP). Interestingly, osmium isotopic analysis performed on sediment at 110 cm gave a low radiogenic reading of $^{187}\text{Os}/^{188}\text{Os} = 1.28$ which would more likely be associated with a more open water environment after major ice sheet retreat (Rooney et al., 2016). Although more radiocarbon dates are needed to determine the exact timings of initial retreat of the GIS from its LGM limits in western Greenland.

Further up core, foraminifera abundances return to near zero between 95-74 cm (LDC layer 1) until after the end of the Older Dryas Stadial at 13.6 ka BP. Above 73 cm marks the start of HDC layer 1 which is associated with coarse-grained sediment of highly variable grain-sizes (diamicton) with high amounts of IRD also present. Ti counts are reduced to around 2% with K counts reduced to approximately 10% as Ca levels rise to very high levels. Magnetic susceptibility rises slightly during HDC layer 1. Highly radiogenic sediment is also present throughout HDC layer 1 with $^{187}\text{Os}/^{188}\text{Os} = 2.26$ at 70 cm, suggesting a significant delivery of glacially eroded material into central Baffin Bay from surrounding ice sheets during the Older Dryas stadial. Levels of barium (productivity marker) evidence increases in water productivity just before and just after the Older Dryas Stadial with rises in benthic and planktonic abundances also present at the end of the Older Dryas Stadial dated at 13.6 ka BP. The end of HDC layer 1 and the start of LDC 2 is marked by rapid drops in carbonate

levels and a return to clay which is rich in Ti. Sediment within LDC 2 is weakly radiogenic with $^{187}\text{Os}/^{188}\text{Os} = 1.43$ at 50 cm indicating that much less in the way of glacially eroded sediments were present in central Baffin Bay during this time between HDC layer 1 and HDC layer 2. HDC layer 2 is associated with the Younger Dryas Stadial (see Table 1 in chapter 4). Sedimentologically and geochemically HDC layer 2 and HDC layer 1 are very similar, characterised by high amounts of IRD, carbonates, highly radiogenic sediment; $^{187}\text{Os}/^{188}\text{Os} = 2.2$ at 32 cm and low levels of Ti. The variations in radiogenic values seen in GC01 are linked to changes in $^{187}\text{Os}/^{188}\text{Os}$ compositions which are likely a result of differing amounts of oceanographic restriction through time (Rooney et al., 2016). This would suggest that highly radiogenic sediment is associated with more restrictive oceanographic conditions in central Baffin Bay during colder periods such as the Younger Dryas and the Older Dryas as evidenced in GC01. Osmium isotopes are also known to respond to changes in continental weathering rates which would suggest that large amounts of glacially eroded material were transported into central Baffin Bay during the Younger Dryas and Older Dryas Stadials. Magnetic susceptibility also increases slightly during HDC 2. Abundances of foraminifera start off high at the start of HDC layer 2 but quickly fall to near zero before rising sharply again at the end of the Younger Dryas Stadial along with levels of Barium. This suggesting short periods of higher water productivity before and after the Younger Dryas Stadial in central Baffin Bay. Reasons for this are likely linked with higher amounts of nutrient deposition as large icebergs melted as warmer conditions set in during interstadials. However, this does not explain the high amounts of productivity before the Younger Dryas. Although it does seem plausible that given the paleoceanographic reconstructions by (Simon et al., 2014), that the edge of the sea-ice would have temporarily been close to the study site before conditions turned cold enough to promote permanent sea-ice coverage in Baffin Bay.

Above 19 cm in GC01, defined as the UBM layer in chapter 4, levels of carbonates fall to very low levels with sharp increases in Mn/K. These increases in Mn/Ka have been suggested to coincide with changes to redox conditions (Croudace et al., 2006; Polyak et al., 2009; Simon et al., 2012) with the relatively warm climatic conditions in Arctic regions causing changes in physical and biogeochemical processes that operate within the water column, and down to the sea floor. Radiogenic values in the uppermost sections of GC01 are very low, $^{187}\text{Os}/^{188}\text{Os} = 1.16$ at 7 cm, this suggests less restrictive oceanographic conditions during what is most likely the Holocene, as shown by this studies age-depth model (see Figure 4.1). The UBM layer is characterised by FI throughout with occasional clasts/intraclasts present until 9 cm, after which material is dominated by mud, massive. Foraminifera abundances are extremely low between 19-7 cm with a marked change from calcareous species (*casidulina neoteritis* and *Trioculina*) to the agglutinated species *Rhizammina algaeformis* with no calcareous species present up core thereafter. Zero identifiable foraminifera were present above 6 cm until the top of GC01. This cyclic pattern of foraminiferal loss in Baffin Bay is well documented in the literature (Asku, 1983) and with such a strong link in terms of foraminiferal abundances with changes in carbonate levels, this suggests that dissolution of foraminifera is severe in central Baffin Bay during the last 22 ka. The pattern of dissolution is not so clear between 168-104 cm in GC01 with foraminifera abundances remaining generally very low throughout except for one major peak in planktonic foraminifers between 114-104 cm which appear to occur during only modest rises in calcium carbonate. The presence of such high abundances of planktonic foraminifera between 114-98 cm in GC01 is of interest as this occurs during only

modest increases in carbonate yet is not evident in similar modest increases in carbonate ratios downcore between 139-122 cm. The relationship between carbonate and foraminiferal loss is particularly evident in-between HDC layer 1, HDC layer 2 and the Holocene (UBM layer), shown by near 0% foraminiferal preservation. Dissolution appears much less severe during the Younger Dryas cold stage and Older Dryas stadials, although abundances do fall during the middle of each period perhaps due to increasingly low supplies of nutrients during the middle of both stadials.

5.4 BC06: Interpretations and correlations to GC01:

Sedimentological analysis of BC06 shows evidence of the presence of HDC 2 (previously defined in GC01 interpretations in this chapter) from 46 cm upwards until 24 cm with a narrow clay present in the bottommost 2 cm of BC06. HDC 2 is characterised by coarse sediment with a range of different grain sizes (diamicton) with high amounts of IRD present throughout the unit. High levels of magnetic susceptibility are present throughout HDC 2 in BC06. High levels of carbonates are also present with foraminifera abundances high both before and after HDC 2 which is also associated with the Younger Dryas Stadial as in GC01. The transition between HDC layer 2 is marked by a salt precipitate layer extending 26-22 cm and a decline in IRD. Above 22

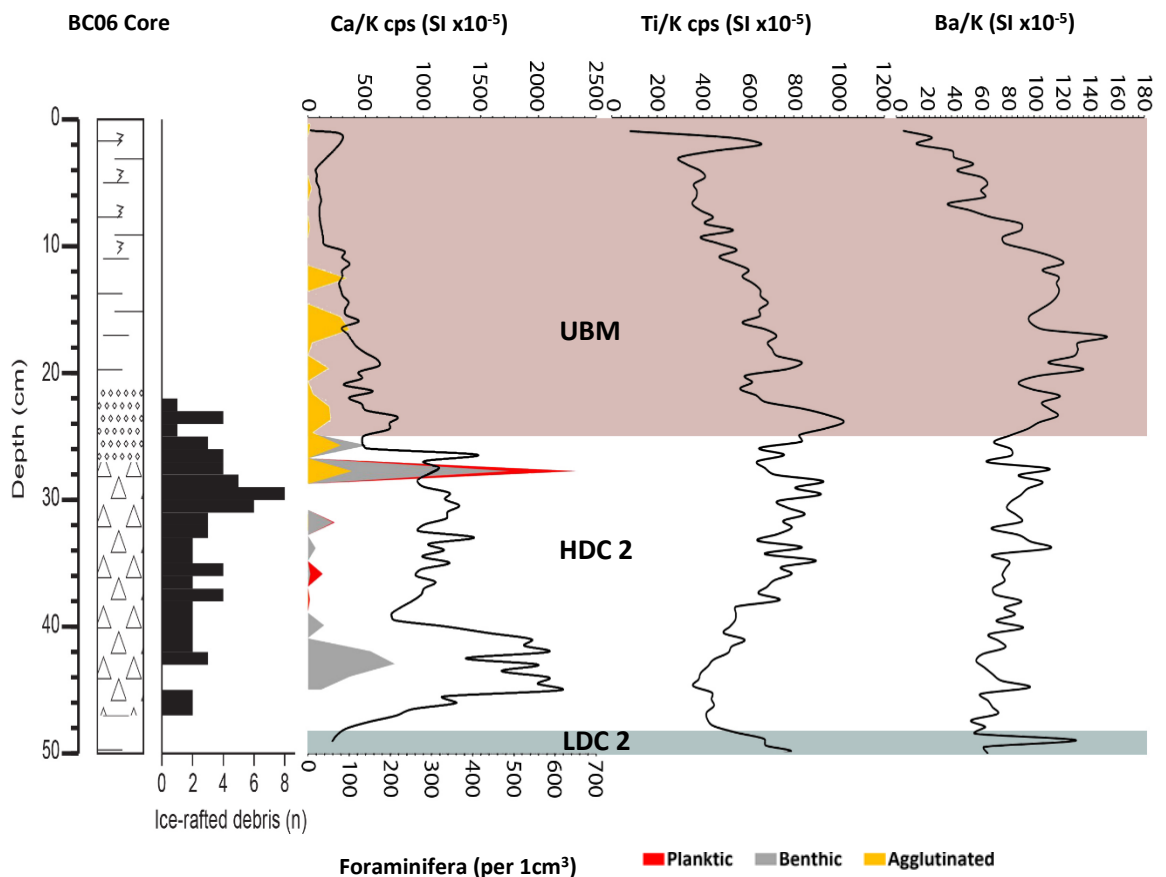


Figure 5.2: High resolution combined images showing geochemical properties of GC01. Moving from left to right; simplified core log illustrating changes in stratigraphy with IRD counts plotted against depth. XRF showing calcium (Ca), manganese (Mn), iron (Fe), barium (Ba) measured against potassium (K). Colour coding has been used in order to split up major lithofacies based on sedimentology, physical and geochemical data. Red layer = uppermost brown mud unit, White layers = high carbonate units, often IRD rich, Dark green layers = low carbonate units. Foraminifera abundances are also shown, split into agglutinated (black), benthics (grey) and planktics (red).

cm is the UBM layer as defined in GC01, characterised by clay which is rich in Ti, very low levels of carbonates and large rises in Mn/K levels. At this point, foraminiferal assemblages change from calcareous to agglutinated with *Rhizomania*. *Algaeformis* dominating, as seen in GC01. No foraminifera are present above 12 cm until the end of BC06. This would support previous work (Asku, 1983; Simon et al., 2012) that suggest

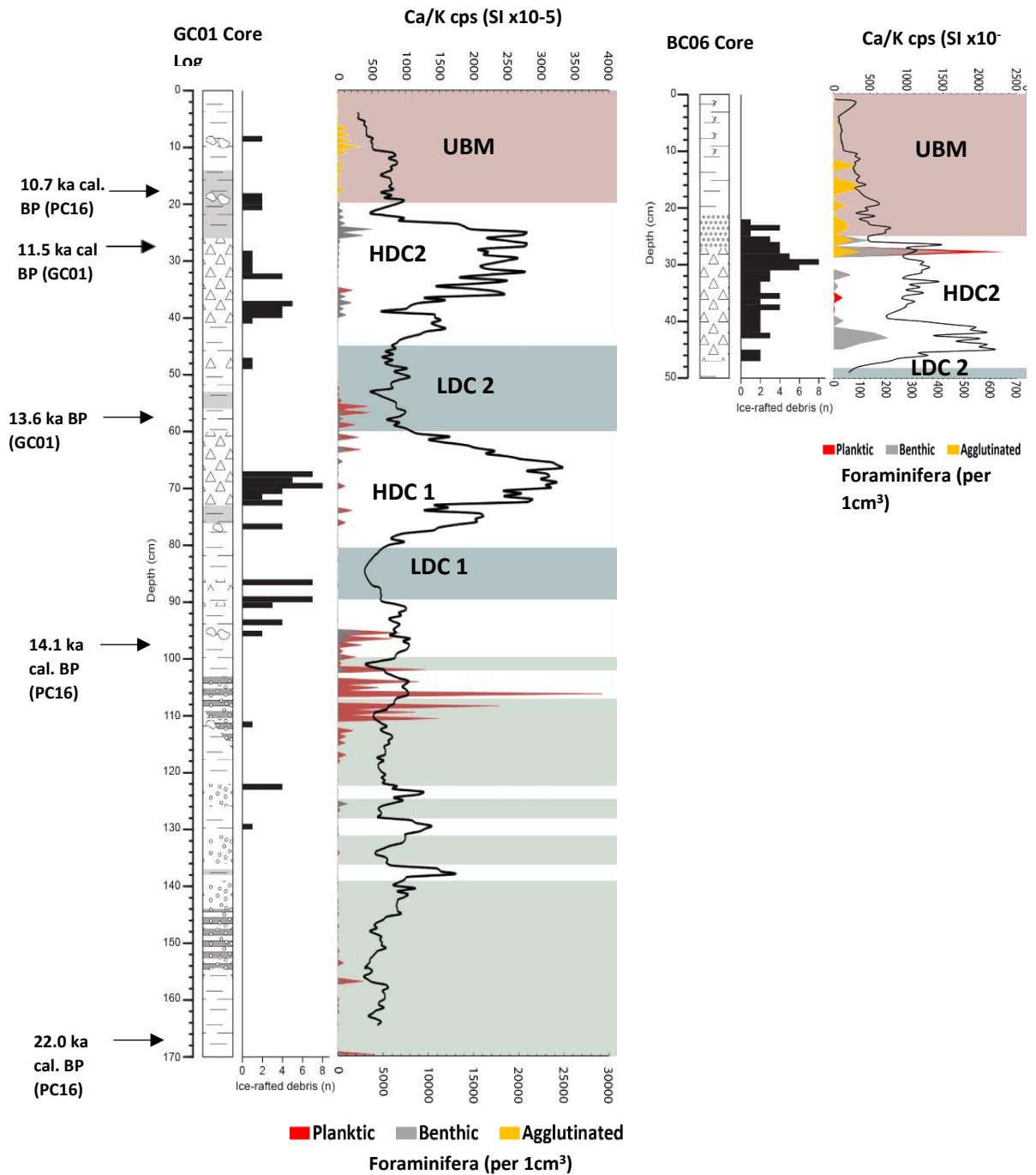


Figure 5.3: Comparisons of GC01 and BC06. Note that no ¹⁴C dates were extracted from BC06. High resolution combined images showing geochemical properties of GC01. Moving from left to right; simplified core log illustrating changes in stratigraphy with IRD counts plotted against depth. XRF showing calcium (Ca), manganese (Mn), iron (Fe), barium (Ba) measured against potassium (K). Colour coding has been used in order to split up major lithofacies based on sedimentology, physical and geochemical data. Red layer = uppermost brown mud unit, White layers = high carbonate units, often IRD rich, Dark green layers = low carbonate units. Foraminifera abundances are also shown, split into agglutinated (black), benthics (grey) and planktics (red).

that bottom water was particularly corrosive during the Holocene in Baffin Bay. Barium levels indicate higher levels of productivity during the Holocene than during the Younger Dryas stadial with levels rising sharply above 21 cm despite little foraminifera species diversity. However, this could reflect increases in other productivity marks not measured in this study such as algae, diatoms and dinocysts etc. In the uppermost 10 cm of BC06 there is evidence of bioturbation taking place with the UBM layer underlain by a darker grey sediment as displayed in Figure 4.4.

5.5 Summary of Interpretations GC01 and BC06:

GC01 and BC06 both exhibit interesting changes up core with large fluctuations in sedimentological, physical, geochemical and micropaleontological properties. This could suggest that during the Older Dryas and the Younger Dryas Stadials increased glacial erosion of carbonate rocks underneath the major ice sheets surrounding central Baffin Bay took place. Due to the vast majority of carbonate rocks being located on Baffin Island and in the Canadian Arctic this would also suggest that HDC layers are associated with large iceberg discharges from the (IIS) and the (LIS). Whereas periods of LDC, which are characterised by fine grained Ti-rich sediments could indicate changes in ice front position of the major ice sheets that surrounded Baffin Bay during the last 22 ka. Since LDC layers appear to occur during interstadial and interglacial periods ice front positions would be significantly less extensive than during HDC layers. This would support detailed studies of sediment origin (Simon et al., 2014;2016) which suggest that during major ice sheet retreats of the GIS, i.e. the initial LGM break up and the Holocene retreat, increased dilution of carbonates occurred in central Baffin Bay. Thus, resulting in low amounts of detrital carbonates during interstadial and interglacial periods. Foraminifera abundances are also supportive of this with near 0% preservation achieved during LDC layers in either GC01 or BC06 with preservation much higher during the Older Dryas and the Younger Dryas Stadials despite falling abundances in the middle of each Stadial. This suggests that dissolution in central Baffin Bay is severe, especially so during interstadial and interglacial periods as first documented by (Asku, 1983) with this corresponding to the Older Dryas and Younger Dryas Stadials and the Holocene in this study. Unfortunately, foraminiferal species diversity remained extremely low throughout both GC01 and BC06 so it was not possible to provide a full reconstruction of oceanographic change based on ecological changes for central Baffin Bay. Although there is evidence of a sharp change from *casidulina reneforme* (associated with glaciomarine conditions (Lloyd, 2008)) to *casidulina neoteritis* in GC01 above 98 cm which could indicate the presence of Atlantic water reaching central Baffin Bay around 15.0 Ka. BP during the initial LGM retreat due to *casidulina neoteritis* linked previously with water of Atlantic origin (Lubinski, Polyak and Forman, 2001; Lloyd, 2008). Although this study does not directly date foraminifera between 128-98 cm it is likely that sediment between this interval is of LGM in age as supported by this studies age-depth model and the presence of and with the presence of an extremely large bloom in planktics occurring just before the proposed end of the LGM at 107-98 cm. This could suggest that the WGC was much weaker during the LGM but began to strengthen again during sometime around 15.0 ka BP supporting recent work by (Jennings et al., 2017).

Chapter Six: Discussion:

6.1 Introduction:

This study synthesises the data presented in chapter 4 and 5 and compares to findings from this to well established long-term records. Due to the poor resolution/lack of proxy data present during the Holocene, (see chapter 4 for details), this chapter will primarily focus on developing a record of ice sheet instability and ocean productivity changes through the Late Pleistocene for central Baffin Bay.

6.2 The Timings and Dynamics of BBDC Events in central Baffin Bay during the last deglacial (15.5- 10.5 ka BP):

It is well-known that the transition from the LGM to the current interglacial was a period of rapid fluctuations in ice sheet volume, sea-level and temperature (Shakun and Carlson, 2010; Jackson et al., 2017). The deglacial chronology of Hudson Bay and the Labrador Sea has been heavily studied over the last several decades (e.g. MacAyeal, 1993; Broecker, 1994; Hemming, 2004) because of this a well-established chronology of meltwater events now exists. A series of significant events known as Heinrich events (Heinrich, 1988), reviewed in detail in chapter 2, primarily focus on discharges of meltwater from the south-eastern sector of the LIS. The driving forces of Heinrich events are likely complex with previous work attributing the events to either internal ice-sheet dynamics such as the binge-purge model (MacAyeal, 1993), which suggests that geothermal heat combined with increasing ice thickness crossed a threshold leading to sub-glacial melting as ice volume increased during the 'binge phase' creating a lubricated surface underneath the ice sheet which initiated the 'purge phase'. Other explanations attribute Heinrich events to external factors such as changes in solar output which could influence the timings of Dansgaard-Oeschger events and the release of freshwater into the North Atlantic (McManus et al., 2004). However, because primary focuses were directed towards the Heinrich events for so long, few studies until recently have researched the deglacial chronology of the ice sheets surrounding central Baffin Bay (Andrews et al., 2012, Simon et al., 2012; 2014; Jackson et al., 2017).

Through recent research it has been documented that large meltwater events also occurred in Baffin Bay as the north-eastern sector of the LIS, IIS and GIS retreated during the last deglaciation as temperatures rose since the LGM. These meltwater events are known as Baffin Bay Detrital Carbonate (BBDC) events, (detailed in chapter 2), occurred throughout the last interglacial-glacial cycle. Evidence from longer cores also raised from the abyssal plain of central Baffin Bay (Asku and Piper, 1987; Andrews et al., 1998; Simon et al., 2012; 2014; 2016) identify two events; BBDC 0 and BBDC 1 occurring during the last deglaciation. The exact timings of BBDC 0 and BBDC 1 have proved difficult to fully define due to very poor preservation of biogenic material for dating purposes, especially so during the Holocene when bottom waters were particularly corrosive (Asku, 1983). Magnetostratigraphic dating appears to have had some success in recent years on longer cores (Simon 2014; 2016) but there remains significant uncertainty surrounding the comparison of data due to significant amounts of noise present within datasets (Simon et al., 2016; Jackson et al., 2017).

Based on the detailed analysis of GC01 and BC06 presented in chapter 5 of this study along with previous work (Asku and Piper, 1987; Andrews and Ebrel, 2011; Simon et al., 2012) it is likely that the major high

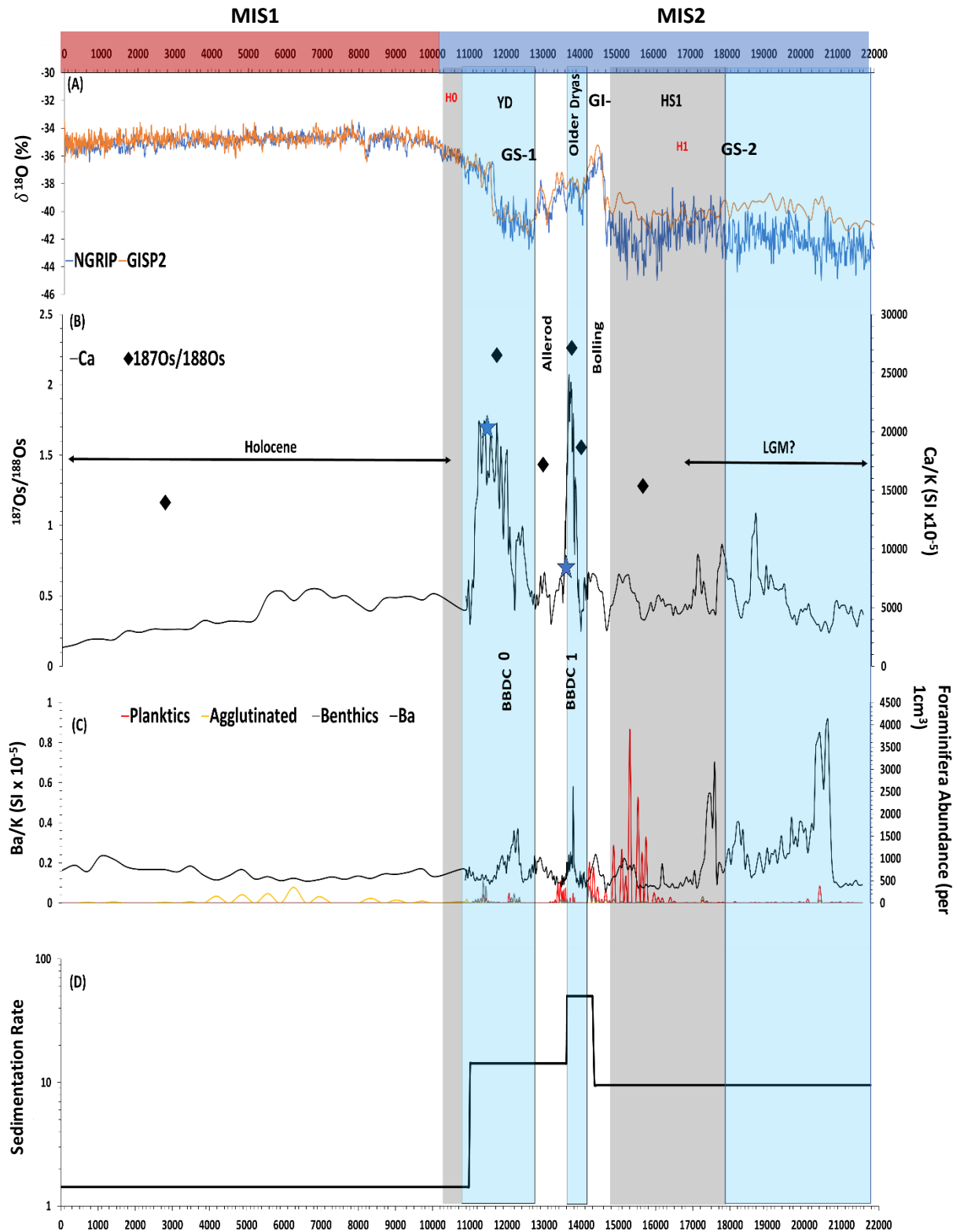


Figure 6.1: Comparisons of key data extracted from GC01 with GISP2 and NGRIP during the last 22ka. **(A)** GISP2 and NGRIP $\delta^{18}\text{O}$ ice core data with major stadials and interstadials highlighted as well as the current interglacial (Holocene) and the LGM. Marine Isotope stages are labelled at the top of the chart. BBDC events are also labelled with Heinrich events timings Hemming, (2004) and Heinrich Stadials timings Jennings, et al., (2015) and Marcott et al., (2011) shown by the grey shading. **(B)** XRF Ca/K data plotted against osmium isotopic ratios, positions of radiocarbon ages are represented by blue stars. **(C)** Ba/K ratios (productivity) plotted against abundances of planktic, agglutinated and benthic foraminifera. **(D)** Average sedimentation rates for GC01.

detrital carbonate (HDC) layers in GC01 and BC06 are associated with BBDC events previously identified (Asku, 1981; Hiscott et al., 1989; Andrews et al., 2014; Simon et al., 2012). In GC01 there are two BBDC events, clearly distinguishable in Figure 5.1 by rapid rises in calcium which is accompanied by significant increases in IRD along with large increases in sedimentation rates. The use of radiocarbon dating of two separate foraminiferal assemblages from GC01 dated the two BBDC events to 13.6 ka BP and 11.5 ka BP which is in very good agreement with recent studies from central Baffin Bay (e.g. Simon et al., 2016; Jackson et al., 2017). Due to the time restraints on this study and the severe dissolution of foraminifera present throughout both cores it was not possible to fully constrain the timings of each BBDC event. Nevertheless, it has been possible to establish a chronology for both BBDC 1 and BBDC 0 based on two ¹⁴C dates from calcareous foraminifera. Working up core, the first detrital carbonate event (BBDC 1), (see Figure 5.1) has been dated at 13.6 ka BP, which would be coeval with the end of the Older Dryas Stadial dated to have occurred between 13.6-14.2 ka BP (Fairbanks, 1990; Friedrich et al., 2001). Due to low foraminifera abundance during the peak in carbonates it was not possible to obtain a sample from the centre of BBDC 1. The second BBDC event (BBDC 0) was dated centrally in regards to the peak in carbonate due to higher foraminiferal abundances compared with BBDC 1. BBDC 0 was dated at 11.5 ka BP which would place it coeval with the middle of the Younger Dryas Stadial and correlates well with these cold events in the Greenland ice core records, GISP2 and NGRIP (see Figure 6.1).

The combination of the direct radio ages obtained from GC01 and the use of two extra tie-points based on correlation with core PC16 (Simon et al., 2012) highlight that both BBDC events are marked by an increase in sedimentation rates to approximately 80 cm/kyr during BBDC 1. Rates decrease slightly during BBDC 0 but still ten-fold higher than during the Holocene.

The timings of BBDC 1 and BBDC 0 while appearing to be coeval with the Older Dryas and the Younger Dryas Stadials respectively, they seem not to be synchronous with either Heinrich event 1 (H1) or Heinrich event 0 (H0), which both saw massive amounts of meltwater enter the North Atlantic through Hudson Strait, see Figure 6.1 for exact timings. The findings of this study suggest that BBDC 1 occurred after H1 and BBDC 0 occurred before H0, see Table 2 for more details.

BBDC EVENT NUMBER	Ages (ka BP) (Shown in Figure 6.1)	HEINRICH EVENT NUMBER	Ages (ka BP) (Jennings, 2015)
0	11.4-12.7	0	11.2-11.5
1	13.6-14.1	1	15.0-17.0

Table 4: BBDC events timings of this study as displayed in Figure 5.1 in comparison to the ages of Heinrich events documented in (Jennings, 2015).

BBDC 1 is likely to have occurred after H1 during the Older Dryas Stadial, completely out-of-phase with H1 by nearly 1 ka. Although it should be noted that the correlation with the Older Dryas is difficult to make due to

the stadial itself only lasting several hundred years, with BBDC 1 likely beginning before the end of the Allerød interstadial, peaking during the Older Dryas, and then ending at the start of the Bølling interstadial. Based on the chronology developed here, it would appear that BBDC 0 occurred within the agreed timeframe for the Younger Dryas but does not correspond with the release of meltwater associated with H0. In terms of the dynamics of sediment delivery during both BBDC 1 and BBDC 0 there are clear rises in sedimentation rates, IRD, and detrital carbonate delivery with osmium isotopic values also peaking, suggestive of significant iceberg calving into central Baffin Bay during the Older Dryas and Younger Dryas Stadials. Based on the surrounding geology of the landmasses that flank Baffin Bay it is likely that glacial erosion of basement carbonate rocks in northern Baffin Bay is the primary source of the influx in detrital carbonate, shown in Figure 6.2. Cores taken in shallower waters close to the western Greenland (Jackson et al., 2017) indicate that during BBDC 1 there is a large rise in Ca/K values whereas just off the coast of Baffin Island Ca/Ka levels were at very low levels. It would appear that this is linked to the counter-clockwise ocean circulation in Baffin Bay with glacially eroded carbonate rocks in northern Baffin Bay being transported south via the Baffin Bay current via major ice rafting from the Nares Strait, Lancaster Sound and Jones Sound (see Figure 5.2). This would then allow for these carbonate rich icebergs to interact with other smaller eastward flowing currents that flow into central Baffin Bay, which would agree with previous interpretations (Andrews et al., 1998; Andrews et al., 2011; Jackson et al., 2017). The mineralogy of both GC01 and BC06 during BBDC 0 and BBDC 1, presented in chapter 4, shows that fine grained material rich in Ti (which can be used as a proxy for terrigenous vs. biogenic influx, e.g. Asku and Piper, 1987; Hiscott et al., 1989; Simon et al., 2014; 2016) increases between these detrital carbonate events and diminishes to very low levels during BBDC events. This alternating pattern of high to low Ti ratios has been interpreted as changes in transport modes within Baffin Bay. Ti-rich sediments are associated with sediment influx from tertiary basalts on western Greenland with feldspar-rich layers also likely related to lateral transport from both Baffin Island and western Greenland (Asku and Piper, 1987; Simon et al., 2012;2016), due to advances and subsequent retreats of ice streams at these locations. Sediment flux from west Greenland and Baffin Island sources (Ti and feldspars) were likely diluted by the increased influx of carbonate rich material from northern Baffin Bay (Andrews and Eberl, 2011) which was delivered into central Baffin Bay via large amounts of iceberg discharge from northern ice streams during BBDC 1 and BBDC 0.

However, it is not possible to fully differentiate between sediment that has been transported from Baffin Island and that transported from west Greenland. Although through the use of XRD it has been proposed that the majority of the fine grained, Ti-rich sediment can be attributed to the Uummannaq region of western Greenland with sediments from eastern Baffin Island mainly found within BBDC layers (Simon et al., 2014;2016).

Oceanographic conditions during the last deglacial period have been investigated using foraminifera and also barium concentration as measures of paleo-productivity, see Figure 5.1. As described in chapter 4, foraminifera abundances appear to peak before and after BBDC 1 and BBDC 0 with near zero identifiable foraminifera present during peaks in detrital carbonate events. This could be due to increases in nutrient supplies from melting icebergs temporarily increasing surface water productivity, enabling blooms in foraminifera after periods of major ice sheet instability i.e. during BBDC 1 and BBDC 0. Barium ratios appear

to follow a similar pattern with peaks occurring before and after both enhanced detrital carbonate delivery events in central Baffin Bay supporting the idea of increased productivity directly before and after each event. Foraminifera abundances are very low throughout large proportions of Holocene sections of cores BC06 and GC01 with a single agglutinated species (*Rhizammina algaeformis*) dominant until the mid-Holocene after which very few foraminifera are preserved.

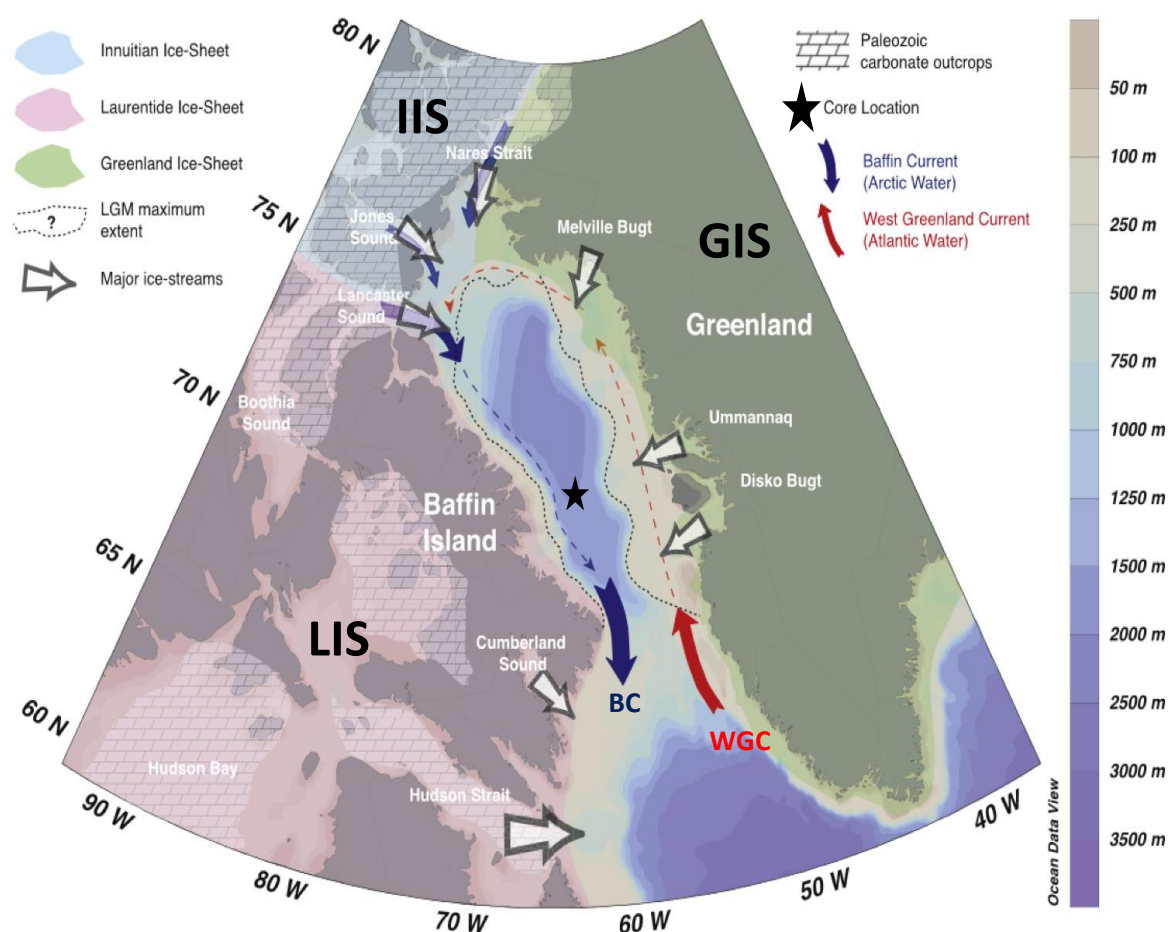


Figure 6.2: Geological map of Baffin Bay's bathymetry and major ocean currents; Baffin Current (BC) and West Greenland Current (WGC). A reconstruction of the LGM limits of the three major ice sheets that surrounded Baffin Bay are labelled; the LIS, IIT and the GIS. Major Palaeozoic outcrops are overlain with white hashed areas showing the locations of carbonate rocks. Modified from (Simon et al., 2016).

The deglacial chronology exhibited in core GC01 and BC06 of this study over the last 17 ka is in agreement with several recent studies from Baffin Bay (Parnell et al., 2007; Andrews et al., 2011; Simon et al., 2014; Jackson et al., 2017). It is therefore in support of two major separate periods of ice sheet instability during the transition from the LGM to the Holocene shown by enhanced detrital carbonate delivery during BBDC 1 and BBDC 0.

6.3 The Dynamics of the LGM in central Baffin Bay (22-15. 6 ka BP):

Interestingly, prior to the BBDC 1 event at 14.1-13. 6 ka BP there is no evidence for any older periods of enhanced carbonate delivery into central Baffin Bay in the last 22 ka, with radiogenic values from osmium isotopes falling back to low levels at 15.9 ka BP. Although, as shown in Figure 5.1, extremely high levels of planktonic foraminifera are present during this period without any notable increases in Barium or Ca/Ka

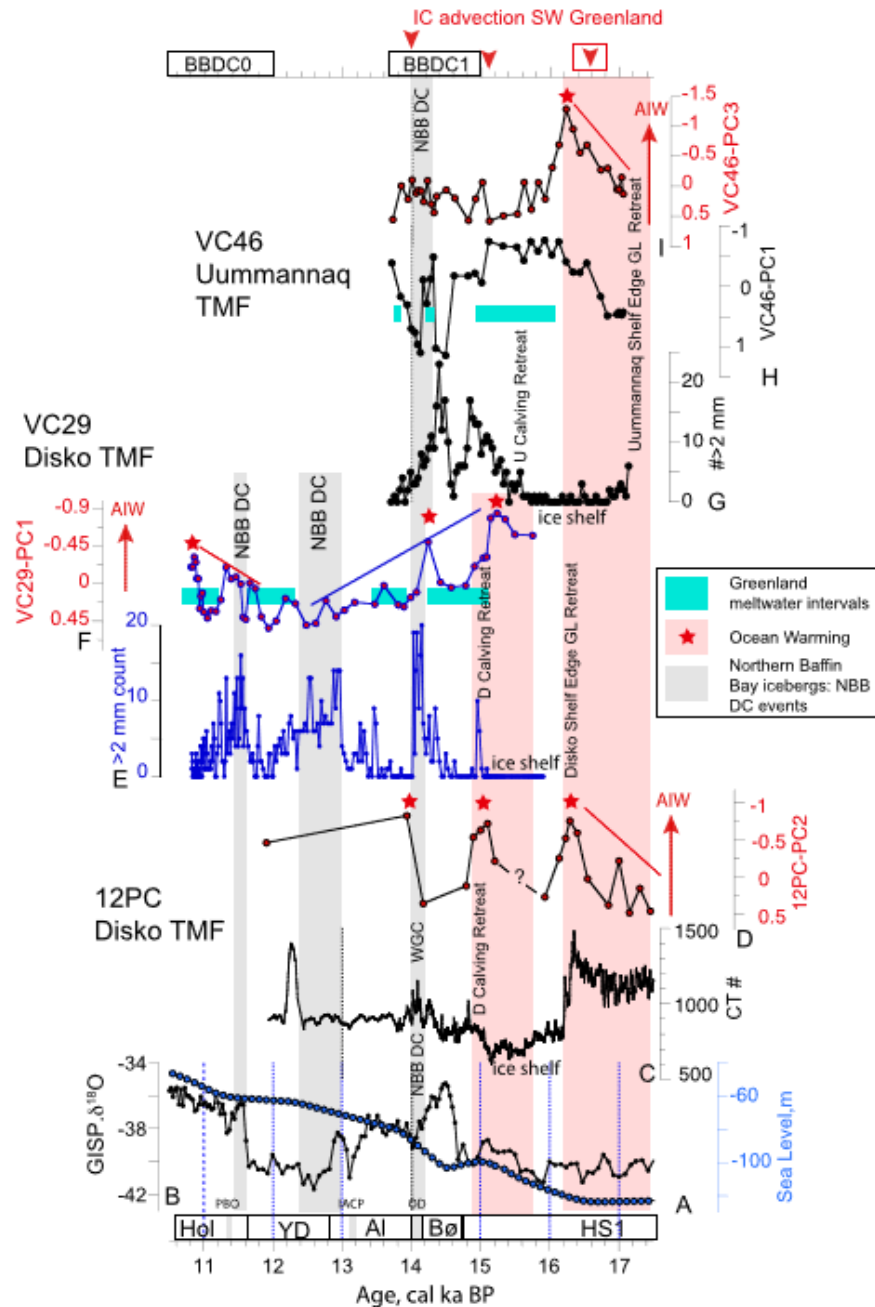


Figure 6.3: Comparison of main proxy records extracted from cores VC46, VC29 and 12PC along the west Greenland coast (Jennings et al., 2017). Proxy records are as follows; (C, E, G) ice rafting, (D, F, I) ocean warming and cooling (D,F,I) meltwater is shown by blue horizontal bars and sediment provenance by the grey bars. The GISP2 ice core record is also shown (A) along with eustatic sea-level (B). Interpretations of grounding line retreat, formation of the ice shelf and calving retreat are also displayed. Taken from (Jennings et al., 2017).

ratios. Nevertheless, a period of very high surface water productivity is indicated to have occurred between approximately 15.5-15.0 ka BP with planktic abundances exceeding 30,000 specimens per 4 ml at times.

Sedimentologically, this period is characterised by a sharp transition from clay to sand before a return to clay. The sand unit itself appears to have been dragged downcore along the edge of the core liner, see Figure 4.2, perhaps due to disturbance of sediment when the core was originally extracted. IRD is present during this period although in much smaller amounts than during BBDC 1 and BBDC 0. Based on the chronology presented here this corresponds to a period when the GIS was still yet to retreat from the shelf edge (O’Cofaigh et al., 2013), see Figure 6.3, it is expected that high amounts of sediment accumulation took place at the edge of the western Greenland continental shelf. It has been documented (Gilbert et al., 1998; Hesse et al., 1999) that sedimentation patterns on submarine slope edges is episodic creating phases of rapid mass movement downslope, as continental slopes become over steepened. This concept would fit well with the interbedding of clay-sand units present in GC01 just prior to, and then during the LGM in central Baffin Bay. Sand units are expected to be associated with turbidites that were transported onto the abyssal plain within large mass movements flowing down from the continental shelf edge on western Greenland. Fine clay units are more likely to be deposited during lower energy environments, in-between mass movements, when sedimentation rates are lower. This is further supported by the mineralogical data presented in Figures 4.8 and 4.9, with higher levels of fine grained Ti-rich sediment present between 22.0-15.5 ka BP which has previously been linked with sediment derived from the Uummannaq region (Simon et al., 2014) via the use of detailed XRD analysis alongside SedUnMix tuning calculation.

However, it should be noted that new research around the deglaciation of the GIS (Jennings et al., 2017) has very recently recovered evidence that indicates the ice retreat via calving began occurring by 15.1ka BP within Uummannaq Trough. This corresponds well to sedimentological data extracted from GC01 which clearly shows an increase in IRD around this period until approximately 14.5ka BP before ceasing until BBDC 1 event begins at approximately 14.1ka BP (Figure 6.1). It is also likely that a second phase and also third phase of calving occurred along the GIS at approximately 13.6ka BP and again at 11.6ka BP (Jennings et al., 2017) although these GIS events are currently difficult to detect in GC01 due to this time period being dominated by material associated with BBDC 1 and BBDC 0 events. Nevertheless, with the use of detailed mineralogical data analysis through the use of XRD it could well be possible in the future to differentiate between different sediment sources around these periods.

6.4 Interpretation of osmium Isotopes in Central Baffin Bay Deep Water:

The Osmium isotope data presented in this study is of particular interest as previous studies have radiogenic isotopes to reconstruct Pleistocene ice sheet fluctuation (Burton et al., 2010; Paquay and Ravizza, 2012). More recent studies (Rooney et al., 2016) have used Osmium isotopes to track Holocene variability of the GIS in Disko and Uummannaq Troughs. As described in chapter 4 of this study and displayed in Figure 6.1, highly radiogenic sediments are present during both BBDC 1 and BBDC 0 with much lower values present before, in-between, and after these events. Previous research (Rooney et al., 2016) found higher osmium isotope values in glaciomarine sediments delivered from Disko Bay ice streams. This would suggest that large

amounts of glaciomarine sediment were transported into central Baffin Bay in two separate phases circa 14.1-13.6 ka BP and 12.7-11.4 ka BP during deglaciation. The fact that highly radiogenic sediment is present in central Baffin Bay is interesting, partly due to this study being the first to use osmium isotopes in deep ocean sediments, but more importantly, because the presence of highly radiogenic material in a location so far away from any ice calving front is unusual.

In the context of tracking ice sheet variability high radiogenic values have previously been interpreted as 'ice proximal' (Rooney et al., 2016) due to high influxes of glacially eroded materials from proximal ice calving. Whereas when radiogenic values are low this would suggest a greater influence from less radiogenic open ocean sources (Rooney et al., 2016). However, this study records high osmium isotope values characteristic of proximal glaciomarine conditions in the centre of Baffin Bay. There is no evidence of any ice sheet in Baffin Bay extending further than the shelf edge over the last 22 Ka hence the location of GC01/BC06 is not expected to have been ice proximal over this time period. This would then suggest that in central Baffin Bay high radiogenic sediments are associated with high amounts of glaciomarine sedimentation from further afield locations. Hence during BBDC 1 and BBDC 0 large-scale ocean currents transported glaciomarine sediments from multiple sources between 15.5 – 10.5 Ka.BP with the IIS likely a major source of glaciomarine sediment during these two BBDC events. The low radiogenic value at approximately 15.5 Ka.BP, see Figure 6.1, is interesting as it falls within the timeframe of the initial LGM break up, when the marine area of Baffin Bay was increasing, although more radiocarbon dates are required to fully constrain this period.

Despite this, it would seem that osmium isotopes can be used in deep-sea locations that have never been ice proximal and still provide evidence of fluctuations in glaciomarine sediment flux from further afield. The results presented here highlight the need for more research investigating osmium isotopes from glaciomarine environments.

6.5 Summary of Central Baffin Bay Sediment Influx and Oceanographic Change (22-10.5 ka BP):

Between 22-10.5 ka BP there was likely to have been marked changes in sediment source origin related to increasing ice sheet instability. During the LGM when the GIS extended to the shelf edge it is likely that rapid deposition of turbidites (episodic in nature) took place from the Uummannaq region of Greenland and flowed into central Baffin Bay. However, it would seem plausible that some sediment influx from other lateral sources, such as the much smaller ice streams located on Baffin Island, could also reach central Baffin Bay, with LGM limits of the LIS also reaching the shelf edge of Baffin Island (Dyke et al., 2002). Although the elemental results presented in chapter 4 go some way in terms of showing the percentage increase of laterally sourced sediment (shown by K- Feldspar (GIS and LIS derived sediment) and Ti ratios (GIS derived sediment)) it is not possible to say exactly how much sediment was sourced from Baffin Island during and just after the LGM. The interbedding of fine grained Ti rich sediments with coarse sand units has been found in other deep-water cores (Simon et al., 2014;2016) extracted to the northwest of GC01 and BC06 and was attributed to stable and long duration GIS advance between 32-16 ka BP. This would support the proposal of a grounded, fast-flowing ice stream that reached the shelf edge and delivered glaciomarine sediments into central Baffin

Bay (O' Cofaigh et al., 2013). Therefore, it is likely that the very large planktonic foraminifera increase at approximately 15.5 ka BP is indicative of the first retreat of the GIS from the Uummannaq trough with large amounts of nutrients deposited in front of the ice calving margin producing very high levels of productivity in central Baffin Bay. These high levels of productivity would then decrease as the calving margin retreated further back onto the continental shelf during deglaciation.

During the transition between the LGM and the Holocene considerable oceanographic change is suggested to have taken place, see Figure 6.4. The LGM is characterised by ice sheet margins which extended to the shelf edge of both west Greenland and Baffin Island, with this acting to reduce the size of current marine area of Baffin Bay significantly. This extended reduction period in marine area of Baffin Bay appears to have reduced foraminifera abundances to almost zero for over 5Ka (between 21-16 ka BP), see Figure 6.1, during GIS advancement to the shelf edge. Results from various numerical simulation models (Ganopolski et al., 2010; Stokes et al, 2012), support the idea of a permanently sea ice-covered surface during the LGM, which would have reduced the strength of oceanic circulation in Baffin Bay. It is likely that the WGC was enhanced

during the Bølling and Allerød Interstadials (Greenland Interstadial 1), see Figure 5.1, resulting in the retreat of the GIS margins after 15.5 ka BP (Jennings et al., 2017) and a significant rise in surface water productivity as the marine area expanded. Along with a retreat of the GIS it has also been suggested (Marshall and Koutnik, 2006; Simon et al., 2014) that during these warmer interstadials events there was an increase in snowfall over the IIS, due to increased cyclonic activity, which combined with warmer temperatures enhanced the flow of icebergs from northern Baffin Bay. These carbonate rich icebergs would then have been transported south via the BC into central Baffin Bay which would produce the short lived BBDC 1 and BBDC 0 events in GC01. It is likely that the contribution of the IIS and the smaller ice streams on Baffin Island (LIS) is mostly during short-lived BBDC events, that occur during periods of major ice sheet instability. The contribution of major western

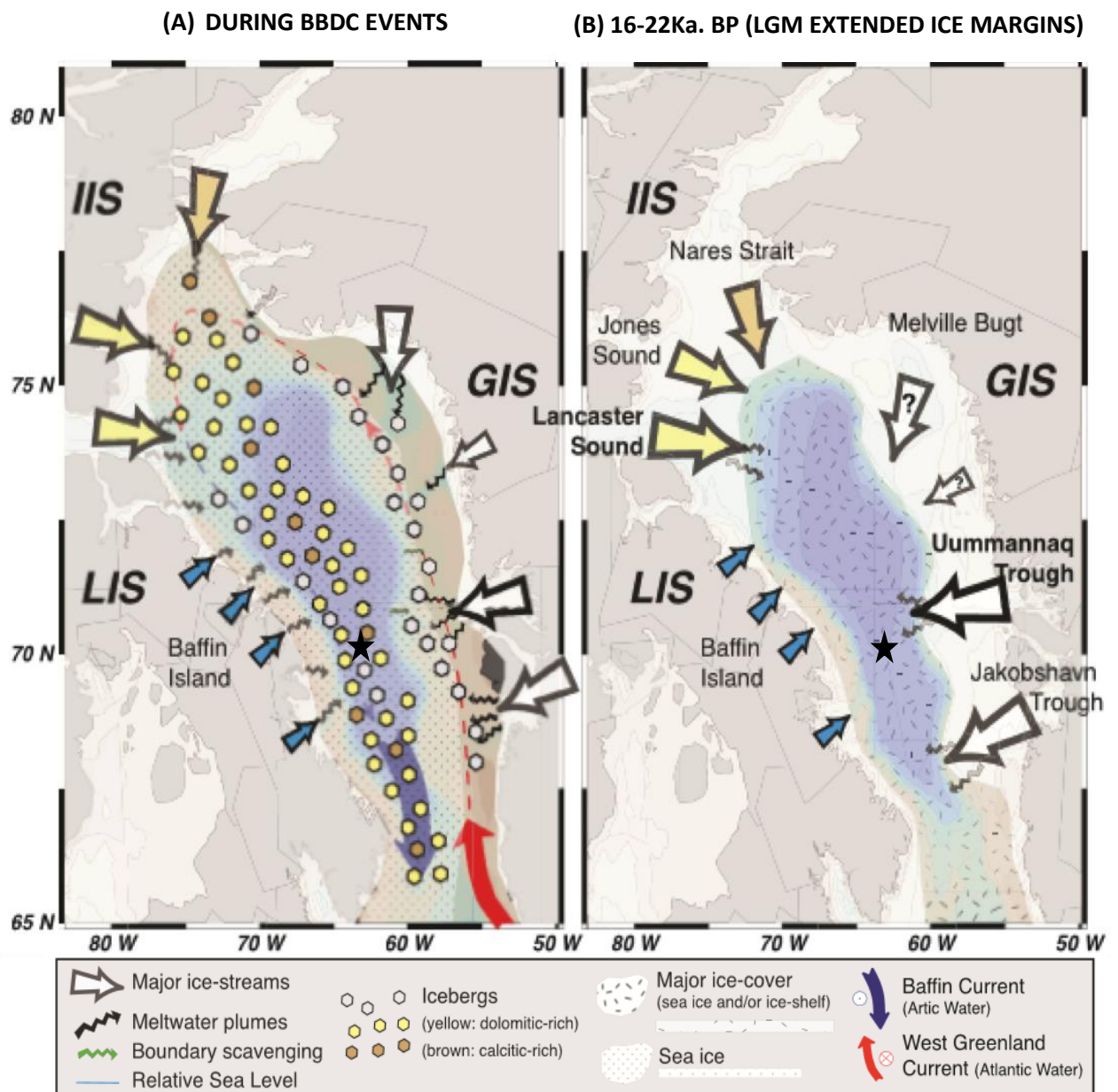


Figure 6.4: Oceanographic change in Baffin Bay between 10.5-22Ka.BP. **(A)** Visual representation of the oceanographic set-up during BBDC 0 and BBDC 1 with significant amounts of calcite laden IRD flowing south from the erosion of basement rocks on the IIS and from Lancaster and Jones Sounds into central Baffin Bay. **(B)** Oceanographic set-up during the LGM with extended ice margins with large influence from major west Greenland ice streams. (Modified from Simon et al., 2016).

Greenland ice streams during deglaciation appears limited (but still present). Due to ice distal conditions in central Baffin Bay during this period it is likely that warmer Atlantic water enhanced retreat after maximum ice extent was reached before 16.0 ka BP (Sheldon et al., 2016). It is also possible that due to such high amounts of material sourced from northern Baffin Bay sources that the finer sediment from western Greenland was simply diluted as represented in this studies XRF analysis (see Figure 4.8).

6.6 Summary of Ice Sheet Instability (22-10.5 ka BP):

Since the end of the LGM and the retreat of the GIS from the shelf edge after 16.0 ka BP there appears to have only been two periods of major ice sheet instability, BBDC 1 and BBDC 0, with only small amounts of sediment/IRD supply coming from the surrounding ice sheets before the onset of BBDC 1 approximately 14.1 ka BP. It is unlikely that these BBDC events are related to Heinrich events that occurred to the south. BBDC 1 and H1 occur very much out of phase with one another with BBDC 1 seemingly beginning during the late Bølling interstadial, perhaps peaking during the Older Dryas and then continuing into the Allerød interstadial. It remains difficult to pin-point the exact timings of BBDC 1 due to a lack of information regarding sedimentation rates but overall it would appear that BBDC 1 lagged Greenland warming, supporting the findings of (Jackson et al., 2017). The driving mechanisms behind BBDC 1 appears to be related to the destabilisation of the north-eastern LIS and the IIS which resulted in enormous and rapid amounts of iceberg calving from these areas. Despite BBDC 1 being completely out of phase with H1 it would seem from this studies timeseries (Figure 6.1), that BBDC 0 occurs just prior to H0 and during the Younger Dryas Stadial. However due to the lower resolution during this period in GC01 combined with the lack of foraminifera and biological constraints available it is not possible to say with certainty that BBDC 0 and H0 overlap with one another. Although recent core extractions which are of higher resolution than GC01 (Jennings et al., 2015) do suggest that BBDC 0 predates H0.

The early Younger Dryas re-advance of the GIS to the mid-outer shelf is likely to have been short-lived, perhaps only remaining at this position for 100 years or so (O'Cofaigh et al., 2013; Hogan et al., 2016) with rapid retreat onto the inner shelf by 12.0 ka BP. It is therefore likely that the instability of the GIS was more influential in terms of sediment delivery into central Baffin Bay during the initial LGM break-up around 16.0 ka BP as represented by high amounts of fine grained Ti-rich sediment and very high planktic abundances, see Figure 4.8. In contrast, the time period between 14.1-10.5 ka BP is dominated by significant ice sheet instability related to major iceberg calving from the north-eastern sector of the LIS and the IIS, although input from the GIS is still present sediment supply to central Baffin Bay is dominated by northern sourced material. Cosmogenic radionuclide dating of terraces in northern Baffin Bay and Lancaster Sound (Zreda et al., 1999; Ledu et al., 2010) support the idea of significant ice retreat from the northern areas of Baffin Bay during BBDC 0. Unfortunately, there is no data for BBDC 1, although it is unlikely given the exceptionally similar sedimentology, grain size and mineralogy of both events that a different mechanism was in place during BBDC 1. While the findings of this study suggest BBDC 0 and BBDC 1 are not coeval with H0 and H1 respectively, it has been documented (Andrews et al., 2014) that due to the oceanographic set-up in Baffin Bay it is likely that detrital carbonate flowed further south at times into the Davis Strait and Labrador Sea during BBDC

6.7 The Role of Ocean circulation changes and Climatic Forcing of major ice sheets surrounding Baffin Bay:

As already discussed based on sedimentological and geochemical data there were likely several periods of ice sheet instability during the last 22 ka relating to major melting of the LIS, IIS and the GIS. As illustrated in Figure 5.5, between 22.0 – 15.8 ka BP the main sediment source is likely to have been from the GIS due to its shelf-edge position, allowing for an enhanced delivery of relatively coarser grained sediment (sands) from turbidity currents onto the abyssal plain in central Baffin Bay. However, there is evidence of large-scale retreat of ice streams between 15.3-15.1 ka BP in cores collected from the shelf-edge of western Greenland adjacent to the Uummannaq trough (Jennings et al., 2017), linked to the retreat of the GIS from the shelf edge as subsurface ocean warming increased. Interestingly, it is likely that during the initial stages of retreat IRD was not produced due to buttressing by a combination of; a fringing ice shelf, persistent sea ice conditions and also the landward shallowing bathymetry of the Uummannaq trough system (Sheldon et al., 2016; Jennings et al., 2017). This interpretation fits well with the sedimentology and geochemical data extracted from GC01. GC01 shows significant changes in sedimentology between 15.8-15.0 ka BP with zero IRD present during this period, IRD levels then increase markedly between 15.0-14.5 ka BP, likely in relation to a second phase of sub-surface ocean warming (Jennings et al., 2017). Sub-surface ocean warming associated with strengthening of the WGC has been linked with earlier increases in the amount of advection of the Irminger Current off the coast of eastern Greenland (Kuijpers et al., 2003). Furthermore, intensification of the thermohaline circulation is likely to have taken place in the Northwest Atlantic and the Labrador Sea during this period, just prior to initial post LGM retreat of the GIS from the shelf-edge of western Greenland (Fagel et al., 1997). Radiocarbon chronologies (Sheldon et al., 2016) indicate that the GIS retreated to the mid-shelf and stabilised forming a large grounding-zone wedge where it remained until after the Younger Dryas cold stage before retreat into the fjords during the Holocene. During this relatively stable period western Greenland sediments would likely have been deposited on the shelf rather than onto the abyssal plain of central Baffin Bay.

However, based on the data extracted from GC01 it is likely that between approximately 14.1-13.6 ka BP and 12.7-11.4 ka BP (i.e. during BBDC 1 and BBDC 0) that regional and local dynamics played a major role in regulating sediment influx from northern Baffin Bay sources (see Figure 6.5). The short lived BBDC events as evidenced in GC01 have previously been correlated to external drivers such as Dansgaard-Oeschger cycles (Simon et al., 2014). Although it would initially appear that BBDC 1 is coeval with Greenland Interstadial 1 in longer-term records (Simon et al., 2012;2014), the higher resolution record extracted from GC01 shows it is more likely associated with the Older Dryas Stadial. Based on the chronology presented here BBDC 0 is likely to overlap with the Younger Dryas Stadial (based on comparison with the GISP2 ice core record see Figure 6.1). Although more radiocarbon dates are needed to fully constrain BBDC 0 which seems to be in relatively good correlation to the Younger Dryas, and especially BBDC 1 which currently appears to start during the Bølling Interstadial and continue into the Allerød Interstadial.

This supports the proposal of the north-eastern sector of the LIS being strongly influenced by local/regional changes in climate, with this sector of the ice sheet appearing to behave differently seemingly independent

of the temperature rises evidenced in the GISP2 record. It is therefore likely that the ice streams associated with the IIS were dynamically different to the larger ice streams present in western Greenland. However further work is needed to fully define the maximum extent of the LIS ice margin on Baffin Island and the to fully constrain the chronology of retreat since the LGM.

The large ice streams which flowed into Baffin Bay from the GIS appear to be influenced significantly by changes in ocean subsurface temperatures associated with strengthening of the WGC which lead to retreat of the GIS during the last deglaciation. This has been previously attributed to the re-invigoration of the Atlantic meridional overturning circulation (AMOC) after the Heinrich event 1 and to the lesser extent during the Younger Dryas (McManus, 2004; Stieglitz et al., 2007). The results of this study build upon and support recent findings by (Jackson et al., 2017) and further add to the evidence that large-scale iceberg discharges (i.e. during BBDC 1 and BBDC 0) acted to slow the AMOC (McManus et al., 2004).

Chapter Seven: Conclusions:

7.1 Conclusions:

This study has used multiple proxies to reconstruct environmental changes in central Baffin Bay linked to past ice sheet dynamics and palaeoceanographic changes over the last 22 ka. The comparison of the data extracted from GC01 and BC06 with previous studies in the area allows for the following conclusions to be made:

1) Two distinct periods of ice sheet instability occurred over the last 14.1 ka corresponding to previously identified Baffin Bay Detrital Carbonate events (BBDC 1 and BBDC 0).

Analysis of GC01 captured two periods of enhanced ice sheet instability characterised by increases in coarse and IRD rich sediment which is rich in carbonate. Based on radiocarbon dating and averaged sedimentation rates BBDC 1 occurred between 14.1- 13.6 ka BP and BBDC 0 occurred between 12.7-11. 4 ka BP. BBDC 1 and BBDC 0 are associated with 'ice distal' environments where ice margins had retreated behind their maximum extents after the LGM, with a more open marine area allowing for enhanced flow of icebergs into central Baffin Bay. These BBDC events therefore must have been produced by major iceberg discharge events to leave such a clear signal in the sedimentological record across much of Baffin Bay.

This is supportive of the high sedimentation rates that occurred during both BBDC 1 and BBDC 0 with the chronology extracted from GC01 matching near perfectly with recent work from eastern and western Baffin Bay by Jackson et al., 2017.

2) BBDC 1 and BBDC 0 are not coeval with Heinrich event 1 and Heinrich event 0.

BBDC 1 and BBDC 0 are not coeval with Heinrich event 1 or Heinrich event 0 in the Labrador Sea and the North Atlantic with recent analysis of Greenland ice core records placing H1 and H0 between 17.0-15. 0Ka.BP and 11.5-11.2 Ka. BP respectively (Jennings, 2015). The start of BBDC 1 (14. 1 ka BP) appears to start at the end of the Bølling Interstadial and end during the Allerød Interstadial with peaks in IRD associated with the Older Dryas Stadial, out-of-phase with Heinrich event 1 which ended approximately 0.9 ka before the start of BBDC 1 (see Figure 6.1). IRD associated with BBDC 0 peaks within the Younger Dryas Stadial which occurred between 12.8 – 11. 4 ka BP, although the correlation of BBDC 0 and the Younger Dryas is not perfect (see Figure 6.1). Also, the end of BBDC 0 is still poorly constrained but likely ends before the start of Heinrich event 0 (11.5-11.2 ka BP) with levels of IRD dropping after 11.4 ka BP. There is evidence that material from BBDC events could be transported further south out of Baffin Bay into the Davis Strait (Jennings, 2014), supporting the large-scale nature of these discharge events from northern Baffin Bay. This would imply that BBDC 0 event could have contributed to meltwater forcing of H0 in the northwest Atlantic.

3) Intense dissolution of biogenic carbonate occurs in-between BBDC 1 and BBDC 0 during interstadials and the Holocene.

Preservation of calcareous foraminifera in central Baffin Bay is near zero during the Bølling and Allerød Interstadials with the Holocene dominated solely by agglutinated species indicating a corrosive bottom water

environment. Productivity in central Baffin Bay increases significantly just after BBDC 1 and BBDC 0 likely due to large increases in nutrient availability from melting icebergs. Preservation of foraminifera in central Baffin Bay is generally low throughout the last 22 ka but does increase during periods of high sedimentation i.e. during BBDC 1 and BBDC 0. It is also likely that increases in marine productivity occurred as openings in the sea-ice began to develop and polynyas emerged creating an environment capable of sustaining marine life (Jennings et al., 2017).

Comparisons of foraminiferal abundances from GC01 to cores extracted from the continental slope of the Disko Trough Mouth Fan e.g. HU2008029-12PC (Jennings et al., 2017b) show very similar patterns in terms of preservation of foraminifera over the last 22ka. GC01 and 12PC also exhibit striking similarities in terms of timings of the large planktic spike at approximately 16. 1ka.BP and also again around BBDC 1 which has recently been linked to an increase in productivity after Heinrich Event 1 but within the Heinrich Stadial when Atlantic Water began to penetrate Baffin Bay and lead to the initial retreat of the GIS from the shelf edge of central west Greenland.

However, foraminiferal species diversity and abundances remain generally very low throughout the last 22 ka in central Baffin Bay. Except for the significant spikes in planktic foraminifera abundance around 15.5-15.3 ka BP, which are likely linked to increased nutrient supply from melting icebergs in central Baffin Bay as the GIS began to retreat from its shelf edge position (Ó Cofaigh et al., 2013) at the end of the LGM.

4) Opening of Baffin Bay to the northwest Atlantic occurred around 15.8-15.6 ka BP.

Analysis of foraminifera shows that as well as very large spikes in planktic foraminifera between 15.8-15.0 ka BP that there was a clear change from *Cassidulina reniforme* (glaciomarine indicator) during the LGM to *Cassidulina neoteretis* (Atlantic Water indicator) after approximately 15. 8 ka BP, (see Figure 4.11) which suggests that the West Greenland Current strengthened during this period and was able to penetrate further north and introduce relatively warmer waters into Baffin Bay. This supports recent work by -Jennings et al., (2017) with both changes in foraminifera ecology and the large spikes in planktic abundances appearing to coincide with the initial stages of retreat of the GIS from the shelf edge of western Greenland.

5) Initial retreat of the GIS from the shelf-edge of western Greenland likely occurred between 15.8-15.0 ka BP.

The first layer of IRD present in GC01 occurring between approximately 15.8-15. 0 ka BP is likely to be associated with initial retreat of the GIS based on sedimentological, physical and geochemical characteristics. Although it is not currently possible to give an exact date, this timeframe is supported by of recent work (Jennings et al., 2017).

6) Significant sediment provenance changes occurred during the last 22 ka in central Baffin Bay.

Analysis of lithofacies and elemental compositions (XRF) of GC01 and BC06 are supportive of a period of increased sediment influx from the GIS between approximately 22-15.5 ka BP characterised by fine grained Ti-rich sediment (Simon et al., 2014). It is likely that maximum ice extent occurred within this period associated with the expansion of the GIS to the shelf-edge during the LGM (Ó Cofaigh et al., 2013), enabling

large amounts of sediment to be transported via slope processes and within turbidity currents onto the abyssal plain. In contrast during the short-lived BBDC 1 and BBDC 0 events coarse-grained sediments rich in carbonates are attributed to the large-scale release of carbonate rich IRD eroded from carbonate-rich basements rocks by the north-eastern sector of the LIS and also the IIS. The amount of carbonate-rich materials preserved in cores GC01 and BC06 suggests a major break up event from these ice sheets surrounding northern Baffin Bay.

The reasons behind the differences in timings of iceberg flux between the GIS and the more northern sourced LIS and IIS are likely complex, however the results from this study suggest there were significant differences in the timings of iceberg discharges from the GIS and the LIS/IIS. It is likely that these differences in timings are related to the more northerly sectors of the LIS and IIS being more susceptible to local/regional changes in climate and/or influenced by internal ice sheet dynamics. In contrast, the major ice streams of western Greenland, appear to have been influenced significantly by the inflow and strengthening of the WGC bringing relatively warmer water after the LGM and general warming driving deglaciation.

The drivers responsible for the different timings in responses of the various ice sheets surrounding Baffin Bay remain poorly understood. Although currently speculative, it remains plausible that due to the reduced inflow of Arctic Water from the Nares Strait due to it being blocked by grounded glacier ice during deglaciation (Knudsen et al., 2008), that relatively warm Atlantic Water may have been able to reach northernmost Baffin Bay during BBDC 1 and BBDC 0. This would aid in the major release of icebergs during BBDC 1 and BBDC 0 from northern Baffin Bay sources and could be responsible for the time lag between the initial GIS retreat around 15.5 ka BP and the start of BBDC 1 at 14.1 ka BP. However, this would not explain why BBDC 1 and BBDC 0 occurred during cold stadial conditions during the Older Dryas and the Younger Dryas therefore the drivers behind both events could be linked to internal ice sheet dynamics of the IIS and LIS.

7) Evidence of decoupling of the LIS and the IIS to the AMOC during deglaciation.

Based on comparisons of sedimentological, geochemical and physical data with the timeseries shown in Figure 5.1, it appears that BBDC 1 began during the Bølling Interstadial and continued into the Allerød Interstadial with peaks in detrital carbonates coinciding with the Older Dryas Stadial. Based on the evidence presented here there does not seem to be a perfect correlation between climate events and BBDC events. However, the timings associated with BBDC events suggest that iceberg flux did occur during both Stadial and Interstadial periods. This would indicate that large amounts of iceberg discharge occurred from the LIS and IIS during Interstadials, meaning that BBDC events may not correlate with the AMOC variability, with the AMOC possibly still influenced by meltwater flux from the LIS and Heinrich events.

This supports recent work (Bohm et al., 2014) with the results of this study suggesting that the AMOC was not directly affected by sub-millennial meltwater pulses, rather major slowdowns only occurred during glacial maximum. This would also suggest that the initial trigger for the start of BBDC events are not necessarily linked to temperatures changes on Greenland with BBDC events occurring during both stadials and interstadial conditions (see Figure 6.1 for details) as seen in the longer records of Simon et al., (2012;2014;2016), in support of interpretations presented by Jackson et al., (2017). This suggests that the

northeastern sector of the LIS and the IIS were likely decoupled from the North Atlantic climate driver during the last deglaciation and perhaps during previous deglaciations too.

8) IP₂₅ is not present in any samples collected from central Baffin Bay.

Variations in sea-ice concentrations over the last 22 ka were not able to be reconstructed for the purposes of this study due to no evidence of IP₂₅ in any of the twelve samples extracted from GC01. Reasons as to why this was the case are not discussed in this study but do require future investigation. Since IP₂₅ has been found in previous cores from Baffin Bay it would be worthwhile to conduct more sampling on GC01 at a higher resolution in order to give a more complete insight into ice conditions in deep central Baffin Bay over the last 22ka.

7.2 Future research in central Baffin Bay:

Further research is needed in Baffin Bay in order to establish both short-term and longer-term ice sheet dynamics of the understudied northern ice streams/glaciers of the LIS/IIS/GIS. The results from this study indicate that the influence of BBDC 1 and BBDC 0 were extensive across Baffin Bay, with material associated with these large-scale discharge events also likely to have been transported and deposited in the Davis Strait and Labrador Sea. Therefore, it is essential that future research focuses on developing a robust high-resolution chronology of BBDC events and also of ice sheet advance and retreat in Baffin Bay since the LGM as well as over the last glacial cycle (e.g. Simon et al., 2016). This in turn will also allow for a greater understanding of the main drivers of ice sheet fluctuations and associated sea-level changes during the late Quaternary.

7.3 Recommendations for future analysis (GC01 and BC06):

1) Development of a stronger age-depth model.

Despite very low abundances of foraminifera it should be possible to extract more samples for radiocarbon dating. This would provide an age estimation for the bottom i.e. the full length of GC01 to better define sedimentation rates and to give a maximum age for the core. It may also be possible to give an age for the initial retreat of the GIS from the shelf edge at the end of the LGM by using the spike in planktic foraminifera at 107 cm. This would provide a stronger age-depth model and give a more detailed look at changes in sedimentation rates over the last 22 ka in central Baffin Bay. Specific attention should be focused on fully constraining BBDC 1 in relation to the GISP2 and NGRIP ice core records to determine its full extent and overlap into the Bølling and Allerød Interstadials. Better time constraint on BBDC 0 would also be beneficial in order to confirm whether there was any overlap between BBDC 0 and H0.

2) XRD analysis of GC01.

XRD analysis would provide specific mineralogical data for central Baffin Bay for the last 22 ka. This should make it possible to pick out Ti-rich layers with XRD that should correspond to clay layers (see Simon et al.,

2014) in GC01. This would allow for a better understanding of provincial sediment delivery patterns during the LGM and during deglaciation.

3) Higher resolution Osmium isotope analysis.

In order to better reconstruct glaciomarine sediment delivery into central Baffin Bay during the LGM, BBDC 1 and BBDC 0, finer sampling intervals for Osmium isotopes are required throughout the full length of GC01. Higher resolution analysis will help in improving our understanding of how osmium isotopes can help in interpretation of glacial erosion and sediment provenance/ delivery from glaciated margins.

4) Re-sample for IP₂₅.

Although IP₂₅ was not found in GC01 at any of the chosen sample points it has been found in other cores extracted from the West Greenland margin (e.g. Jennings et al., 2014; Jennings et al., 2017). Therefore, it would be beneficial for future research to take samples for IP₂₅ at a much higher resolution especially so between approximately 100-20 cm in GC01 in order to assess the level of sea ice in central Baffin Bay since the LGM.

References:

- Arctic Monitoring And Assessment Programme, (2016), Research Projects, 'Major Currents in the North Atlantic Ocean', Available at: <http://www.amap.no/documents/doc/major-surface-currents-in-the-north-atlantic-ocean/458>, (Accessed 6/1/16).
- Aksu, A.E., (1981) 'Late Quaternary stratigraphy, paleoenvironmentology and sedimentation history of Baffin Bay and Davis Strait' PhD, Thesis, to be published by *Dalhousie University*, Halifax, NS.
- Asku, A.E, (1983) 'Holocene and Pleistocene dissolution cycles in deep sea cores of Baffin Bay and Davis Strait: Paleoceanographic implications' *Marine Geology*, Volume: 53, 331-348.
- Aksu, A.E., (1984)., 'Subaqueous debris flow deposits in Baffin Bay'. *Geo-Marine Letters*, 4(2), pp.83-90.
- Aksu, A.E. and Hiscott, R.N., (1989) 'Slides and debris flows on the high-latitude continental slopes of Baffin Bay' *Geology*, 17(10), pp.885-888.
- Aksu, A. & Piper, D. J. W. (1979) 'Baffin Bay in the past 100,000yr' *Geology*, Volume: 7, 245–248.
- Aksu, A.E, Piper, D.J.W., (1987) 'Late Quaternary sedimentation in Baffin Bay' *Canadian Journal of Earth Sciences*, 24, pp. 1833–1846.
- Aksu, A.E., De Vernal, A. and Mudie, P.J., (1989) 'High resolution foraminifer, palynologic and stable isotopic records of Upper Pleistocene sediments from the Labrador Sea: paleoclimatic and paleoceanographic trends' In: S.P. Srivastava, M. Arthur, B. Clement et al., *Proc. ODP Sci. Res.*, Volume: 105: pp.617-652.
- Alvarez-Solas, J. and Ramstein, G., (2011) 'On the triggering mechanism of Heinrich events', *Proceedings of the National Academy of Sciences*, 108(50), pp.1359-1360.
- Andrews, J.T., (1998) 'Abrupt changes (Heinrich events) in late Quaternary North Atlantic marine environments: a history and review of data and concepts' *Journal of Quaternary Science*, 13(1), pp.3-16.
- Andrews, J.T. and Eberl, D.D., (2011) 'Surface (sea floor) and near-surface (box cores) sediment mineralogy in Baffin Bay as a key to sediment provenance and ice sheet variations' *Canadian Journal of Earth Sciences*, 48(9), pp.1307-1328.
- Andrews, J.T., Evans, L.W., Williams, K.M., Briggs, W.M., Jull, A.J.T., Erlenkeuser, H. and Hardy, I., (1990) 'Cryosphere/ocean interactions at the margin of the Laurentide Ice Sheet during the Younger Dryas chron: SE Baffin shelf, Northwest Territories' *Paleoceanography*, 5(6), pp.921-935.
- Andrews, J.T., Gibb, O.T., Jennings, A.E. and Simon, Q., (2014) 'Variations in the provenance of sediment from ice sheets surrounding Baffin Bay during MIS 2 and 3 and export to the Labrador Shelf Sea: site HU2008029-0008 Davis Strait' *Journal of Quaternary Science*, 29(1), pp.3-13.
- Andrews, J.T. and Ives, J.D., (1978) 'Cockburn Nomenclature and the Late Quaternary History of the Eastern Canadian Arctic' *Arctic and Alpine Research*, pp.617-633.
- Azetsu-Scott, K., Clarke, A., Falkner, K., Hamilton, J., Jones, E.P., Lee, C., Petrie, B., Prinsenberg, S., Starr, M. and Yeats, P., (2010) 'Calcium carbonate saturation states in the waters of the Canadian Arctic Archipelago and the Labrador Sea' *Journal of Geophysical Research: Oceans*, 115(C11).

- Bard, E., Fairbanks, R.G. and Hamelin, B., (1992) 'How accurate are the U-Th ages obtained by mass spectrometry on coral terraces' *In Start of a Glacial* (pp. 15-21). Springer: Berlin, Heidelberg.
- Belt, S.T, Brown, T.A, Rodriguez, A.N, Sanz, P.C, Tonkin.A., Ingle.R., (2012) 'A reproducible method for the extraction, identification and quantification of Arctic sea ice proxy IP25 from marine sediments' *Analytical Methods*, 4, pp. 705.
- Belt, S.T., Massé, G., Rowland, S.J., Poulin, M., Michel, C. and LeBlanc, B., (2007) 'A novel chemical fossil of palaeo sea ice: IP 25' *Organic Geochemistry*, 38(1), pp.16-27.
- Belt, S.T. and Müller, J., (2013) 'The Arctic sea ice biomarker IP 25: a review of current understanding, recommendations for future research and applications in palaeo sea ice reconstructions' *Quaternary Science Reviews*, 79, pp.9-25.
- Benn, D.I., and Evans, D.J.A., (1998) 'Glaciers and glaciation' London: Arnold, p.734.
- Bennike, O., (2004) 'Holocene sea-ice variations in Greenland: onshore evidence' *The Holocene*, 14(4), pp.607-613.
- Bennike, O. and Björck, S., (2002) 'Chronology of the last recession of the Greenland Ice Sheet' *Journal of Quaternary Science*, 17(3), pp.211-219.
- Berger, A., (1988) 'Milankovitch theory and climate' *Reviews of geophysics*, 26(4), pp.624-657.
- Berger, W.H., (1990) 'The Younger Dryas cold spell—a quest for causes' *Global and Planetary Change*, 3(3), pp.219-237.
- Berger, A., Mélice, J.L. and Loutre, M.F., (2005) 'On the origin of the 100-kyr cycles in the astronomical forcing', *Paleoceanography*, 20(4).
- Berger, A., Li, X.S. and Loutre, M.F., (1999) 'Modelling northern hemisphere ice volume over the last 3Ma', *Quaternary Science Reviews*, 18(1), pp.1-11.
- Bernhard, J.M. and Sen Gupta, B.K., (1999) 'Foraminifera of oxygen-depleted environments' *Modern foraminifera*, pp.201-216.
- Bernier, M.M., de Vernal, A., Hillaire-Marcel, C. and Moros, M., (2014). 'Paleoceanographic changes in the Disko Bugt area, West Greenland, during the Holocene'. *The Holocene*, 24(11), pp.1573-1583.
- Blake Jr, W., (1992) 'Holocene emergence at Cape Herschel, east-central Ellesmere Island, Arctic Canada: implications for ice sheet configuration' *Canadian Journal of Earth Sciences*, 29(9), pp.1958-1980.
- Blott, S.J. and Pye, K., (2001) 'GRADISTAT: a grain size distribution and statistics package for the analysis of unconsolidated sediments' *Earth surface processes and Landforms*, 26(11), pp.1237-1248.
- Böhm, E., Lippold, J., Gutjahr, M., Frank, M., Blaser, P., Antz, B., Fohlmeister, J., Frank, N., Andersen, M.B. and Deininger, M., (2015) 'Strong and deep Atlantic meridional overturning circulation during the last glacial cycle' *Nature*, 517(7532), p.73.
- Bond, G., Broecker, W., Johnsen, S., McManus, J., Labeyrie, L., Jouzel, J. and Bonani, G., (1993) 'Correlations between climate records from North Atlantic sediments and Greenland ice', *Nature*, 365(6442), pp.143-147.
- Bond, G.C. and Lotti, R., (1995) 'Iceberg discharges into the North Atlantic on millennial time scales during the last glaciation' *Science*, 267(5200), pp.1005.

- Bond, G., Showers, W., Cheseby, M., Lotti, R., Almasi, P., Priore, P., Cullen, H., Hajdas, I. and Bonani, G., (1997) 'A pervasive millennial-scale cycle in North Atlantic Holocene and glacial climates' *Science*, 278(5341), pp.1257-1266.
- Briner, J.P., Miller, G.H., Davis, P.T., Bierman, P.R. and Caffee, M., (2003) 'Last Glacial Maximum ice sheet dynamics in Arctic Canada inferred from young erratics perched on ancient tors' *Quaternary Science Reviews*, 22(5), pp.437-444.
- Briner, J.P., Overeem, I., Miller, G. and Finkel, R., (2007) 'The deglaciation of Clyde Inlet, northeastern Baffin Island, Arctic Canada' *Journal of Quaternary Science*, 22(3), pp.223-232.
- Broecker, W.S., (1994) 'Massive iceberg discharges as triggers for global climate change', *Nature*, 372, pp.421-424.
- Broecker, W.S., Bond, G., Klas, M., Bonani, G. and Wolfli, W., (1990) 'A salt oscillator in the glacial Atlantic? 1. The concept', *Paleoceanography*, 5(4), pp.469-477.
- Broecker, W., Bond, G., Klas, M., Clark, E. and McManus, J., (1992), 'Origin of the northern Atlantic's Heinrich events', *Climate Dynamics*, 6(3-4), pp.265-273.
- Broecker, W.S. and Donk, J., (1970) 'Insolation changes, ice volumes, and the O18 record in deep-sea cores' *Reviews of Geophysics*, 8(1), pp.169-198.
- Bromwich, D.H., Toracinta, E.R., Wei, H., Oglesby, R.J., Fastook, J.L. and Hughes, T.J., (2004) 'Polar MM5 simulations of the winter climate of the Laurentide Ice Sheet at the LGM' *Journal of Climate*, 17(17), pp.3415-3433.
- Brown, T.A., Belt, S.T., Philippe, B., Mundy, C.J., Massé, G., Poulin, M. and Gosselin, M., (2011) 'Temporal and vertical variations of lipid biomarkers during a bottom ice diatom bloom in the Canadian Beaufort Sea: further evidence for the use of the IP25 biomarker as a proxy for spring Arctic sea ice' *Polar Biology*, 34(12), pp.1857-1868.
- Buch, E., (2002) 'Present oceanographic conditions in Greenland waters' *Copenhagen: Danish Meteorological Institute*, pp. 1-39, Scientific Report 02-02.
- Buch, E. and Stein, M., (1989) 'Environmental Conditions off West Greenland, 1980-85', J. Northwest. Atlantic' *Fish. Science*, 9(8), pp.1-89.
- Carlson, A.E., LeGrande, A.N., Oppo, D.W., Came, R.E., Schmidt, G.A., Anslow, F.S., Licciardi, J.M. and Obbink, E.A., (2008) 'Rapid early Holocene deglaciation of the Laurentide ice sheet' *Nature Geoscience*, 1(9), pp.620-624.
- Carlson, A.E. and Winsor, K., (2012) 'Northern Hemisphere ice-sheet responses to past climate warming' *Nature Geoscience*, 5(9), pp.607-613.
- Carstens, J., Hebbeln, D. and Wefer, G., (1997) 'Distribution of planktic foraminifera at the ice margin in the Arctic (Fram Strait)' *Marine Micropaleontology*, 29(3), pp.257-269.
- Charles, C.D. and Fairbanks, R.G., (1992) 'Evidence from Southern Ocean sediments for the effect of North Atlantic deep-water flux on climate', pp.416-419.
- Chapman, M.R. and Shackleton, N.J., (2000) 'Evidence of 550-year and 1000-year cyclicities in North Atlantic circulation patterns during the Holocene', *The Holocene*, 10(3), pp.287-291.
- Clemens, S.C. and Tiedemann, R., (1997) 'Eccentricity forcing of Pliocene–early Pleistocene climate revealed in a marine oxygen-isotope record', *Nature*, 385(6619), pp.801-804.

- Cofaigh, C.Ó., Dowdeswell, J.A., Jennings, A.E., Hogan, K.A., Kilfeather, A., Hiemstra, J.F., Noormets, R., Evans, J., McCarthy, D.J., Andrews, J.T. and Lloyd, J.M., (2013) 'An extensive and dynamic ice sheet on the West Greenland shelf during the last glacial cycle' *Geology*, 41(2), pp.219-222.
- Coope, G.R., Lemdahl, G., Lowe, J.J. and Walkling, A., (1998) 'Temperature gradients in northern Europe during the last glacial–Holocene transition (14-9 14C kyr BP) interpreted from coleopteran assemblages' *Journal of Quaternary Science*, 13(5), pp.419-433.
- Coulthard, R.D., Furze, M.F., Pieńkowski, A.J., Nixon, F.C. and England, J.H., (2010). 'New marine ΔR values for Arctic Canada'. *Quaternary Geochronology*, 5(4), pp.419-434.
- Crane, R.G., (1978) 'Seasonal variations of sea ice extent in the Davis Strait-Labrador Sea area and relationships with synoptic-scale atmospheric circulation' *Arctic*, pp.434-447.
- Croudace, I., A. Rindby and Rothwell.R., (2006) 'ITRAX: Description and evaluation of a new multi-function X-ray core scanner', *New Techniques in Sediment Core Analysis, Geological Society. Special. Publication*, 51 pp. 267.
- Cuffey, K.M. and Clow, G.D., (1997) 'Temperature, accumulation, and ice sheet elevation in central Greenland through the last deglacial transition' *Journal of Geophysical Research: Oceans*, 102(C12), pp.26383-26396.
- Cuny, J., Rhines, P.B. and Kwok, R., (2005) 'Davis Strait volume, freshwater and heat fluxes' *Deep Sea Research Part I: Oceanographic Research Papers*, 52(3), pp.519-542.
- Darling, K.F., Wade, C.M., Stewart, I.A., Kroon, D., Dingle, R. and Brown, A.J.L., (2000) 'Molecular evidence for genetic mixing of Arctic and Antarctic subpolar populations of planktonic foraminifers' *Nature*, 405(6782), pp.43-47.
- Davis, P.T., (1985) 'Neoglacial moraines on Baffin Island. *Quaternary Environments: Eastern Canadian Arctic, Baffin Bay and Western Greenland*', Allen and Unwin: London, pp.682-718.
- Dey, B., (1981) 'Monitoring winter sea ice dynamics in the Canadian Arctic with NOAA-TIR images' *Journal of Geophysical Research: Oceans*, 86(C4), pp.3223-3235.
- Dowdeswell, J.A., Maslin, M.A., Andrews, J.T. and McCave, I.N., (1995) 'Iceberg production, debris rafting, and the extent and thickness of Heinrich layers (H-1, H-2) in North Atlantic sediments' *Geology*, 23(4), pp.301-304.
- Dunbar, M., (1973) 'Ice regime and ice transport in Nares Strait' *Arctic*, pp.282-291.
- Dunbar, M.J., (1951) 'Eastern Arctic Waters: A Summary of Our Present Knowledge of the Physical Oceanography of the Eastern Arctic Area, from Hudson Bay to Cape Farewell and from Belle Isle to Smith Sound' *Fisheries Research Board of Canada*.
- Dunbar, M. & Dunbar, M. J. (1972) 'The history of the North Water' *Proceedings of the Royal Society of Edinburgh B*, 72, 231–241.
- Dyke, A.S., Andrews, J.T., Clark, P.U., England, J.H., Miller, G.H., Shaw, J. and Veillette, J.J., (2002) 'The Laurentide and Innuitian ice sheets during the last glacial maximum' *Quaternary Science Reviews*, 21(1), pp.9-31.
- Dymond, J., Collier, R., McManus, J., Honjo, S., Manganni, S., (1992) 'Can the aluminium and titanium contents of ocean sediments be used to determine the paleoproductivity of the oceans?' *Paleoceanography*, 12, pp.586–593.

- Elkibbi, M. and Rial, J.A., (2001) 'An outsider's review of the astronomical theory of the climate: is the eccentricity-driven insolation the main driver of the ice ages?' *Earth-Science Reviews*, 56(1), pp.161-177.
- Enderlin, E.M. and Howat, I.M., (2013) 'Submarine melt rate estimates for floating termini of Greenland outlet glaciers (2000–2010)', *Journal of Glaciology*, 59(213), pp.67-75.
- England, J., (1999) 'Coalescent Greenland and Innuitian ice during the last glacial maximum: revising the Quaternary of the Canadian High Arctic', *Quaternary Science Reviews*, 18(3), pp.421-456.
- England, J., Atkinson, N., Bednarski, J., Dyke, A.S., Hodgson, D.A. and Cofaigh, C.Ó., (2006) 'The Innuitian Ice Sheet: configuration, dynamics and chronology', *Quaternary Science Reviews*, 25(7), pp.689-703.
- Fagel, N., Hillaire-Marcel, C. and Robert, C., (1997) 'Changes in the Western Boundary Undercurrent outflow since the Last Glacial Maximum, from smectite/illite ratios in deep Labrador Sea sediments' *Paleoceanography*, 12(1), pp.79-96.
- Fairbanks, R.G., (1990) 'The age and origin of the "Younger Dryas climate event" in Greenland ice cores' *Paleoceanography*, 5(6), pp.937-948.
- Fairbanks, R.G., Charles, C.D. and Wright, J.D., (1992) 'Origin of global meltwater pulses, In Radiocarbon after four decades' *Springer: New York*, pp. 473-500.
- Falconer, G., Andrews, J.T. (1965) 'Ives Late-Wisconsin and moraines in northern Canada' *Science*, 147 (3658), pp. 608-610.
- Feyling-Hanssen, R.W., (1964) '*Foraminifera in Late Quaternary deposits from the Oslofjord area*' *Universitets for laget*, (No. 225).
- Fissel, D.B., Lemon, D.D. and Birch, J.R., (1982) 'Major features of the summer near-surface circulation of western Baffin Bay, 1978 and 1979' *Arctic*, pp.180-200.p-374.
- Fredskild, B., (1983), 'The Holocene vegetational development of the Godthåbsfjord area, West Greenland' *Commission for Scientific Research in Greenland*, Volume: 10.
- Friedrich, M., Kromer, B., Kaiser, K.F., Spurk, M., Hughen, K.A. and Johnsen, S.J., (2001) 'High-resolution climate signals in the Bølling–Allerød Interstadial (Greenland Interstadial 1) as reflected in European tree-ring chronologies compared to marine varves and ice-core records' *Quaternary Science Reviews*, 20(11), pp.1223-1232.
- Funder, S. and Hansen, L., (1996) 'The Greenland ice sheet—a model for its culmination and decay during and after the last glacial maximum' *Bulletin of the Geological Society of Denmark*, 42(2), pp.137-152.
- Ganopolski, A., Calov, R. and Claussen, M., (2010) 'Simulation of the last glacial cycle with a coupled climate ice-sheet model of intermediate complexity' *Climate of the Past*, 6(2), pp.229-244.
- Ghil, M., (1994) 'Cryothermodynamics: The chaotic dynamics of paleoclimate', *Physical D: Nonlinear Phenomena* 77(1-3), pp.130-159.
- Gilbert, I.M., Pudsey, C.J. and Murray, J.W., (1998) 'A sediment record of cyclic bottom-current variability from the northwest Weddell Sea'. *Sedimentary geology*, 115(1-4), pp.185-214.

- Gilbert, R., Nielsen, N., Desloges, J.R. and Rasch, M., (1998) 'Contrasting glacial marine sedimentary environments of two arctic fiords on Disko, West Greenland' *Marine Geology*, 147(1-4), pp.63-83.
- Grumet, N.S., Wake, C.P., Mayewski, P.A., Zielinski, G.A., Whitlow, S.I., Koerner, R.M., Fisher, D.A. and Woollett, J.M., (2001) 'Variability of sea-ice extent in Baffin Bay over the last millennium', *Climatic Change*, Volume: 49(1-2), pp.129-145.
- Hald, M. and Steinsund, P.I., (1996) 'Benthic foraminifera and carbonate dissolution in the surface sediments of the Barents and Kara Seas. *Surface-sediment composition and sedimentary processes in the central Arctic Ocean and along the Eurasian Continental Margin*' *Berichte zur Polarforschung*, 212, pp.285-307.
- Hamel, D., de Vernal, A., Gosselin, M. and Hillaire-Marcel, C., (2002) 'Organic-walled microfossils and geochemical tracers: sedimentary indicators of productivity changes in the North Water and northern Baffin Bay during the last centuries', *Deep Sea Research Part II: Topical Studies in Oceanography*, 49(22), pp.5277-5295.
- Hayes, I.I., (1867) 'The Open Polar Sea', *Hud and Houghlin*, New York, pp.454.
- Hays, J.D., Imbrie, J. and Shackleton, N.J., (1976) 'Variations in the Earth's orbit: pacemaker of the ice ages', *American Association for the Advancement of Science*.
- Heinrich, H., (1988), 'Origin and consequences of cyclic ice rafting in the northeast Atlantic Ocean during the past 130,000 years' *Quaternary research*, 29(2), pp.142-152.
- Hemming, S.R., (2004) 'Heinrich events: Massive late Pleistocene detritus layers of the North Atlantic and their global climate imprint' *Reviews of Geophysics*, 42(1).
- Hesse, R., Klauk, I., Khodabakhsh, S. and Piper, D., (1999) 'Continental slope sedimentation adjacent to an ice margin. III. The upper Labrador Slope' *Marine Geology*, 155(3), pp.249-276.
- Hillaire-Marcel, C., Vernal, A.D., Bilodeau, G. and Wu, G., (1994) 'Isotope stratigraphy, sedimentation rates, deep circulation, and carbonate events in the Labrador Sea during the last 200 ka' *Canadian Journal of Earth Sciences*, 31(1), pp.63-89.
- Hiscott, R.N., Aksu, A.E. and Nielsen, O.B., (1989) 'Provenance and dispersal patterns, Pliocene-Pleistocene section at site 645, Baffin Bay' In *Proc. Ocean Drill. Program Sci. Results*, 105, pp. 31-52.
- Hogan, K.A., Cofaigh, C.Ó., Jennings, A.E., Dowdeswell, J.A. and Hiemstra, J.F., (2016) 'Deglaciation of a major palaeo-ice stream in Disko Trough, West Greenland' *Quaternary Science Reviews*, 147, pp.5-26.
- Holland, D.M., Thomas, R.H., De Young, B., Ribergaard, M.H. and Lyberth, B., (2008) 'Acceleration of Jakobshavn Isbrae triggered by warm subsurface ocean waters', *Nature geoscience*, 1(10), pp.659-664.
- Hulbe, C.L., (1997) 'An ice shelf mechanism for Heinrich layer production' *Paleoceanography*, 12(5), pp.711-717.
- Hulbe, C.L., MacAyeal, D.R., Denton, G.H., Kleman, J. and Lowell, T.V., (2004) 'Catastrophic ice shelf breakup as the source of Heinrich event icebergs', *Paleoceanography*, 19(1).
- Imbrie, J., Boyle, E.A., Clemens, S.C., Duffy, A., Howard, W.R., Kukla, G., Kutzbach, J., Martinson, D.G., McIntyre, A., Mix, A.C. and Molino, B., (1992) 'On the structure and origin of major

- glaciation cycles 1. Linear responses to Milankovitch forcing', *Paleoceanography*, 7(6), pp.701-738.
- Jackson, R., Carlson, A.E., Hillaire-Marcel, C., Wacker, L., Vogt, C. and Kucera, M., (2017) 'Asynchronous instability of the North American-Arctic and Greenland ice sheets during the last deglaciation'. *Quaternary Science Reviews*, 164, pp.140-153.
- Jennings, A., Andrews, J., Pearce, C., Wilson, L. and Ólafsdóttir, S., (2015) 'Detrital carbonate peaks on the Labrador shelf, a 13–7ka template for freshwater forcing from the Hudson Strait outlet of the Laurentide Ice Sheet into the subpolar gyre' *Quaternary Science Reviews*, 107, pp.62-80.
- Jennings, A., Andrews, J., O'Coifagh, C., Guillaume St.Onge, Sheldon, C., Belt, S., Cabedo-Sanz, P., Hillaire-Marcel, C., (2017) ' Ocean forcing of Ice Sheet retreat in central west Greenland from LGM to the early Holocene' *Elsevier*, 472, 1-13.
- Jennings, A.E. and Helgadottir, G., (1994) 'Foraminiferal assemblages from the fjords and shelf of eastern Greenland' *Journal of Foraminiferal Research*, 24(2), pp.123-144.
- Jennings, A.E., Sheldon, C., Cronin, T.M., Francus, P., Stoner, J. and Andrews, J., (2011) 'The Holocene history of Nares Strait: Transition from glacial bay to Arctic-Atlantic throughflow' *Oceanography*, 24(3):26–41.
- Jennings, A.E., Walton, M.E., Ó Cofaigh, C., Kilfeather, A., Andrews, J.T., Ortiz, J.D., De Vernal, A. and Dowdeswell, J.A., (2014) 'Paleoenvironments during Younger Dryas-Early Holocene retreat of the Greenland Ice Sheet from outer Disko Trough, central west Greenland'. *Journal of Quaternary Science*, 29(1), pp.27-40.
- Jiang, H., Seidenkrantz, M.S., Knudsen, K.L. and Eriksen, J., (2002) 'Late-Holocene summer sea-surface temperatures based on a diatom record from the north Icelandic shelf' *The Holocene*, 12(2), pp.137-147.
- Jones, E.P., Rudels, B. and Anderson, L.G., (1995) 'Deep waters of the Arctic Ocean: origins and circulation. Deep Sea Research Part I' *Oceanographic Research Papers*, 42(5), pp.737-760.
- Jones, E. P., Swift, J. H., Anderson, L. G., Lipizer, M., Civitarese, G., Falkner, K. K., Kattner, G. & McLaughlin, F. (2003) 'Tracing Pacific water in the North Atlantic Ocean' *Journal of Geophysical Research*, 108 (C4), pp. 346-374.
- Joughin, I., Alley, R.B. and Holland, D.M., (2012) 'Ice-sheet response to oceanic forcing', *science*, 338(6111), pp.1172-1176.
- Kaminski, H.S, (1955) 'Distribution of ice in Baffin Bay and Davis Strait', *Technical Report, U.S Navy Hydrographic Office, Washington D.C.*
- Kaminski, M.A., Boersma, E., Tyszka, J.A.R.O.S.L.A.W. and Holbourn, A.E.L., (1995) 'Response of deep-water agglutinated foraminifera to dysoxic conditions in the California Borderland basins' Grzybowski Foundation.
- Keigwin, L.D., Curry, W.B., Lehman, S.J. and Johnsen, S., (1994) 'The role of the deep ocean in North Atlantic climate change between 70 and 130 kyr ago' *Nature*, 371(6495), pp.323-326.
- Kellogg, T.B., (1976) 'Late Quaternary climatic changes: evidence from deep-sea cores of Norwegian and Greenland Seas', *Geological Society of America Memoirs*, 145, pp.77-110.
- Kiilerich, A.B., (1939) 'The Godthaab Expedition, 1928: A Theoretical Treatment of the Hydrographical Observation Material'. *CA Reitzel*.

- Kinnard, C., Zdanowicz, C.M., Fisher, D.A., Isaksson, E., de Vernal, A. and Thompson, L.G., (2011) 'Reconstructed changes in Arctic sea ice over the past 1,450 years' *Nature*, 479(7374), pp.509-512.
- Knudsen, K.L., Stabell, B., Seidenkrantz, M.S., Eiriksson, J. and Blake, W., (2008) 'Deglacial and Holocene conditions in northernmost Baffin Bay: sediments, foraminifera, diatoms and stable isotopes' *Boreas*, 37(3), pp.346-376.
- Kominz, M.A., Heath, G.R., Ku, T.L. and Pisias, N.G., (1979) 'Brunhes time scales and the interpretation of climatic change' *Earth and Planetary Science Letters*, 45(2), pp.394-410.
- Kuijpers, A., Troelstra, S.R., Prins, M.A., Linthout, K., Akhmetzhanov, A., Bouryak, S., Bachmann, M.F., Lassen, S., Rasmussen, S. and Jensen, J.B., (2003) 'Late Quaternary sedimentary processes and ocean circulation changes at the Southeast Greenland margin' *Marine Geology*, 195(1), pp.109-129.
- Kutzbach JE, Webb T, (1993) 'Conceptual basis for understanding Late-Quaternary climates. In Global Climates since the Last Glacial Maximum' In: Wright HR Jr, Kutzbach JE, Webb T III, Ruddiman WE, Street-Perrott FA, Bartlein PJ (eds). *University of Minnesota Press*; 5–23.
- Kwok, R., Toudal Pedersen, L., Gudmandsen, P. and Pang, S.S., (2010) 'Large sea ice outflow into the Nares Strait in 2007' *Geophysical Research Letters*, 37(3).
- Lamb, H.H., (1995) 'Climate History of The Modern World' *Routledge*, pp. 433.
- Langway, C.C., Oeschger, H. and Dansgaard, W., (1985) 'Greenland ice core: geophysics, geochemistry, and the environment', *American Geophysical Union*, 33.
- Lassen, S.J., Kuijpers, A., Kunzendorf, H., Hoffmann-Wieck, G., Mikkelsen, N. and Konradi, P., (2004) 'Late-Holocene Atlantic bottom-water variability in Igaliku Fjord, South Greenland, reconstructed from foraminifera faunas' *The Holocene*, 14(2), pp.165-171.
- Ledu, D., Rochon, A., de Vernal, A. and St-Onge, G., (2010) 'Holocene paleoceanography of the northwest passage, Canadian Arctic Archipelago' *Quaternary Science Reviews*, 29(25), pp.3468-3488.
- Levac, E., Vernal, A.D. and Blake Jr, W., (2001) 'Sea-surface conditions in northernmost Baffin Bay during the Holocene: Palynological evidence', *Journal of Quaternary Science*, 16(4), pp.353-363.
- Li, G., Piper, D.J. and Calvin Campbell, D., (2011) 'The Quaternary Lancaster Sound trough-mouth fan, NW Baffin Bay' *Journal of Quaternary Science*, 26(5), pp.511-522.
- Lin, Z.S. and Wang, S.G., (2004) 'The 100ka period problem of solar radiation' *Chinese Journal of Geophysics*, 47(6), pp.1093-1097.
- Liu, T., Ding, Z. and Rutter, N., (1999) 'Comparison of Milankovitch periods between continental loess and deep sea records over the last 2.5 Ma', *Quaternary Science Reviews*, 18(10), pp.1205-1212.
- Lloyd, J.M. (2006) 'Late Holocene environmental change in Disko Bugt, west Greenland: interaction between climate, ocean circulation and Jakobshavn Isbrae' *Boreas*, 35, 35–49.
- Lowe.J.J and Walker.M.J.C., (1998) 'Reconstructing Quaternary Environments', *Pearson*: London.
- Lynch-Stieglitz, J., Adkins, J.F., Curry, W.B., Dokken, T., Hall, I.R., Herguera, J.C., Hirschi, J.J.M., Ivanova, E.V., Kissel, C., Marchal, O. and Marchitto, T.M., (2007) 'Atlantic meridional overturning circulation during the Last Glacial Maximum' *Science*, 316(5821), pp.66-69.

- MacAyeal, D.R., (1993) 'Binge/purge oscillations of the Laurentide ice sheet as a cause of the North Atlantic's Heinrich events' *Paleoceanography*, 8(6), pp.775-784.
- MacLean, B., Jansa, L.F., Falconer, R.K.H. and Srivastava, S.P., (1977) 'Ordovician strata on the southeastern Baffin Island shelf revealed by shallow drilling' *Canadian Journal of Earth Sciences*, 14(8), pp.1925-1939.
- Manabe, S. and Broccoli, A.J., (1985), 'The influence of continental ice sheets on the climate of an ice age', *Journal of geophysical Research*, 90(D1), pp.2167-2190.
- Marko, J.R., Birch, J.R. and Wilson, M.A., (1982) 'A study of long-term satellite-tracked iceberg drifts in Baffin Bay and Davis Strait' *Arctic*, pp.234-240.
- Marshall, S.J. and Koutnik, M.R., (2006) 'Ice sheet action versus reaction: Distinguishing between Heinrich events and Dansgaard-Oeschger cycles in the North Atlantic' *Paleoceanography*, 21(2).
- Mauritzen, C., (1996) 'Production of dense overflow waters feeding the North Atlantic across the Greenland-Scotland Ridge. Part 1: Evidence for a revised circulation scheme' *Deep Sea Research Part I: Oceanographic Research Papers*, 43(6), pp.769-806.
- McIntyre, A., Kipp, N.G., Bé, A.W., Crowley, T., Kellogg, T., Gardner, J.V., Prell, W. and Ruddiman, W.F., (1976) 'Glacial North Atlantic 18,000 years ago: a CLIMAP reconstruction' *Geological Society of America Memoirs*, 145, pp.43-76.
- McManus, J.F., Francois, R., Gherardi, J.M., Keigwin, L.D. and Brown-Leger, S., (2004) 'Collapse and rapid resumption of Atlantic meridional circulation linked to deglacial climate changes' *Nature*, 428(6985), pp.834-837.
- McManus, J.F., Oppo, D.W., Keigwin, L.D., Cullen, J.L. and Bond, G.C., (2002) 'Thermohaline circulation and prolonged interglacial warmth in the North Atlantic' *Quaternary Research*, 58(1), pp.17-21.
- Mead A. Allison, Arthur T. DeGaetano, & Jay M. Pasachoff, (2012), Holt McDougal Earth Science ??**
- Mertz, G., Narayanan, S. and Helbig, J., (1993) 'The freshwater transport of the Labrador Current' *Atmosphere-Ocean*, 31(2), pp.281-295.
- Melling, H., Gratton, Y. and Ingram, G., (2001) 'Ocean circulation within the North Water polynya of Baffin Bay' *Atmosphere-Ocean*, 39(3), pp.301-325.
- Milankovitch, M., (1941) 'Kanon der Erdebestrahlung und seine Anwendung auf das Eiszeitenproblem' *Königlich Serbische Akademie*.
- Miller, G.H., Wolfe, A.P., Briner, J.P., Sauer, P.E. and Nesje, A., (2005) 'Holocene glaciation and climate evolution of Baffin Island, Arctic Canada' *Quaternary Science Reviews*, 24(14), pp.1703-1721.
- Miller, G.H., Wolfe, A.P., Steig, E.J., Sauer, P.E., Kaplan, M.R. and Briner, J.P., (2002) 'The Goldilocks dilemma: big ice, little ice, or "just-right" ice in the Eastern Canadian Arctic' *Quaternary Science Reviews*, 21(1), pp.33-48.
- Mix, A.C., Pisias, N.G., Rugh, W., Wilson, J., Morey, A. and Hagelberg, T.K., (1995) 'Benthic foraminifer stable isotope record from Site 849 (0-5 Ma): local and global climate changes' *Proceedings of the Ocean Drilling Program, Scientific Results*.

- Mudelsee, M. and Schulz, M., (1997) 'The Mid-Pleistocene climate transition: onset of 100 ka cycle lags ice volume build-up by 280 ka' *Earth and Planetary Science Letters*, 151(1), pp.117-123.
- Müller, J., Wagner, A., Fahl, K., Stein, R., Prange, M., Lohmann, G. (2011) 'Towards quantitative sea ice reconstructions in the northern North Atlantic: a combined biomarker and numerical modelling approach' *Earth Planet. Sci. Lett.*, 306 (3-4) (2011), pp. 137–148.
- Muench, R.D., (1971) 'The physical oceanography of the northern Baffin Bay region (No. AINA-TR-7)' *ARCTIC INST OF NORTH AMERICA WASHINGTON DC*.
- Münchow, A., Melling, H. and Falkner, K.K., (2006) 'An observational estimate of volume and freshwater flux leaving the Arctic Ocean through Nares Strait' *Journal of Physical Oceanography*, 36(11), pp.2025-2041.
- Murray, J.W., (1991) 'Ecology and distribution of benthic foraminifera. *Biology of Foraminifera*' *Academic Press, London*, pp.221-253.
- Myers, P.G., Kulan, N. and Ribergaard, M.H., (2007) 'Irminger water variability in the West Greenland Current' *Geophysical Research Letters*, 34(17).
- Ohlenschlaeger, R., (2000) 'Reente foraminiferers fordeling og Sen-Holocene Klimavariationer fra fjordsystemer I det centrale Vestgrønland.' M.S.c Thesis, *Department of Earth Sciences University of Aarhus, Denmark*.
- Nick, F.M., Vieli, A., Andersen, M.L., Joughin, I., Payne, A., Edwards, T.L., Pattyn, F. and van de Wal, R.S., (2013) 'Future sea-level rise from Greenland's main outlet glaciers in a warming climate' *Nature*, 497(7448), pp.235-238.
- NOAA (2017) National Centres for Environmental Information. Available at: <https://maps.ngdc.noaa.gov/viewers/bathymetry/> (Accessed:28 June 2017).
- Osterman, L. E. & Nelson, A. R. (1989) 'Latest Quaternary and Holocene paleoceanography of the eastern Baffin Island continental shelf, Canada: Benthic foraminiferal evidence' *Canadian Journal of Earth Science*, 26, 2236–2248.
- Palfrey Jr, K.M. and Day, G.G., (1968) 'Oceanography of Baffin Bay and Nares Strait in the summer of 1966 and current measurements in Smith Sound, summer 1963' *COAST GUARD WASHINGTON DC OCEANOGRAPHIC UNIT*.
- Parkinson, C.L. and Cavalieri, D.J., (1989) 'Arctic sea ice 1973–1987: Seasonal, regional, and interannual variability' *Journal of Geophysical Research: Oceans*, 94(C10), pp.14499-14523.
- Parkinson, C.L., Cavalieri, D.J., Gloersen, P., Zwally, H.J. and Comiso, J.C., (1999) 'Arctic sea ice extents, areas, and trends, 1978–1996' *Journal of Geophysical Research: Oceans*, 104(C9), pp.20837-20856.
- Parnell, J., Bowden, S., Andrews, J.T. and Taylor, C., (2007) 'Biomarker determination as a provenance tool for detrital carbonate events (Heinrich events?): Fingerprinting Quaternary glacial sources into Baffin Bay' *Earth and Planetary Science Letters*, 257(1), pp.71-82.
- Pearce, C., Jessen, C., Solignac, S., Reynisson, N.F., Kuijpers, A. and Seidenkrantz, M.S., (2011) 'Younger Dryas-Early Holocene sea surface conditions offshore Newfoundland: Original title: Southwestern Labrador Sea ocean-and atmospheric circulation in the mid to late Holocene' In *XVIII INQUA Congress*.

- Peck, V.L., Hall, I.R., Zahn, R., Elderfield, H., Grousset, F., Hemming, S.R. and Scourse, J.D., (2006) 'High resolution evidence for linkages between NW European ice sheet instability and Atlantic Meridional Overturning Circulation' *Earth and Planetary Science Letters*, 243(3), pp.476-488.
- Petterson, O, (1900) 'Die wasser Ziukulation im Nordatlantschen Ozean', *Pettermann's Geographische Mitteil'* 46 (3), pp.61-65.
- Polyak, L., Bischof, J., Ortiz, J.D., Darby, D.A., Channell, J.E., Xuan, C., Kaufman, D.S., Løvlie, R., Schneider, D.A., Eberl, D.D. and Adler, R.E., (2009) 'Late Quaternary stratigraphy and sedimentation patterns in the western Arctic Ocean' *Global and Planetary Change*, 68(1), pp.5-17.
- Praeg, D.B., MacLean, B., and Sonnichsen, S. (2006) 'Quaternary geology of the Northeast Baffin Island continental shelf, Cape Aston to Buchan Gulf (70° to 72°N)' *Geological Survey of Canada*.
- Qvale, G. and Van Weering, T.C., (1985) 'Relationship of surface sediments and benthic foraminiferal distribution patterns in the Norwegian Channel (northern North Sea)' *Marine Micropaleontology*, 9(6), pp.469-488.
- Rahman, A., (1995) 'Reworked nannofossils in the North Atlantic Ocean and subpolar basins: implications for Heinrich events and ocean circulation', *Geology*, 23(6), pp.487-490.
- Raymo, M.E. and Nisancioglu, K.H., (2003) 'The 41 kyr world: Milankovitch's other unsolved mystery' *Paleoceanography*, 18(1).
- Rial, J.A., (1999) 'Pacemaking the ice ages by frequency modulation of Earth's orbital eccentricity' *Science*, 285(5427), pp.564-568.
- Rial, J.A. and Anaclerio, C.A., (2000), 'Understanding nonlinear responses of the climate system to orbital forcing' *Quaternary Science Reviews*, 19(17), pp.1709-1722.
- Rignot, E. and Kanagaratnam, P., (2006) 'Changes in the velocity structure of the Greenland Ice Sheet' *Science*, 311(5763), pp.986-990.
- Rignot, E. and Mouginot, J., (2012) 'Ice flow in Greenland for the international polar year 2008–2009', *Geophysical Research Letters*, 39(11).
- Schroeder-Adams, C.J. and Van Rooyen, D., (2011) 'Response of recent benthic foraminiferal assemblages to contrasting environments in Baffin Bay and the Northern Labrador Sea, Northwest Atlantic', *Arctic*, pp.317-341.
- Rignot, E., Velicogna, I., van den Broeke, M.R., Monaghan, A. and Lenaerts, J.T., (2011) 'Acceleration of the contribution of the Greenland and Antarctic ice sheets to sea level rise' *Geophysical Research Letters*, 38(5).
- Roncaglia, L. and Kuijpers, A., (2004) 'Palynofacies analysis and organic-walled dinoflagellate cysts in late-Holocene sediments from Igaliku Fjord, South Greenland' *The Holocene*, 14(2), pp.172-184.
- Rooney, A.D., Selby, D., Lloyd, J.M., Roberts, D.H., Lückge, A., Sageman, B.B. and Prouty, N.G., (2016) 'Tracking millennial-scale Holocene glacial advance and retreat using osmium isotopes: Insights from the Greenland ice sheet' *Quaternary Science Reviews*, 138, pp.49-61.
- Ruddiman, W.F. and Heezen, B.C., (1967) 'Differential solution of planktonic foraminifera', *In Deep Sea Research and Oceanographic Abstracts*, 14, No. 6, pp. 801-808.
- Ruddiman, W.F. and McIntyre, A., (1981) 'The North Atlantic Ocean during the last deglaciation' *Palaeogeography, Palaeoclimatology, Palaeoecology*, 35, pp.145-214.

- Sadler, H.E., (1976) 'Water, heat, and salt transports through Nares Strait, Ellesmere Island' *Journal of the Fisheries Board of Canada*, 33(10), pp.2286-2295.
- Sakshaug, E. and Holm-Hansen, O., (1984) 'Factors governing pelagic production in polar oceans' *In Marine phytoplankton and productivity*, Springer: Berlin Heidelberg (pp. 1-18).
- Schmieder, F., von Dobeneck, T. and Bleil, U., (2000), 'The Mid-Pleistocene climate transition as documented in the deep South Atlantic Ocean: initiation, interim state and terminal event', *Earth and Planetary Science Letters*, 179(3), pp.539-549.
- Schroder-Adams, C. J., Cole, F. E., Medioli, F. S., Mudie, P. J., Scott, D. B. & Dobbin, L, (1990) 'Recent arctic shelf foraminifera: Seasonally ice covered vs. perennially ice covered areas' *Journal of Foraminiferal Research*, 20, 8–36.
- Scott, D.B., Medioli, F.S. and Schafer, C.T., (2001) '*Monitoring in coastal environments using foraminifera and thecamoebian indicators*' Cambridge University Press.
- Scott, D.B., Mudie, P.J., Baki, V., MacKinnon, K.D. and Cole, F.E., (1989) 'Biostratigraphy and late Cenozoic paleoceanography of the Arctic Ocean: foraminiferal, lithostratigraphic, and isotopic evidence' *Geological Society of America Bulletin*, 101(2), pp.260-277.
- Scott, D.B., Mudie, P.J., de Vernal, A., Hillaire-Marcel, C., Baki, V., Mackinnon, K.D., Mediolo, F.S., Mayer, L., (1989) 'Lithostratigraphy, biostratigraphy, and stable-isotope stratigraphy of cores from ODP Leg 105 site surveys, Labrador Sea and Baffin Bay' In: Srivastava, S.P., Arthur, M., Clement, B., et al. (Eds.). *Proc. Ocean Drill. Programme, Science Results*, 195, PP. 561-582.
- Seidenkrantz, M.S., (2013) 'Benthic foraminifera as palaeo sea-ice indicators in the subarctic realm—examples from the Labrador Sea–Baffin Bay region' *Quaternary Science Reviews*, 79, pp.135-144.
- Seidenkrantz, M.S., Aagaard-Sørensen, S., Sulsbrück, H., Kuijpers, A., Jensen, K.G. and Kunzendorf, H., (2007) 'Hydrography and climate of the last 4400 years in a SW Greenland fjord: implications for Labrador Sea palaeoceanography', *The Holocene*, 17(3), pp.387-401.
- Seidenkrantz, M.S., Roncaglia, L., Fischel, A., Heilmann-Clausen, C., Kuijpers, A. and Moros, M., (2008) 'Variable North Atlantic climate seesaw patterns documented by a late Holocene marine record from Disko Bugt, West Greenland' *Marine Micropaleontology*, 68(1), pp.66-83.
- Shakun, J.D. and Carlson, A.E., (2010) 'A global perspective on Last Glacial Maximum to Holocene climate change' *Quaternary Science Reviews*, 29(15), pp.1801-1816.
- Sheldon, C., Jennings, A., Andrews, J.T., Cofaigh, C.Ó., Hogan, K., Dowdeswell, J.A. and Seidenkrantz, M.S., (2016) 'Ice stream retreat following the LGM and onset of the west Greenland current in Uummannaq Trough, west Greenland' *Quaternary Science Reviews*, 147, pp.27-46.
- Shackleton, N.J., (2000) 'The 100,000-year ice-age cycle identified and found to lag temperature, carbon dioxide, and orbital eccentricity' *Science*, 289(5486), pp.1897-1902.
- Simon, Q., Hillaire-Marcel, C., St-Onge, G. and Andrews, J.T. (2014) 'North-eastern Laurentide, western Greenland and southern Inuitian ice stream dynamics during the last glacial cycle' *Journal of Quaternary Science*, 29(1), pp.14-26.
- Simon, Q., St-Onge, G. and Hillaire-Marcel, C., (2012) 'Late Quaternary chronostratigraphic framework of deep Baffin Bay glaciomarine sediments from high-resolution paleomagnetic data' *Geochemistry, Geophysics, Geosystems*, 13(11).

- Simon, Q., Thouveny, N., Bourles, D.L., Nuttin, L., Hillaire-Marcel, C. and St-Onge, G., (2016) 'Authigenic $^{10}\text{Be}/^9\text{Be}$ ratios and ^{10}Be -fluxes (^{230}Th xs-normalized) in central Baffin Bay sediments during the last glacial cycle: Paleoenvironmental implications'. *Quaternary Science Reviews*, 140, pp.142-162.
- Smith, E.H., Soule, F.M. and Mosby, O., (1937) 'The Marion and General Greene Expeditions to the Davis Strait and Labrador Sea Under the Direction of the United States Coast Guard, 1928-1931-1933-1934-1935', *Scientific Results Part 2, Physical Oceanography*. US Government Printing Office.
- Soua, M., (2011) 'Productivity and bottom water redox conditions at the Cenomanian-Turonian Oceanic Anoxic Event in the southern Tethyan margin, Tunisia', *Revue méditerranéenne de l'environnement*, 4, pp.653-664.
- Stanford, J.D., Rohling, E.J., Bacon, S., Roberts, A.P., Grousset, F.E. and Bolshaw, M., (2011) 'A new concept for the paleoceanographic evolution of Heinrich event 1 in the North Atlantic', *Quaternary Science Reviews*, 30(9), pp.1047-1066.
- Stein, R. and Stax, R., (1991) 'Late Quaternary organic carbon cycles and paleoproductivity in the Labrador Sea' *Geo-Marine Letters*, 11(2), pp.90-95.
- Straneo, F., Sutherland, D.A., Holland, D., Gladish, C., Hamilton, G.S., Johnson, H.L., Rignot, E., Xu, Y. and Koppes, M., (2012) 'Characteristics of ocean waters reaching Greenland's glaciers', *Annals of Glaciology*, 53(60), pp.202-210.
- Stokes, C.R., Margold, M., Clark, C.D. and Tarasov, L., (2016) 'Ice stream activity scaled to ice sheet volume during Laurentide Ice Sheet deglaciation' *Nature*, 530(7590), pp.322-326.
- Stokes, C.R. and Tarasov, L., (2010) 'Ice streaming in the Laurentide Ice Sheet: A first comparison between data-calibrated numerical model output and geological evidence', *Geophysical Research Letters*, 37(1).
- Stokes, C.R., Tarasov, L. and Dyke, A.S., (2012) 'Dynamics of the North American Ice Sheet Complex during its inception and build-up to the Last Glacial Maximum' *Quaternary Science Reviews*, 50, pp.86-104.
- Stötter, J., Wastl, M., Caseldine, C. and Häberle, T., (1999) 'Holocene palaeoclimatic reconstruction in northern Iceland: approaches and results' *Quaternary Science Reviews*, 18(3), pp.457-474.
- Sutton, R.T. and Hodson, D.L., (2005) 'Atlantic Ocean forcing of North American and European summer climate', *Science*, 309(5731), pp.115-118.
- Tang, C.C., Ross, C.K., Yao, T., Petrie, B., DeTracey, B.M. and Dunlap, E., (2004) 'The circulation, water masses and sea-ice of Baffin Bay' *Progress in Oceanography*, 63(4), pp.183-228.
- Tan, F.C. and Strain, P.M., (1980) 'The distribution of sea ice meltwater in the eastern Canadian Arctic' *Journal of Geophysical Research: Oceans*, 85(C4), pp.1925-1932.
- Tribovillard, N., Algeo, T.J., Lyons, T., Armelle, R., (2006) 'Trace metals as paleoredox and paleoproductivity proxies: An update Chemical Geology', *Environmental*.
- The Pew Charitable Trusts, (2016) Research and Analysis: 'From the North Water Polynya to Lancaster Sound' Available at: <http://www.pewtrusts.org/en/research-and-analysis/factsheets/0001/01/01/from-the-north-water-polynya-to-lancaster-sound>, (Accessed 6/1/17).
- Tribovillard, N., Algeo, T.J., Lyons, T., Armelle, R., (2006) 'Trace metals as paleoredox and paleoproductivity proxies: An update Chemical Geology', *Environmental*.

- Trouet, V., Esper, J., Graham, N.E., Baker, A., Scourse, J.D. and Frank, D.C., (2009) 'Persistent positive North Atlantic Oscillation mode dominated the medieval climate anomaly', *Science*, 324(5923), pp.78-80.
- Tuenter, E., Weber, S.L., Hilgen, F.J., Lourens, L.J. and Ganopolski, A., (2005) 'Simulation of climate phase lags in response to precession and obliquity forcing and the role of vegetation' *Climate Dynamics*, 24(2-3), pp.279-295.
- Valeur, H.H., Hansen, C., Hasen, K.Q., Rasmussen, L., Thingvad, N., (1996) 'Weather, sea and ice conditions in eastern Baffin Bay, offshore northwest Greenland, a review' *Danish Meteorological Institute Technical Report Number: 96-12*.
- Vare, L.L., Massé, G., Gregory, T.R., Smart, C.W. and Belt, S.T., (2009) 'Sea ice variations in the central Canadian Arctic Archipelago during the Holocene' *Quaternary Science Reviews*, 28(13), pp.1354-1366.
- Vilks, G., (1975) 'Comparison of *Globorotalia pachyderma* (Ehrenberg) in the water column and sediments of the Canadian Arctic' *Journal of Foraminiferal Research*, 5(4), pp.313-325.
- Volkman, J.K. (1986) 'A review of sterol markers for marine and terrigenous organic matter' *Org. Geochem*, 9 (2), pp. 83–99.
- Walker, M. and Lowe, J., (2007) 'Quaternary science 2007: a 50-year retrospective' *Journal of the Geological Society*, 164, 1073-1092.
- Wang, J., Mysak, L.A. and Ingram, R.G., (1994) 'Interannual variability of sea-ice cover in Hudson Bay, Baffin Bay and the Labrador Sea' *Atmosphere-ocean*, 32(2), pp.421-447.
- Weckström, K., Massé, G., Collins, L.G., Hanhijärvi, S., Bouloubassi, I., Sicre, M.A., Seidenkrantz, M.S., Schmidt, S., Andersen, T.J., Andersen, M.L. and Hill, B., (2013) 'Evaluation of the sea ice proxy IP 25 against observational and diatom proxy data in the SW Labrador Sea' *Quaternary Science Reviews*, 79, pp.53-62.
- Weidick, A. and Bennike, O., (2007) 'Quaternary glaciation history and glaciology of Jakobshavn Isbræ and the Disko Bugt region, West Greenland: a review' *Geological Survey of Denmark and Greenland*, 14.
- Williams, K.M., (1986) 'Recent Arctic marine diatom assemblages from bottom sediments in Baffin Bay and Davis Strait' *Marine Micropaleontology*, 10(4), pp.327-341.
- Williams, D.F. and Fillon, R.N., (1986) 'Meltwater influences and palaeocirculation changes in the North Atlantic during the last glacial termination' *Geological Society, London, Special Publications*, 21(1), pp.175-180.
- Winograd, I., Coplen, T., Landwehr, J., Riggs, A., Ludwig, K., Szabo, B., Kolesar, P and Revesz, K., (1992) 'Continuous 500, 000-year climate record from vein calcite in Devils Hole, Nevada' *Science*, 258(5080), pp.255-260.
- Young, N.E., Briner, J.P., Rood, D.H. and Finkel, R.C., (2012) 'Glacier extent during the Younger Dryas and 8.2-ka event on Baffin Island, Arctic Canada', *Science*, 337(6100), pp.1330-1333.
- Zucker, F., Stocker, T.F. and Broecker, W.S., (1994) 'Atmospheric freshwater fluxes and their effect on the global thermohaline circulation' *Journal of Geophysical Research: Oceans*, 99(C6), pp.12443-12457.
- Zreda, M., England, J., Phillips, F., Elmore, D. and Sharma, P., (1999) 'Unblocking of the Nares Strait by Greenland and Ellesmere ice-sheet retreat 10,000 years ago' *Nature*, 398(6723), p.139.

Zwally, H.J., Abdalati, W., Herring, T., Larson, K., Saba, J. and Steffen, K., (2002) 'Surface melt-induced acceleration of Greenland ice-sheet flow', *Science*, 297(5579), pp.218-222.

Appendices:

8.1 GC01 Foraminifera Data Log:

Depth (cm):+G64D40B2:G58B2 :G71B2:B2:H106	JR175 GC01 Total abunda nces:	JR175 GC01 Species Identification:	Aggluti nated (TA)	Plan ktic (TA)	Ben thic (TA)
4-5cm	Zero forams	N/A	0	0	0
5-6cm	20 aggluti nated	20 Rhizammina algaeformis	20	0	0
6-7cm	25 aggluti nated, 6 plankti cs	25 Rhizammina algaeformis	25	6	0
7-8cm *	No materia l left to sample	N/A	0	0	0
8-9cm	20 aggluti nated	19 Rhizammina algaeformis, 1 unknown A	20	0	0
9-10cm	28 aggluti nated	27 Rhizammina algaeformis, 1 unknown A	28	0	0
10-11cm	154 aggluti nated	154 Rhizammina algaeformis	154	0	0
11-12cm	187 aggluti nated	184 Rhizammina algaeformis, 3 unknown A	187	0	0

12-13cm	209 agglutinated	209 Rhizammina algaeformis	209	0	0
13-14cm *	351 agglutinated	351 Rhizammina algaeformis	351	0	0
14-15cm	144 agglutinated	144 Rhizammina algaeformis	144	0	0
15-16cm *	N/A	N/A			
16-17cm	106 agglutinated	106 Rhizammina algaeformis	106	0	0
17-18cm *	66 agglutinated	66 Rhizammina algaeformis	66	0	0
18-19cm	41 agglutinated	41 Rhizammina algaeformis	41	0	0
19-20cm	33 agglutinated	33 Rhizammina algaeformis	33	0	0
20-21cm	85 agglutinated	85 Rhizammina algaeformis	85	0	0
21-22cm *	33 agglutinated	33 Rhizammina algaeformis	33	0	0
22-23cm	3 agglutinated, 2 benthics	1 cassidlunia neoteretis	3	0	2
23-24cm *	2 agglutinated, 1 benthic	1 cassidlunia neoteretis		0	1

24-25cm	32 planktics, 30 benthics, 1 agglutinated	28 cass. Neoteretis, 4 unknown Ask Jerry, 1 Rhizamina algaeformis	1	32	30
25-26cm	77 benthics, 56 planktics, 2 agglutinated	70 cass. Neoteretis, (1 unknown box 8), 6 nonion orbiculare, 2 Rhizamina algaeformis	2	56	77
26-27cm	92 benthics, 23 planktics, 4 agglutinated	88 cass. neoteretis, 2 cass. reneforme, 4 Rhizamina algaeformis	4	23	92
27-28cm *	107 benthics, 35 planktics, 1 agglutinated	103 cass. Neoteretis, 4 trioculina, 1 Rhizamina algaeformis	1	35	107
28-29cm	507 benthics, 175 planktics	236 cass. neoteretis, 6 cibicides lobatus, 16 trioculina	0	175	507
29-30cm	261 benthics, 102 planktics	236 cass. neoteretis, 28 trioculina, 4 cibicides lobatis	0	102	361
30-31cm	39 planktics, 27 benthics, 1	23 cass. neoteretis, 1 agg benthic (unidentifiable), 3 Elphidium Foraclaucta, 1 Rhizamina Algaeformis	1	39	27

	agglutinated				
31-32cm *	24 planktics, 25 benthics	17 cass. neoteretis, 6 trioculina, 2 cass. Reneforme	0	24	25
32-33cm	22 planktics, 22 benthics, 1 agglutinated	16 cass. neoteretis, 6 trioculina, 1 Rhizammina Algaeformis	1	22	22
33-34cm	20 benthics, 5 planktics, 2 agglutinated	15 cass. Neoteretis, 5 trioculina, 2 Rhizammina Algaeformis	2	5	20
34-35cm	18 planktics, 8 benthics	4 cass. Neoteretis, 4 trioculina	0	18	8
35-36cm	7 planktics, 4 benthics	3 cass. Neoteretis, Elphidium Formaclaucta	0	7	4
36-37cm	4 planktics, 4 benthics, 1 agglutinated	1 cass. Neoteretis, trioculina, 1 Rhizammina Algaeformis	1	4	4
37-38cm *	5 benthics, 2	4 cass. Neoteretis, 1 trioculina	0	2	5

	plankti cs					
38-39cm	216 benthic s and 31 plankti c	194 cass. Neoteretis, 22 trioculina	0	216	31	
39-40cm *	119 benthic s, 20 plankti cs, 1 aggluti nated	105 cass. Neoteretis, 14 trioculina, 1 Rhizammina Algaeformis	1	20	119	
40-41cm	204 benthic s, 48 plankti cs	185 cass.neoteretis, 17 trioculina, 2 Elphidium... (ASK JERRY)	0	204	204	
41-42cm *	89 benthic s, 34 plankti cs	83 cass.neoteretis, 6 trioculina	0	34	89	
42-43cm	127 benthic s, 44 plankti cs, 1 aggluti nated	75 cass.neoteretis, 1 Rhizammina algaeformis	1	44	127	
43-44cm *	7 benthic s, 2 plankti cs	3 cass.neoteretis, 2 trioculina, 1 cass. Reneforme	0	2	7	
44-45cm	1 benthic , 1 plankti c	1 cass.neoteretis	0	1	1	

45-46cm	2 agglutinated	2 Rhizammina algaeformis	2	0	0
46-47cm	Zero forams	N/A	0	0	0
47-48cm	N/A	N/A			
48-49cm	1 benthic	1 cass.neoteretis	0	0	0
49-50cm	1 benthic	1 cass.neoteretis	0	0	1
50-51cm	Zero forams	N/A	0	0	0
51-52cm	N/A	N/A			
52-53cm	Zero forams	N/A	0	0	1
53-54cm	4 benthic s, 1 agglutinated	3 cass. neoteretis, 1 tricolina, 1 Rhizammina algaeformis	1	0	4
54-55cm	23 planktics	N/A	0	23	0
55-56cm *	23 planktics, 2 benthics	1 unidentifiable (agglutinated benthic), 1 cass.neoteretis	0	23	2
56-57cm	66 planktics, 7 benthics	1 unknown S (ASK JERRY), 6 cass. Neoteretis	0	66	7
57-58cm *	459 planktics, 36 benthics	5 cass. Reneforme, 30 cass. Neoteretis	0	459	7

58-59cm	491 planktic and 83 benthics	79 cass.neoteretis, 3 trioculina, 1 cass. Reneforme	0	491	73
59-60cm *	279 planktics, 60 benthics	54 cass.neoteretis, 6 trioculina	0	279	81
60-61cm	267 planktics, 24 benthics	6 trioculina, 18 cass.neoteretis	0	267	29
61-62cm *	177 planktics, 13 benthics	6 trioculina, 6 cass. neoteretis	0	177	26
62-63cm	312 planktics and 53 benthics	53 trioculina	0	312	51
63-64cm *	N/A	N/A			
64-65cm	337 planktics, 115 benthics	115 trioculina	0	337	147
65-66cm *	N/A	N/A			
66-67cm	72 planktic and 49 benthics	46 trioculina, 3 cass. Neoteretis	0	72	55
67-68cm *	N/A	N/A			

68-69cm	13 benthic s, 9 plankti cs	16 trioculina	0	9	13
69-70cm *	N/A	N/A			
70-71cm	109 plankti cs and 17 benthic s	16 unknow L, 1 cass. Neoteretis	0	109	17
71-72cm *	N/A	N/A			
72-73cm	Facies bounda ry layer	N/A	0	0	0
73-74cm *	N/A	N/A			
74-75cm	213 plankti c and 39 benthic s	37 trioculina, 1 cass. reneforme	0	213	49
75-76cm *	N/A	N/A			
76-77cm	120 plankti cs, 2 benthic s	1 cass.reneforme, 1 cass. Neoteretis	0	120	4
77-78cm *	N/A	N/A			
78-79cm	5 plankti cs and 2 benthic s	1 trioculina, 1 cass.reneforme	0	5	2
79-80cm	N/A	N/A			

80-81cm	3 plankti cs	N/A	0	3	0
81-82cm	N/A	N/A			
82-83cm	8 plankti cs and 2 benthic s	2 trioculina	0	8	4
83-84cm	N/A	N/A			
84-85cm	1 benthic	1 cass. Neoteretis	0	0	2
85-86cm	N/A	N/A			
86-87cm	4 plankti cs and 1 benthic	1 agglutinated benthic (unidentifiable)	0	4	1
87-88cm	N/A	N/A			
88-89cm	4 plankti cs, 1 benthic	1 cass. Neoteretis	0	4	1
89-90cm	N/A	N/A			
90-91cm	4 plankti cs	N/A	0	4	0
91-92cm	N/A	N/A			
92-93cm	1 benthic , 1 plankti c	1 trioculina	0	1	1
93-94cm	N/A	N/A			
94-95cm	Zero forams	N/A	0	0	0
95-96cm	N/A	N/A			

96-97cm	6 plankti cs	N/A	0	6	0
97-98cm *	N/A	N/A			
98-99cm	917 plankti cs, 374 bethics	8 trioculina, 28 cass.reneforme, 1 fissurina species, 2 stainforthia feylingi, 1 stainforthia fuilformas, 1 lagna clauata, 1 melonis barleenus, 1 onionella labradesrica, 1 laryngosigma labradonica	0	917	374
99-100cm	799 plankti cs and 183 benthic s	1 melonis barleenus, 1 onionella labradonica, 1 Laryngosigma trilocularis, 9 trioculina, cass. reneforme	0	799	183
100-101cm	358 plankti cs, 59 benthic s	8 cass. Reneforme, 1 (ASK JERRY), 1 melonis barleenus	0	358	59
101-102cm	80 plankti cs, 17 benthic s	3 trioculina, 6 cass.reneforme, 1 stainforthia feylingi	0	80	17
102-103cm	271 plankti cs, 83 benthic s	12 cass.reneforme, 12 Orbulina universa, 2 unknown S (ASK JERRY)	0	271	83
103-104cm	53 plankti cs and 10 benthic s	3 cass.reneforme, 4 Orbulina universa, 1 unknown S, 1 Stainforthia feylingi	0	53	10

104-105cm	1,292 plankti cs, 88 benthic s	12 orbulina universa, 2 cass.reneforme, 5 furgnkenia acuta	0	129 2	88
105-106cm *	N/A	N/A			
106-107cm	13,171 Plankti cs, 31 benthic s	20 cass.reneforme, 3 cass. Neoteretis, 2 orbulina universa, 3 furgenkenia acuta	0	131 71	31
107-108cm	600 plankti cs and 6 benthic s	5 cass. Reneforme, 1 unknown S, 1 cass.neoteretis	0	600	6
108-109cm	3,901 plankti cs, 24 benthic s	8 cass. Reneforme, 15 orbulina universa, 1 furgenkenia acuta	0	390 1	16
109-110cm *	N/A	N/A			
110-111cm	2,377 plankti cs, 12 benthic s	7 cass.reneforme, 2 unknown S (ASK JERRY), 2 orbulina universa, 1 cass.neoteretis	0	237 7	23
111-112cm	1,134 plankti c and 28 benthic s	4 orbulina universa, 8 cass. Reneforme, 1 unknown S	0	113 4	28
112-113cm	1,483 plankti cs, 27 benthic s	4 orbulina universa, 1 unknown S, 2 cass. reneforme	0	148 3	27
113-114cm *	N/A	N/A			

114-115cm	229 plankti cs, 10 benthic s	3 orbulina universa, 2 cass.reneforme	0	229	10
115-116cm	128 plankti cs and 4 benthic s	2 laryngosigma trilocularis, 1 unknown S, 1 cass. Reneforme	0	128	4
116-117cm	111 plankti cs, 4 benthic s	1 laryngosigma trilocularis, 3cass. Reneforme,	0	111	19
117-118cm	N/A	N/A			
118-119cm	126 plankti cs, 10 benthic s	6 cass. Reneforme	0	126	10
119-120cm	35 plankti cs and 2 benthic s?	1 cass. Reneforme	0	35	2
120-121cm	3 plankti cs, 2 benthic s	1 laryngosigma trilocularis, 1 cass. Neoteretis	0	0	0
121-122cm	N/A	N/A			
122-123cm	6 benthic s, 6 plankti cs	1 Ellphidium incertum, 1 cass. Renefrome	0	6	6
123-124cm	4 plankti	2 cass. Reneforme, 1 laryngosigma trilocularis	0	4	2

	cs and 2 benthic s				
124-125cm	2 benthic s	2 cass. reneforme	0	0	4
125-126cm *	N/A	N/A			
126-127cm	105 benthic s, 57 plankti c, 1 aggluti nated	92. cass reneforme, 13 unknown S, 1 Rhizamina algaeformis	1	57	144
127-128cm	37 plankti cs and 2 benthic s	26 cass. Reneforme, 7 unknown S, 2 agglutinated benthics (unidentifiable), 1 buccella frigida	0	37	2
128-129cm	4 plankic s, 11 benthic s	6. cass reneforme	0	4	11
129-130cm	N/A	N/A			
130-131cm	10 plankti cs, 1 benthic	1 cass. Reneforme	0	10	1
131-132cm	16 plankti cs 4 benthic s	3 cass. Reneforme, 1 tricolina	0	16	3
132-133cm	1 plankti c, 1 benthic	1 unknown S	0	1	1

133-134cm *	N/A	N/A			
134-135cm	27 planktics, 3 benthics	1 Ellipdum..., 1 Ellipdum incertum, 1 cass. Reneforme	0	27	5
135-136cm	1 planktic and 1 benthics	1 cass. reneforme	0	1	2
136-137cm	boundary layer?	N/A	0	0	0
137-138cm *	N/A	N/A			
138-139cm	5 planktics, 1 benthic	1 cass. Neoteretis, 1 agglutinated benthic (unidentifiable)	0	5	1
139-140cm	8 planktics and 1 benthic	1 cass. Reneforme	0	8	1
140-141cm	6 planktics, 3 benthics	1 cass. Renenforme, 2 unknown S	0	6	3
141-142cm	N/A	N/A			
142-143cm	15 planktics, 2 benthics	1 unknown B, 1 cass. Reneforme	0	15	8
143-144cm	8 planktics and 1 benthic	1 Orbulina universa	0	8	1

144-145cm	18 benthic s, 6 plankti cs	1 cass.reneforme, 6 buccella frigida	0	18	6
145-146cm	N/A	N/A			
146-147cm	21 benthic s, 13 plankti cs	7 cass. Renenforme, 5 unknown S	0	13	21
147-148cm	5 plankti cs and 6 benthic s	4 cass. Reneforme, 3 cibisidis labatus	0	5	6
148-149cm	10 plankti cs, 4 benthic s	2 cass. Reneforme, 2 buccella frigida	0	10	6
149-150cm	N/A	N/A			
150-151cm	27 plankti cs, 12 benthic s	1 cass. Neoteretis, 3 cass. Reneforme	0	27	12
151-152cm	10 plankti cs and 2 benthic s	2 cass. Reneforme	0	10	2
152-153cm	85 plankti cs, 12 benthic s	1 cass. Neoteretis, 7 cass. Reneforme	0	85	12
153-154cm	N/A	N/A			

154-155cm	31 planktics, 6 benthics	4 cass. Reneforme, 1 buccella frigida, 1 unknown S	0	0	0
155-156cm	379 planktics and 34 benthics	26 unknown S (one larger), 6 cass. Reneforme, 1 agglutinated benthic, 1 buccella frigida	0	379	59
156-157cm	132 planktics, 21 benthics	16 unknown S, 5 cass. Reneforme	0	0	0
157-158cm *	N/A	N/A			
158-159cm	17 planktics, 3 benthics	1 unknown S (large), 2 cass. Reneforme	0	17	3
159-160cm	11 planktics and 11 benthics	10 cass. Reneforme, 1 unknown S	0	11	21
160-161cm	22 planktics, 5 benthics	2 unknown S, 3 cass. Reneforme	0	22	5
161-162cm	N/A	N/A			
162-163cm	9 planktics, 2 benthics	1 cass. Neoteretis	0	9	2

163-164cm	6 plankti cs	N/A	0	6	0
164-165cm	2 plankti cs	N/A	0	2	0
165-166cm	N/A	N/A			
166-167cm	4 plankic s	N/A	0	4	0
167-168cm	543 plankti cs and 56 benthic s	2	0	543	53

8.2 BC06 Foraminifera Data Log:

JR175 BC06 A Total abundances:	JR175 BC06A Species identification List:	Agglutinated (TA)	Planktic (TA)	Benthic (TA)
6 agglutinated, 2 benthics	6 unknown A, onion?	6	0	2
N/A	N/A	0	0	0
N/A	N/A	0	0	0
N/A	N/A	0	0	0
N/A	N/A	0	0	0
8 agglutinated	5 Rhizammina algaeformis, 3 unknown A	8	0	0
N/A	N/A	0	0	0
N/A	N/A	0	0	0
4 agglutinated	2 Rhizammina algaeformis, 2 unknown A	4	0	0
N/A	N/A	0	0	0
N/A	N/A	0	0	0
N/A	N/A	0	0	0
94 agglutinated	94 Rhizammina algaeformis	94	0	0
N/A	N/A	0	0	0
N/A	N/A	0	0	0
79 agglutinated	79 Rhizammina algaeformis	79	0	0
100 agglutinated	100 Rhizammina algaeformis	100	0	0
10 agglutinated	10 Rhizammina algaeformis	10	0	0
N/A	N/A	0	0	0
49 agglutinated	48 Rhizammina algaeformis, 1 unknown A	49	0	0
N/A	N/A	0	0	0

12 agglutinated (precipitate layer)	12 Rhizammina algaeformis	12	0	0
52 agglutinated	52 Rhizammina algaeformis	52	0	0
55 agglutinated	55 Rhizammina algaeformis	55	0	0
11 agglutinated	11 Rhizammina algaeformis	11	0	0
145 benthics, 99 planktics, 80 agglutinated	145 cass. Neoteretis, 80 Rhizammina algaeformis	80	99	145
N/A	N/A	0	0	0
655 planktics, 489 benthics, 107 agglutinated	210 cass. Neoteretis, 4 trioculina, 15 Oridorsalis umbonatus	107	655	489
N/A	N/A	0	0	0
N/A	N/A	0	0	0
N/A	N/A	0	0	0
61 benthics, 65 planktics, 1 agglutinated	21 cass. Neoteretis, 6 Oridorsalis umbonatus, 4 trioculina	1	65	61
N/A	N/A	0	0	0
19 benthics, 9 planktics	11 cass. Neoteretis, 1 Oridorsalis umbonatus, 4 trioculina	0	9	19
N/A	N/A	0	0	0
36 planktics, 3 benthics	3 cass. Neoteretis	0	36	6
N/A	N/A	0	0	0
5 planktics, 1 benthic, 1 agglutinated	1 trioculina	1	5	1
N/A	N/A	0	0	0
9 planktics, 40 benthics	29 cass. Neoteretis, 2 trioculina	0	9	40
N/A	N/A	0	0	0

152 benthics, 18 planktics	3 trioculina, 148 cass. Neoteretis	0	18	152
212 benthics, 100 planktics	17 trioculina, 195 cass. Neoteretis	0	100	212
102 benthics, 68 planktics	5 trioculina, 97 cass. neoteretis	0	68	102
33 benthics,31 planktics	28 cass. Neoteretis, 5 trioculina	0	31	33

8.3 XRF data GC01:

Section Depth (cm)	Ca-Ka cps	Ti-Ka cps	Fe-Ka cps	Mn-Ka cps	Ba-Ka cps	K -Ka cps
3	1598.5 7	345.7 9	3736.2 3	193.15	0.7199488 49	897.4
3.5	1840.9 9	379.0 6	4101.2	211.68	1.0228898 43	994.9 1
4	2248.7 7	563.8 4	6379.5 3	229.3	0.8021680 22	1346. 57
4.5	2316.3 2	502.4 7	6392.9 3	270.76	0.8855421 69	1331. 38
5	2257.2 2	499.3 6	6384.9 2	183.17	0.8682539 68	1260. 07
5.5	2995.7 8	662.6 7	9225.0 7	265.67	0.6079228 03	1757. 65
6	2878.2 8	621.1 7	6871.3 3	189.85	0.4770852 43	1729. 2
6.5	3157.6 1	659.3 4	8391.9 3	176.01	0.4460112 81	1961. 12
7	3140.4 6	630.9 7	7309.8 9	171.89	0.3978819 97	1949. 61
7.5	3164.6 7	668.9	7510.7 4	149.71	0.3843311 16	2023. 29
8	3196.3 1	591.1 5	7067.9 4	181.52	0.4103240 39	1947. 17
8.5	3891.8 6	823.7 8	10277. 56	149.88	0.3353765 32	2375. 22
9	3649.1 9	690.2 7	7939.0 4	148.43	0.2299651 57	2256. 79
9.5	3841.5 7	717.4 4	8016.6 5	145.44	0.2448370 24	2323. 73
10	3810.1 2	694.8 1	7983	166.35	0.3435001 48	2345. 27
10.5	3984.3 8	734.2 8	8291.5 9	187.1	0.2615933 41	2413. 49
11	6039.4 7	1075. 83	12636. 03	196.34	0.2109020 6	3767. 64
11.5	6406.6 3	1121. 17	12688. 23	162.78	0.1824306 59	3890. 4
12	5595.4 5	955.0 4	11486. 2	235.1	0.2035505	3239. 35
12.5	6482.5 8	1124. 27	14695. 17	324.52	0.2290888 72	3646. 34
13	6548.7 5	1092. 75	14135. 42	253.96	0.2324904 49	3509. 59

13.5	5833.1 3	958.2	11115. 57	252.58	0.3017637 11	3023. 03
14	6017.5 7	918.3 1	10795. 48	278.1	0.2386713 59	3161. 64
14.5	5273.6 4	885.9 1	11620. 07	208.15	0.3070017 95	2756. 85
15	4716.5 1	729.1 2	8430.4 9	169.42	0.1922663 8	2497. 91
15.5	5758.2 1	856.1 3	11599. 8	235.06	0.2338177 01	2886. 77
16	5846.9 7	834.5 3	9558.3 2	241.1	0.2676812 89	2939. 06
16.5	5956.7 8	775.7 8	9410.4 1	177.78	0.2373417 72	2900. 21
17	5654.6 2	754.3 6	8832.6 5	177.63	0.2751548 81	2640. 82
17.5	6160.8 3	751.5 2	8503.4	228.95	0.1819354 84	2797. 2
18	4755.3 3	597.4 8	7413.2	215.73	0.2490824 57	2071. 62
18.5	5954.1 2	721.9 9	8133.6 3	215.9	0.2049827 33	2604. 56
19	5166.9 8	609.6 1	7358.8 6	246.95	0.3205985 35	2030. 98
19.5	7327.3 3	871.6 7	10223. 78	226.93	0.2770716 83	2956. 9
21.5	3640.3 9	413.4 6	4325.7 1	316.26	0.4904163 91	1231. 96
22	5027.0 4	471.4 1	5021.0 4	313.41	0.3826086 96	1509. 53
22.5	7358.4 1	605.6 8	6661.6 4	243.58	0.2343308 87	2216. 59
23	6761.6 5	560.2 6	7012.8 5	275.3	0.3359283 77	1871. 29
23.5	12963. 94	989.8 4	11961. 24	257.75	0.2672238 54	3586. 22
24	13982. 77	803.4 2	8258.9 9	242.49	0.2085450 35	3208. 39
24.5	14759. 26	691.6 7	6658.7 5	220.35	0.2282051 28	2810. 29
25	20846. 38	923.9	9557.8 1	222.14	0.2063120 98	3594. 87
25.5	20400. 22	832.3 4	7799.7 4	207.81	0.1641778 59	3704. 98
26	16489. 08	783.0 3	7252.4 8	257.48	0.2949756 89	2877. 83
26.5	18558. 72	708.8 4	6416.9 7	175.59	0.2670018 52	2991. 75

27	20916.68	714.95	6803.15	266.26	0.181743421	3327.31
27.5	20633.64	771.25	7030.64	230.39	0.176313785	3456.54
28	15582.89	738.89	7518.28	217.45	0.352718513	2703.48
28.5	16640.65	845.5	8546.69	206.68	0.248951782	3147.33
29	16136.65	829.69	9908.51	152.46	0.332643202	2914.98
29.5	19812.01	997.85	11628.39	119.85	0.195364238	3666.12
30	18646.05	853.28	8824.99	97.77	0.205869751	3402.7
30.5	17024.79	851.96	8431.86	161.54	0.290705128	2991.83
31	15710.16	727.29	7853.85	141.22	0.570815451	2478.99
31.5	16633.07	727.13	7785.62	126.23	0.491609082	2522.17
32	20725.18	722.97	7177.23	227.67	0.205307263	3173.42
32.5	16662.99	514.06	5617.45	194.95	0.35442575	2171.45
33	13482.78	412.33	5004.13	248.67	0.430643127	1675.18
33.5	18665.28	475.89	5073.35	190.03	0.39706499	2162.46
34	16022.25	410.62	5153.65	219.78	0.570900123	1817.75
34.5	10853.58	352.65	5086.75	150.52	0.853305785	1236.1
35	15021.73	439.75	5893.56	162.27	0.824630542	1668.37
35.5	17734.8	506.22	5961.94	198.13	0.749098774	2016.65
36	18371.97	504.42	5783.73	208.87	0.380664653	2112.83
36.5	9756.99	369.37	5132.04	94.55	0.921135647	1085.83
37	11869.1	350.12	4644.73	174.29	0.510006901	1308.55
37.5	8914.07	316.51	4306.03	148.48	0.863938053	959.98
38	7962.9	250.18	3681.27	91.8	0.700879765	852.29
38.5	7497.37	313.97	3656.37	144.24	1.077102804	856.16

39	4835.1 7	234.1 4	2971.7 4	413.21	1.8228941 68	587.5 3
39.5	10721. 47	337.1 4	3974.4 6	363.05	1.0839694 66	1131. 06
40	10708. 53	325.8 2	4084.2 1	213.7	0.7026841 02	1388. 23
40.5	11388. 36	262.7 3	3316.1 6	262.56	0.6839488 64	1373. 68
41	10337. 44	389.4 6	4595.5 2	182.84	0.4427390 79	1504. 81
41.5	11038. 35	538.9 6	8394.1 3	232.15	0.4123314 07	1968. 86
42	11895. 88	633.4 4	9443.7 1	224.41	0.2335396 74	2267. 23
42.5	9787.7 8	694.9 8	12028. 87	170.48	0.1721174 5	2376. 08
43	9037.5	766.5 2	11343. 77	197.21	0.2089825 85	2451. 45
43.5	7743.9	801.3 2	10839. 66	180.11	0.2006465 52	2405. 89
44	6842.4 7	752.2 6	11261. 32	209.05	0.2137515 08	2162. 02
44.5	6521.4	772.9 8	10928. 87	142.14	0.2524002 02	2086. 33
45	5939.3 3	706.9 7	10382. 8	180.96	0.2851701 98	1938. 06
45.5	6421.2 7	782.4 9	10223. 96	192.04	0.1868725 87	2217. 2
46	5255.2 1	577.0 6	8145.5	178.95	0.2588485 13	1625. 38
46.5	6148.6 4	773.7 4	11600. 86	172.28	0.2334905 66	1983. 81
47	4876.5 8	451.6 4	7425.4 5	200.89	0.2602873 14	1421. 11
47.5	6094.9 6	713.1 2	11132. 73	167.45	0.2281776 42	1786. 48
48	5189.8 3	502.5 2	7701.2 7	185.22	0.2553191 49	1385. 68
48.5	6034.6 7	499.4 9	7098.9 4	223.44	0.2470728 79	1558. 08
49	7686.7 2	564.7 4	8281.9 3	271.75	0.2603765 94	1914. 67
49.5	6230.9 4	494.1 8	7401.3	140.97	0.2419646 9	1669. 44
50	7089.6 9	636.7 8	8156.7 3	223.24	0.2516184 72	2011. 28
50.5	7992.9 3	589.8 1	7802.7 4	126.74	0.1706881 14	2200. 28

51	6792.9	637.3	7802.1	95.76	0.2224168	2022.
		9	3		13	38
51.5	5933.1	655.6	10712.	157.71	0.2509075	1767.
	6	6	27		38	48
52	5901.7	648.6	9260.9	139.57	0.1873152	1836.
	4	8	1		99	37
52.5	6073.6	704.3	10375.	174.79	0.2034354	1960.
	3	1	63		3	18
53	3644.0	252.0	2780.1	133.12	0.1241621	822.5
	1	2	3		45	8
53.5	4289.2	345.2	4062.5	140.51	0.1541248	1097.
	3		1		61	74
54	4983.2	446.7	4983.3	155.11	0.1361490	1441.
	9	9			03	33
54.5	5794.2	574.2	6350.3	230.11	0.1805070	1797.
	1		4		95	88
55	6433.2	668.1	6900.0	126.05	0.1449893	1900.
	5	3	7		39	22
55.5	6442.4	546.1	6872.9	96	0.1614269	1915.
	7	2	2		79	48
56	6523.1	671.1	7603.5	143.57	0.1466101	2099.
	9	7	9		69	36
56.5	7474.3	885.9	9873.8	123.65	0.1251969	2851.
		4	7		39	93
57	7316.2	940.5	12125.	107.23	0.1306376	2828.
	1	4	77		8	51
57.5	6700.2	890.4	9499.3	120.55	0.1161634	2812.
	8	9	6		5	43
58	5396.8	690.1	7781.8	120.86	0.1695340	2195.
	4	1	6		5	86
58.5	6833.7	913.1	11060.	105.25	0.1553290	2612.
	4	7	27		67	68
59	6201.2	718.0	7917.9	124.88	0.1150550	2311.
	4	6	4		8	1
59.5	7432.7	777.8	8094.1	43.32	0.1598188	2572.
	4	5	9		83	29
60	8076.8	820.0	8289.4	105.16	0.1435914	2651.
	3	5	5		17	57
60.5	8918.3	776.2	7857.3	163.35	0.1802841	2516.
	6	8	1		92	21
61	12364.	946.5	11616.	223.82	0.1193236	3260.
	55	3	82		52	22
61.5	10029.	766.2	8209.1	293.55	0.1341314	2705.
	4	3	3		87	63
62	11714.	704.2	7315.5	326.34	0.1233579	2699.
	71	1	1		23	65
62.5	14157.	669.0	7296.6	285.02	0.1073456	3033.
	17	7	4		47	75

63	15294.8	684.98	7862.6	223.26	0.147882823	3012.17
63.5	17336.34	757	8348.74	260.86	0.118225088	3331.27
64	16370.09	560.79	5948.15	268.43	0.189821414	2862.31
64.5	18881.62	559.23	5386.55	248.97	0.209560867	2945.37
65	20504.88	638.28	6326.18	262.82	0.151650773	3115.7
65.5	23587.13	675.03	7449.2	220.44	0.174996664	3221.65
66	24242.36	553.19	5693.02	353.58	0.199105982	3154.3
66.5	24804.76	539.73	4365.28	241.61	0.14255517	2985.74
67	20892.22	493.16	4215.78	225.37	0.250611519	2527.74
67.5	23046.51	448.37	4127.22	276.85	0.215890851	2753.12
68	23394.06	498.67	4386.25	402.7	0.179371276	2855.25
68.5	22416.17	479.6	4061.86	0.60453834	0.152320508	2722.05
69	24221.1	492.31	5364.89	0.48617363	0.180788754	2974.07
69.5	22952.25	499.72	4250.29	0.35500852	0.263859942	2769.47
70	23541.93	438.11	4254.46	0.57352256	0.183733284	2968.49
70.5	18357.92	376.82	3937.02	0.48317067	0.192230855	2408.62
71	20300.98	416.95	4582.84	0.58019218	0.151145602	2774.99
71.5	18367.93	431.22	4873.99	0.34518182	0.212445003	2558.94
72	21529.66	503.25	5077.57	0.40573997	0.164833116	3134.38
72.5	20903.97	491.05	5907.24	0.38661718	0.153991987	2898.5
73	10787.6	267.44	2588.49	0.39595345	0.355991591	1827.31
73.5	12209.45	569.07	6277.22	0.42770971	0.488615155	3132.64
74	9618.75	223.75	2925.82	0.24880478	0.179480841	1457.48
74.5	15689.1	489.71	5310.95	0.31045806	0.164921915	2614.74

75	16107.95	496.75	5586.61	0.24427276	0.131973701	2708.42
75.5	15165.47	568.51	6040.36	0.32433223	0.162306559	2642.65
76	15396.37	673.73	6879.08	0.46323347	0.203547751	2795.47
76.5	13056.51	708.53	7859.56	0.37412348	0.187022901	2752.47
77	11146.77	842.45	8533.27	0.33632231	0.154855316	2853.82
77.5	10531.03	853.03	8525.69	0.41361717	0.139958337	2855.36
78	7456.01	778.13	8183.19	0.53445323	0.137598899	2367.57
78.5	6284.87	691.74	7364.44	0.51408907	0.162141637	2044.16
79	5900.57	770.63	9878.25	0.38555946	0.166433846	1957.04
79.5	7357.63	772.69	8328.77	0.46936709	0.157923202	2345.35
80	5802.63	866.54	8882.17	0.4264495	0.157218443	2288.98
80.5	5089.23	750.74	8794.7	0.62958008	0.145932519	2090.57
81	4673.72	790.18	9617.32	0.41684696	0.122604615	2104.57
81.5	4403.66	720.21	9114.67	0.29574839	0.168031021	1864.48
82	4026.23	635.96	8003.17	0.33998853	0.149500852	1583.83
84.5	2976.06	178.53	1798.37	0.41619025	0.092010478	608.28
87	3704.74	400.11	4706.15	0.66017878	0.145044543	1216.71
87.5	4544.52	570.67	5842.08	0.64725473	0.11620603	1587.09
88	4744.51	673.5	6679.33	0.35977337	0.146316438	1755.83
88.5	4712.18	690.84	8025.02	0.45867385	0.195933457	1880.22
89	4830.68	858.21	10163.41	0.57846036	0.158281999	2378.07
89.5	4711.31	894.88	11645.65	0.51499756	0.121942381	2377.59
90	4877.99	949.01	11824.94	0.94829047	0.147183099	2640.83
90.5	6436.72	946.93	10819.09	0.67698722	0.137011931	2804.88

91	7492.0 6	1014. 94	10782. 9	0.772230 01	0.1921994 16	3032. 5
91.5	7530.0 6	824.7 9	9131.4 4	0.477757 18	0.1590894 7	2572. 64
92	6725.9 6	841.7	9480.6 2	0.605165 96	0.2105177 99	2459. 2
92.5	6991.4 7	995.0 4	13055. 33	0.509362	0.1850113 13	2550. 3
93	5673.7 8	857.3 7	10112. 87	0.419607 1	0.1384824 5	2409. 64
93.5	6078.2	1069. 25	11475. 86	0.516683 24	0.1685418 85	2721. 55
94	6853.0 6	1222. 69	16386. 14	0.425375 85	0.1489619 95	2841. 39
94.5	6497.8 8	1081. 37	12197. 3	0.316435 39	0.1718397 42	2713. 27
95	6132.3 8	976.9 7	11709. 51	0.478971 04	0.1442341 4	2494. 46
95.5	6458.1	1025. 14	14473. 29	0.458852 82	0.1992292 34	2421. 17
96	5769.9 9	780.6 5	9798.4 8	0.310518 65	0.2117433 69	1996. 66
96.5	7966.6 9	1173. 57	15033. 87	0.366194 19	0.1857082 84	2873. 8
97	7202.2 8	968.3 9	10913. 46	0.281239 62	0.1744596 8	2677. 69
97.5	7876.6 8	838.7	8737.5 4	0.299176 24	0.1969641 19	2594. 82
98	7809.2 8	670.4 9	6772.0 9	0.261417 11	0.1960282 96	2268. 67
98.5	7548.6	627.8 3	6553.2 9	0.437303 74	0.2438751 18	2160. 14
99	6693.9 1	655.1 1	6774.7 3	0.381985 39	0.2437987 24	2110. 91
99.5	6382.4 1	815.2 1	9020.0 6	0.335361 32	0.2247767 43	2114. 18
100	6288.2 7	894.4	9593.5 8	0.288321 26	0.1945343 58	2409. 82
100.5	4682.8 4	536.6 9	6864.0 6	193.15	0.1818627 45	1472. 8
101	3062.7 3	863	7498.0 6	211.68	50.8	1814. 57
101.5	3726.5 9	981.8 9	9941.8 3	229.3	95.9	2143. 92
102	5061.0 4	1223. 64	13556. 58	270.76	108.6	2976. 61
102.5	5247.2 9	1129. 69	13504. 8	183.17	132.9	2568. 42

103	5969.7 9	1052. 16	10040. 42	265.67	139.3	2595. 76
103.5	6746.1 9	1094. 49	9633.1 5	189.85	145.8	2856. 34
104	7823.8 2	956.5 2	7874.7 7	176.01	152	2923. 91
104.5	7546.9	776.5 3	6720.0 3	171.89	143.6	2804. 98
105	7112.2 1	850.4 4	6941.1 1	149.71	151.2	2600. 82
105.5	7554.7 9	715.5 2	5492.4 4	181.52	158.5	2446. 77
106	7756.8 9	754.5 7	6484.6 9	149.88	158.1	2656. 12
106.5	7740.9 1	891.9	7970.1 9	148.43	147.8	2968. 09
107	6615.5 4	781.5	6644.1 1	145.44	146.4	2626. 3
107.5	6280.3 2	944.9 6	8012.2 3	166.35	154.5	2827. 17
108	6196.7 7	931.7 3	8205.7 1	187.1	178	2698. 77
108.5	5571.6 1	1026. 24	10275. 59	196.34	141.6	2828. 45
109	5431.7 1	1264. 92	12741. 24	162.78	96.8	3298. 23
109.5	4174.6 3	1248. 36	13555. 34	235.1	110.7	3029. 72
110	3976.2	1341. 9	14204. 6	324.52	106.5	3139. 79
110.5	3973.9 8	1357. 65	15704. 7	253.96	104.2	3231. 39
111	4363.9 6	1311. 65	13472. 74	252.58	121.8	3155. 12
111.5	4869.0 6	1411. 94	14015. 79	278.1	115.7	3272. 01
112	5432.4 2	1455. 27	16413. 95	208.15	126.9	3485. 18
112.5	4721.1 7	1176. 89	12818. 04	169.42	99.3	2704. 27
113	5095.4 9	1142. 17	12095. 95	235.06	97.8	2480. 52
113.5	5891.1 6	1308. 95	16586. 51	241.1	97.6	3164. 39
114	6033.8 6	1344. 83	13393. 45	177.78	95.1	3425. 61
114.5	5542.1 4	1174. 02	12124. 58	177.63	102.6	2783. 49

115	5735.0 5	839.0 5	7888.3 3	228.95	163.9	2040. 85
115.5	5116.5 9	1122. 93	12299. 02	215.73	111.5	2550. 73
116	5245.5 6	1249. 15	14660. 5	215.9	115.3	2789. 7
116.5	5262.0 5	1316. 55	13489. 91	246.95	108	3121. 52
117	5215.2 2	1300. 93	13576. 99	226.93	104.1	3092. 16
117.5	4330.2 5	1108. 42	12728. 86	316.26	107.2	2471. 75
118	5083.5 4	1413. 55	17409. 49	313.41	108.9	3314. 37
118.5	4553.2 5	1358. 53	15057. 11	243.58	106	2931. 34
119	4450.0 3	1331. 85	16055. 54	275.3	102.5	2775. 82
119.5	4592.1 4	1311. 16	15242. 66	257.75	133.3	2813. 33
120	4849.9 4	1269. 71	14716. 54	242.49	107.6	3000. 36
120.5	5279.5 1	1298. 29	17443. 76	220.35	133.9	2910. 54
121	4829.2 2	978.1	12006. 6	222.14	126.5	2532. 23
121.5	5231.1 5	1378. 87	17917. 11	207.81	145.4	3108. 54
122	4963.7 4	1025. 97	11846. 33	257.48	118.9	2297. 56
122.5	6557.1 7	1239. 84	12123. 08	175.59	117.2	2671. 75
123	6068.9 1	814.5 7	8374.3 2	266.26	131.9	2325. 7
123.5	9452.3 6	1588. 59	11820. 36	230.39	122.8	1947. 79
124	8888.0 7	1187. 71	10758. 77	217.45	116.6	1726. 6
124.5	6211.6 3	935.2 5	9413.6 9	206.68	147	2381. 31
125	7225.7 3	724.9 8	7916.4 2	152.46	138.5	2167. 58
125.5	6122.0 4	527.7 5	6003.1 4	119.85	124.1	2072. 36
126	4903.6 3	271.5 4	3509.0 5	97.77	120.8	1672. 12
126.5	4465.6 3	284.7	3195.5 6	161.54	155.1	1741. 07

127	4746.2 7	251.6 4	3354.4 5	141.22	136.6	1588. 41
127.5	4786.2 5	342.1 5	3981.3 2	126.23	128.8	1602. 24
128	4420.3 1	188.3 5	3086.2 1	227.67	131.7	1730. 98
128.5	8035.5 2	1231. 47	10960. 69	194.95	126.4	2697. 31
129	8638.8 5	634.3 5	6661.4 6	248.67	127.3	2191. 31
129.5	10365. 18	914.5 6	10465. 05	190.03	174.8	2666. 55
130	9666.3 8	888.7 3	8089.6 8	219.78	134.7	2032. 02
130.5	8982.3 7	780.4 1	8136.8 2	150.52	135.4	2261. 73
131	7429.0 4	630.6 5	6259.5 2	162.27	143.6	2235. 1
131.5	7493.0 6	616.7 9	6027.1 9	198.13	167.2	2121. 41
132	7398.9 6	752.9 7	6917.7 2	208.87	145.4	2202. 04
132.5	7123.9 9	571.0 5	6228.3 4	94.55	159.3	2139. 56
133	5835.4 1	461.3 9	4666.6 7	174.29	140.4	1970. 67
133.5	5037.5 5	379.4 1	3790.1 8	148.48	152.1	1686. 96
134	4257.2 2	353.5	3366.7 5	91.8	141.9	1610. 14
134.5	4159.5 2	453.7 4	4720.7 7	144.24	131.6	1699. 34
135	5227.4 8	398.7 7	5192.3 3	413.21	145.5	2203. 67
135.5	5525.0 1	780.6 8	7961.8 1	363.05	134	2270. 74
136	5371.7 9	579.4 2	6883.4 6	213.7	140.2	2290. 93
136.5	5993.4 6	559.3 2	5454.0 7	262.56	112.9	2185. 13
137	10933. 69	1023. 83	11393. 93	182.84	132	2917. 31
137.5	11372. 75	911.9 7	6445.5 7	232.15	127.3	2631. 42
138	12929. 62	956.7 4	9133.7	224.41	142.8	3167. 41
138.5	7677.8 8	721.4	7531.3 2	170.48	147.3	2561. 22

139	7366.9 4	647.8 1	6554.6 5	197.21	162.6	2437. 94
139.5	6666.2 8	697.5 3	7076.0 1	180.11	142.1	2487. 88
140	6170.2 8	894.6 6	9520.4 1	209.05	134.9	2755. 08
140.5	8593.1	690.1 3	6898.3 1	142.14	134	2693. 98
141	6574.3 2	524	5349.4 2	180.96	143.7	2654. 9
141.5	7753.2 4	652.2 7	6453.2 2	192.04	127.1	2421. 97
142	7406.3 1	685.8 8	6516.0 1	178.95	168.5	2437. 46
142.5	6647.9 3	650.3 8	6421.1 7	172.28	157.8	2291. 58
143	6595.0 3	609.2 6	6339.4 8	200.89	161	2325. 49
143.5	6475.0 8	641.3 9	6912.7 6	167.45	127.5	2483. 3
144	6575.7 8	594.5 2	6173.1 4	185.22	155.9	2466. 7
144.5	6608.1 2	503.3 4	5592.5	223.44	169.1	2256. 69
145	6981.1 1	663.9 3	6335.9 7	271.75	163	2336. 47
145.5	5387.9 9	714.3 8	6277.2 5	140.97	158.6	3355. 67
146	5056.2 5	658.4 5	5935.8 8	223.24	162.4	3159. 6
146.5	4372.1 1	608.4 8	5873.5 7	126.74	152.8	2552. 98
147	4012.2 5	333.9 5	3404.8 6	95.76	142.8	2035. 46
147.5	4337.1	495.5 7	4650.6 6	157.71	146.9	2689. 87
148	3530.7 4	488.9	4935.2 2	139.57	162	2374. 63
148.5	4169.0 9	610.9 4	5300.3 8	174.79	172.9	2948. 53
149	4836.6 7	441.4	4294.8 3	133.12	178.5	2516. 11
149.5	4638.6 5	438.2	3742.4 9	140.51	176.7	2088. 82
150	4903.8 1	434.6 2	4355.6 9	155.11	153	2544. 84
150.5	4822.1 1	525.2 4	4910.4 6	230.11	194.5	2924. 72

151	5321.0 3	707.9 6	6298.9 4	126.05	177.8	3036. 18
151.5	4429.9 2	545.3 5	5101.4 2	96	174	2766. 17
152	4122.0 3	371.3 9	3884.8 9	143.57	147.6	2406. 63
152.5	3826.3 3	332.8 7	3670.5 5	123.65	122.3	2309. 39
153	3547.5 5	206.3 2	2684.9 6	107.23	160.8	2084. 76
153.5	3533.7 5	186.2 9	2328.1 2	120.55	152	1847. 62
154.5	2979.7 2	192.8 2	2075.9 4	120.86	163.3	1942. 72
154.5	3347.2 6	210.9 8	2634.9 8	105.25	149.6	1877. 7
155	3810.4	254.9 1	2616.8 5	124.88	145.8	1856. 77
155.5	3520.5 1	185.4 9	2501.4 2	43.32	161.6	2111. 35
156	2850.0 5	168.1 5	2000.4 6	105.16	153.5	1772
156.5	3308.4 2	288.5 9	2833.3 8	163.35	145	2019. 71
157	3791.8 7	714.9 5	6565.0 7	223.82	139.3	2178. 45
157.5	5345.1	1277. 89	11401. 56	293.55	136	3347. 75
158	5583.7 6	1319. 08	12742. 91	326.34	137.6	3437. 2
158.5	4938.5 5	1364. 95	13247. 84	285.02	123.8	3343. 54
159	5148.4 9	1447. 76	14084. 04	223.26	115.1	3604. 5
159.5	5206.8	1562. 9	15475. 63	260.86	128.2	3949. 06
160	5153.3 8	1544. 9	15561. 17	268.43	139	3814. 04
160.5	4597.3 2	1381. 37	14633. 99	248.97	135.3	3204. 34
161	4527.3	1337. 95	14117. 26	262.82	117.1	3078. 29
161.5	5102.6 7	1489. 75	16669. 89	220.44	143.2	3385. 6
162	4247.6 7	1250. 08	13734. 93	353.58	109.9	2747. 63
162.5	3848.2 6	1180. 66	13616. 6	241.61	124.6	2453. 08

163	3383.8	1039. 11	12754. 82	225.37	116.8	1989. 8
163.5	4267.9 6	1162. 2	13739. 32	276.85	107.6	2504. 69
164	4796.6	1237	14772. 54	402.7	110.9	2866. 14

8.4 XRF Data BC06:

Section Depth (cm)	K -Ka cps	Ca-Ka cps	Ti-Ka cps	Mn-Ka cps	Fe-Ka cps	Ba-Ka cps
1	-146.55	244.75	79.94	42.16	109.97	5.1
1.5	1704.08	2596.15	528.25	554.25	6409.94	25.8
2	2151.25	3266.75	657.44	442.05	6096.51	14.6
2.5	1429.71	2320.54	446.27	427.64	4587.98	40.4
3	447.14	998.67	294.44	82.07	2256.96	41.9
3.5	652.09	1310.4	326.87	77.87	3019.64	55.9
4	914.62	1527.74	389.53	280.25	4003.68	44.1
4.5	900.45	1656.15	408.77	533.77	4709.46	61.9
5	880.42	1513.28	359.85	529.64	3844.89	66.3
5.5	846.38	1559.76	372.74	621.89	4168.91	61.3
6	911.24	1598.41	370.27	656.1	4096.43	64.3
6.5	821.86	1497.8	352.76	599.73	3994.18	37.2
7	950.04	1677.38	389.51	657.81	5020.4	53.5
7.5	1084.25	1877.16	444.63	788.11	5695.03	68.5
8	1053.1	1789.44	408.81	703.91	4964.02	90.6
8.5	1189.54	2049.99	533.16	839.39	6377.56	90.4
9	744.33	1501.04	390.01	537	4598.36	77.4
9.5	1139.34	1961.6	468.17	680.5	5722.85	78.9
10	1362.21	2365.47	549.14	769.25	6646.53	97.6
10.5	1137.88	1982.22	471.78	591.07	5631.69	113.7
11	1504.14	2462.47	536.41	658.88	6651.99	121.4
11.5	1610.01	2686.78	601.65	752.25	7078.88	106.1
12	1424.57	2514.64	573.28	717.09	6849.84	117.8
12.5	1564.56	2679.93	619.28	731.1	7209.28	116.4

13	1675.05	2927.44	651.96	792.5 2	8742.61	118.3
13.5	1767.79	2986.46	654.61	786.3 7	8301.87	116.6
14	1931.38	3430.63	686.87	894.5 9	9803.85	111.8
14.5	1749.03	3067.41	647.61	685.2 1	7307.45	104.1
15	1897.45	3259.94	649.82	818.9 4	7732.82	96.6
15.5	1647.97	2808.78	573.28	694.4 2	7032.31	97.6
16	1855.09	3223.57	674.83	759.4 8	8016.67	107.3
16.5	1771.56	3192.13	724.5	924.3 5	9678.08	152.7
17	1551.76	2900.84	685.16	897.1	9748.53	131.9
17.5	1766.57	3245.76	704.7	821.8 9	10245.77	132
18	1639.35	3231.93	725.32	874.6 7	10036.52	129
18.5	2052.5	3953.56	835.98	995.1 7	10872.71	110.3
19	1743.96	3590.34	772.75	978.2 7	10639.31	136
19.5	1251.83	3002.41	586.08	669.6 8	8627.65	102.7
20	1471.71	3364.73	617.45	606.0 8	10253.31	88.7
20.5	1186.71	2889.31	563.19	471.8	8529.62	98.6
21	1530.18	3585.35	634.97	492.7 2	8915.5	118.9
21.5	1622.37	3881.1	675.23	506.4 3	9533.62	105.8
22	2629.2	5845.94	837.61	554.7 9	10725.97	111.3
22.5	3079.61	6602.47	952.56	524.3 8	11006.09	117.4
23	3370.95	7519.34	1021.0 7	674.3 5	13691.93	103.8
23.5	2890.77	6521.53	940.32	627.4 4	11739.3	95.2
24	2638.1	5951.35	824.04	659.4 5	9896.7	82.2
24.5	2591.22	5805.63	834.23	629.6 9	11494.79	70.8
25	1856.41	4502.97	647.52	516.8	8467.79	83

25.5	2483.13	5952.87	757.8	671.3 9	10110.62	83.5
26	2319.15	7136.03	638.88	502.5 3	7122.06	66
26.5	2738.7	16073.55	672.89	460.1 6	7006.39	111.2
27	2649.18	9141.76	716.52	467.0 8	7593.76	88.6
27.5	3346.67	10473.16	930.33	590.7 4	11026.99	106.3
28	3046.07	9384.02	805.89	339.7	8552.96	95.5
28.5	3113.18	9487.17	919.19	323.2 1	10090.47	90.2
29	2675.2	8813.92	729.58	296.2 9	8498.47	83
29.5	2912.2	10067.24	771.45	278.1 1	8028.76	80.4
30	3243.77	11519.24	848.85	296.5 7	8438.66	87.4
30.5	2843.48	10928.03	753.27	188.2 2	7794.17	90.9
31	3007.25	12653.01	791.75	246.6 5	8297.49	68.9
31.5	2931.79	13254.95	729.3	276.2 1	6935.5	88.7
32	2715	12671.62	640.35	175.2 4	6811.73	97.6
32.5	3185.02	15998.73	836.34	287.7	9689.21	111.9
33	2651.27	14580.81	671.35	363.7 3	7475.23	70.2
33.5	3274.3	17559.51	897.43	377.2 2	10434.76	81.9
34	3014.67	16836.72	744.29	180.2 9	7574.05	79.5
34.5	3046.51	16033.62	791.57	252.5 8	9144.67	77
35	2793.91	14319.19	714.08	172.2 2	7366.37	78.5
35.5	2969.68	17741.54	681.96	138.5 8	6745.89	70.2
36	2845.28	18375.5	644.95	82.9	5747.97	71.9
36.5	3276.77	20170.7	737.68	155.6 1	6906.16	90.9
37	2744.33	23360.49	544.74	116.1 8	5613.87	78.3
37.5	2814.35	24056.34	545.29	140.2 4	5996.06	86.2

38	2871.97	23971.27	542.3	169.3 3	6455.99	72.6
38.5	2558.12	23298.19	518.99	137.5 5	5331.72	92.2
39	2690.73	24412.39	491.68	134.0 7	5594.22	67.2
39.5	2764.43	25142.3	583.97	146.4 8	5772.24	74.5
40	2686.68	25600.53	527.25	130.0 5	5275.45	78.9
40.5	2766.86	24877.24	509.39	157.7 3	5287.85	62.4
41	2519.39	24615.29	447.01	126.4 1	4250.85	57.9
41.5	2180.44	21773.81	422.19	170.7 8	3873.19	63.9
42	2042.13	21442.69	391.06	127.4 4	3718.86	69.8
42.5	2084.03	19675	380.84	162.6 6	3389.21	76.4
43	2094.09	18605.28	356.93	256.5	3456.32	97
43.5	2257.45	20125.25	439.35	297.3 1	3517.32	61.2
44	2163.45	18693.86	437.35	301.8 6	3684.39	66.5
44.5	2324.62	19684.37	448.42	367.4 1	3679.5	69.8
45	2159.32	17300.86	416.56	533.4 3	4223.84	73.5
45.5	2186.01	16992.58	418.83	327.9 5	4352.37	54.1
46	2177.75	17642.99	443.57	305.2 7	4259.19	64.7
46.5	2323	13947.76	540.42	559.6 1	5986.04	57.2
47	2388.2	11501.04	669.08	647.6 5	7196.1	130.7
47.5	2344.33	9648.4	676.47	345.8	7458.28	63.7
48	2147.37	6649.31	783.09	277.3 1	9517.23	66.4